MUONIUM AND POSITRONIUM
AS MICROPROBES OF SURFACES AND SOLIDS

by

ROBERT FRANCIS XAVIER KIEFL
B.Sc. Carleton University, 1976
M.Sc. The University of British Columbia, 1978

A THESIS SUBMITTED IN PARTIAL FULFILMENT
OF THE REQUIREMENTS FOR THE DEGREE OF
DOCTOR OF PHILOSOPHY

in

THE FACULTY OF GRADUATE STUDIES
Physics Department

We accept this thesis as conforming
to the required standard

THE UNIVERSITY OF BRITISH COLUMBIA
January 1982

In presenting this thesis in partial fulfilment of the requirements for an advanced degree at the University of British Columbia, I agree that the Library shall make it freely available for reference and study. I further agree that permission for extensive copying of this thesis for scholarly purposes may be granted by the head of my department or by his or her representatives. It is understood that copying or publication of this thesis for financial gain shall not be allowed without my written permission.

Department of Physics

The University of British Columbia
2075 Wesbrook Place
Vancouver, Canada
V6T 1W5

Date Feb 12, 1982

ABSTRACT

The properties of muonium(μ^+e^-) and positronium(e^+e^-) are altered significantly in the presence of matter. The study of these exotic H-like atoms provides a unique perspective on atomic interactions with atoms, surfaces, and solids. This theme is explored in a variety of hosts.

The cross section for spin 1 positronium to be converted to spin 0 positronium during collisions with O_2 molecules has been measured from 120 °K to 630 °K in an SiO_2 powder moderator using a positron lifetime technique. The results indicate that positronium does not thermalize in the powder below 450 °K. The spin conversion cross section increases slightly with temperature above 450 °K. A theory for spin conversion of positronium by a spin 1 molecule is developed and used to interpret the data.

Muon Spin Rotation measurements in SiO_2, Al_2O_3, and MgO powders at low temperature in an atmosphere of He indicate that muonium emerges from the surfaces regardless of the ambient temperature of the powder. The muonium spin relaxation rate in Al_2O_3 in a He(or Ne) atmosphere is found to be a linear function of the fraction of surface area not covered by adsorbed He(or Ne). The cross sections for muonium to scatter elastically off adsorbed He and Ne atoms have been measured to be 11.0±0.2 Å^2 and 8.9±0.2 Å^2, respectively.

The first observations of muonium in the condensed phases of Ar, Kr, and Xe are presented. The data indicate that there is a high probability of muonium formation in all cases. The spin

relaxation rate of muonium in solid Xe is ten times that in the liquid, where the random local fields from the nuclear moments of ^{139}Xe and ^{141}Xe are averaged by additional translational motion.

TABLE OF CONTENTS

LIST OF FIGURES

LIST OF TABLES

ACKNOWLEDGEMENT

I feel very fortunate to have had the opportunity to work (and at times laugh) with the numerous people who directly and indirectly helped me during the course of this research. My supervisors Dr. John B. Warren and Dr. Jesse H. Brewer have been invaluable sources of advice and encouragement while never infringing upon my scientific freedom. I offer them my sincerest thanks. Much of the work contained in this thesis required the expertise of very capable people in the execution stage of the experiments. For this I thank Dr. Chris J. Oram, Dr. Glen M. Marshall, Carl W. Clawson, Dave P. Spencer, Dale R. Harshman, and C.A. Fry. The entire MSR group has always been accomodating and helpful so I take pleasure in thanking them. Dr. Dave M. Garner deserves special thanks for his assistance in the computing aspect of the experiments (even at 3:00 AM in the morning). I am very grateful to Dr. Birger Bergersen for several helpful discussions on the question of Ps thermalization in a powder and to Dr. John Berlinsky for discussions on the theory of spin exchange. I would also like to thank all the staff at UBC, especially Al Morgan, Al Bishop, Chris Stevens, Doug Maas, for their technical assistance and Jean Holt for drafting many of the figures in this thesis.

My wife Robin still loves me after all those owl shifts. Her understanding support and love have always been a source of comfort and strength and I dearly thank her for them.

Finally I thank Richard and Theresa Kiefl who have gave me love, encouragement and the opportunity to do my best. I am

forever grateful and I dedicate this thesis to you both.

INTRODUCTION

Pure leptonic atoms such as muonium (Mu) (μ^+e^-) and positronium (Ps) (e^+e^-) play an important role in particle physics. Their properties are free from strong interaction effects so they provide an ideal testing ground for electromagnetic and weak interaction theories. Thus the particle physicist is interested in the properties of free atoms, such as:

1. The annihilation rate and decay mode of 1^3S and 1^1S states of Ps (electromagnetic interaction).
2. $Mu(\mu^+e^-) \rightarrow \overline{Mu}(\mu^-e^+)$ conversion probability (weak interaction).
3. The hyperfine splitting (1^3S-1^1S) and the Lamb shift ($2P_{\frac{1}{2}}$-$2S_{\frac{1}{2}}$ splitting) of both Mu and Ps (electromagnetic interaction).

In contrast, it is the deviations from free atom behaviour in the presence of matter that are of interest to the muon or positron scientist, concerned with the chemical or physical properties of the probe and/or host. The Ps or Mu atom may function as a microprobe of its environment and can provide a unique perspective on atom-molecule, atom-surface, or atom-solid interactions. Very few techniques are sensitive to the action of individual atoms on a time scale as small as 10^{-9} s. The fundamental decay properties of the e^+ and μ^+ in matter, well known from particle physics, make such observations possible.

This thesis is a collection of four experiments concerned with the behaviour of these H-like atoms in matter:

1. 1^3S --> 1^1S spin conversion of Ps off O_2 molecules in an SiO_2 powder moderator between 120-630 °K.

2. Mu production in the voids of SiO_2, Al_2O_3, and MgO powders at 6°K.

3. Mu interaction with Al_2O_3 powder surfaces with adsorbed He or Ne between 7-30°K.

4. The first observations of Mu in the condensed phases of Ar, Kr, and Xe.

The first three chapters are devoted to Ps. The first chapter provides the necessary background information on Ps and the methods of study. The second chapter is concerned primarily with the characteristics of Ps decay in SiO_2 powder, with and without paramagnetic O_2 gas. The reader is referred to Appendix II for a theory of spin exchange scattering of Ps incident off a spin 1 atom or molecule. The first experiment is presented in Chapter III.

The last four chapters may be classified as the Mu part of the thesis. Chapter IV provides background information on Mu and the Muon Spin Rotation (μ^+SR) technique. The characteristics of Mu and the μ^+SR spectrum in oxide powders are of primary concern in Chapter V. The second and third experiments are presented in Chapter VI whereas the last experiment is the subject of Chapter Chapter VII.

CHAPTER I : POSITRONS AND POSITRONIUM

In the beginning there was Dirac (1930), who postulated that vacancies in a filled sea of negative energy electron states would manifest themselves physically as positively charged particles or anti-electrons. Anderson (1933) was the first to observe positrons in cloud chamber photographs of cosmic ray showers. The production of positron-electron pairs from high energy gamma rays was observed shortly afterwards (Blackett 1933). These experimental results sparked a large effort to develop a theory for positrons in matter. Pirenne (1946) was one of the first to perform calculations on the energy levels of positronium (e^+e^-) whose existence was first postulated by Mahorovicii (1934). Wheeler (1946) and Ore and Powell (1949a) calculated annihiliation rates from s=0 and s=1 ground states. Meanwhile experimental studies on Ps were just becoming possible as positron sources such as ^{22}Na and ^{64}Cu became available. The work of Deutsch (1951) firmly established the existence of positronium. Despite the great amount of experimentation since those early days it was not until 1974 that the first excited state of Ps was observed (Canter 1975), made possible by the development of monoenergetic beams of low energy positrons (Canter 1972).

In this chapter, the decay properties of free positrons and Ps in matter and the experimental techniques in positron annihilation are reviewed.

I·1 Conservation of Charge Conjugation Parity in e^+e^- Annihilation

Since positrons are anti-electrons, the positron-electron state is unstable to annihilation into gamma rays through electromagnetic interaction. The charge conjugation operator transforms every particle into its antiparticle. For a fermion antifermion state such as e^+e^-, the charge conjugation or C-parity is $(-1)^{\ell+s}$ where ℓ is the relative orbital angular momentum and s is the total spin (Williams 1971). Gammas or photons are self conjugate with C-parity -1 by virtue of the transformation properties of the electromagnetic vector potential under the C operation. Since electromagnetic interactions conserve C-parity, the annihilation of Ps into n gammas must be such that $\ell+s+n$ is even. If the annihilation occurs from an $\ell=0$ state (i.e.: the ground state of Ps), this restricts the annihilation from s=0 and s=1 states (i.e.: 1^1S and 1^3S atomic states of Ps) to an even and odd number of gammas respectively. Annihilation into a single gamma cannot conserve both momentum and energy so the s=1 state must decay into on odd numbers of photons greater than 1. The annihilation rate into n gammas is proportional to α^n where α (=1/137) is the fine structure constant, so that the s=0 and s=1 states decay primarily into two and three gammas respectively.

I·2 Ps Annihilation

When positrons are injected into matter they may capture an electron to form para-Ps (written p-Ps or $Ps(1^1S)$) or ortho-Ps (written o-Ps or $Ps(1^3S)$), in a statistical ratio of one to three. As stated above, the p-Ps decays in two 511 KeV gammas whereas o-Ps decays in three gammas with a continuous energy spectrum (see Figure I.1). The mean decay rate (1/lifetime) in

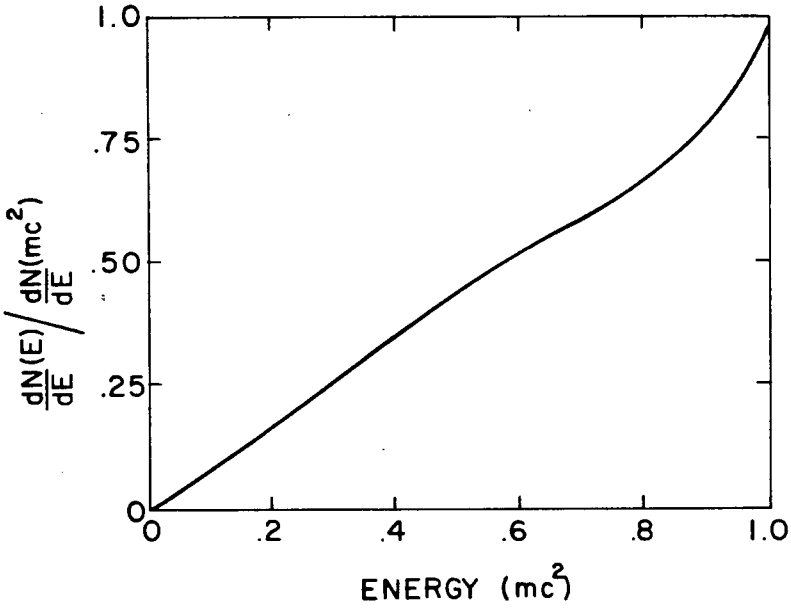

Figure I·1 The energy spectrum for o-Ps annihilation (Ore 1949a).

vacuum for p-Ps and o-Ps have been measured to be 799±11 x 10^7 s^{-1} (Theriot 1967) and 0.7056±0.0007 x 10^7 s^{-1} (Gidley 1978) respectively.

I·3 Experimental Techniques

The study of positrons in matter is based on detection of the annihilation quanta. The relevant observables are the mean annihilation rate, the angle between the gammas, the energy, polarization and number of gammas. The most commonly used means of carrying out investigations of positrons are the lifetime, angular correlation and doppler broadening techniques (West 1973).

I·3·1 Lifetime Technique

^{22}Na sources are often used for measuring positron lifetimes because the decay positron is followed in most decays by the emission of a nuclear gamma of energy 1274 KeV within 10^{-11}s (see Figure I·2). The time delay between the nuclear gamma and the annihilation quanta can be measured with

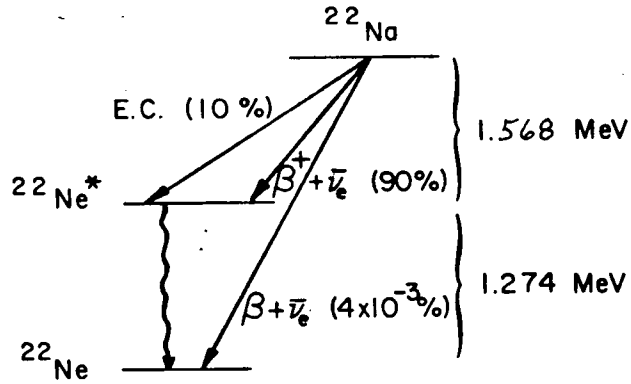

Figure I·2 Decay scheme for ^{22}Na .

scintillation detectors. Small plastic scintillators (2cm long x 2cm diameter) provide excellent timing resolution (2.5×10^{-10} s) but suffer from poor efficiency and energy

resolution. They are essential when studying short lifetimes in solids and liquids. The relatively long lifetime of o-Ps in gases and powders may be studied using larger NaI detectors which have much better energy resolution and efficiency, although the timing resolution (4 to 5 x 10^{-9} s) is not as good as may be achieved with plastic scintillators.

I·3·2 Angular Correlation

The angle between two photons from e^+e^- (s=0) annihilation is given as

$$\theta = p_\perp / m_o c \quad p_\perp \ll m_o c$$ (West, 1973) Equation I·1

where $p_\perp$ is the pair momentum component perpendicular to direction of emission and m_0 is the electron rest mass. The angular distribution between the annihilation quanta can be measured using a long slit angular correlation apparatus which measures the coincidence counting rate between two detectors as a function of angle defined by detector 1, the positron source, and detector 2. A typical angular resolution is 0.5 mrad. The decay of mean thermalized p-Ps contributes a narrow component to the angular distribution of the annihilation quanta since the pair momentum (of order $(kT2m)^{\frac{1}{2}}$)is small in comparison to annihilations involving high momentum valence electrons.

I·3·3 Doppler Broadening

Information on the pair momentum distribution can also be obtained by using a high resolution Ge or Ge-Li gamma detector to measure the Doppler broadening of the annihilation line at 511 KeV. In first order the shift in energy

$$\Delta E = h\nu - m_o c^2 \sim p_{11} c/2$$ (Hotz, 1968) Equation I·2

where $h\nu$ is the energy of the detected gamma and p_{11} is the component of pair momentum along the direction of emission. The Doppler broadening technique analyzes all momentum channels simultaneously and is therefore much faster and does not require high e^+ stopping densities nor strong sources as does the angular correlation technique. However the resolution of present day detectors is limited to around 1 KeV at 511 KeV.

I·4 Quenching of o-Ps in Matter

The properties of o-Ps are significantly altered in the presence of matter. The decay rate of o-Ps in matter can be expressed $\lambda=\lambda_0+\lambda_q$ where λ_0 is the free decay rate and λ_q is the quenching rate associated with the medium, due primarily to spin conversion and/or pickoff. Spin conversion is when o-Ps is converted to p-Ps via a spin exchange interaction with paramagnetic species such as H, NO, and O_2. This is covered in more detail in Appendix II. In short, collisions involving o-Ps and a paramagnetic molecule do not conserve the z component of spin of the electron on Ps and thus o-Ps-->p-Ps conversion is possible. Pickoff quenching occurs when the positron in o-Ps

annihilates with a valence electron from the host. These two quenching processes are easily distinguishable using angular correlation or doppler broadening. Spin conversion to p-Ps results in a narrow pair momentum distribution determined by the thermal motion of the p-Ps atom. In contrast, pickoff annihilation with a valence electron from the host results in a relatively broad pair momentum distribution, determined primarily by the high momentum of the valence electron. For example the mechanism for quenching of o-Ps by O_2 in silica gel (Chuang 1974)and silica powder (Kiefl 1978)moderators has been determined to be spin conversion as opposed pickoff annihilation resulting from a chemical reaction.

CHAPTER II : POSITRONIUM IN SiO_2 POWDER

Positron lifetime spectra in oxide powders exhibit three components (Brandt 1968). A very fast (< 1 ns) component is due to p-Ps and free e^+ decay(while slowing down or thermalized). A second 2-3 ns component is attributed to pickoff annihilation of o-Ps within the powder grains and the longest lived component (~140 ns) is thought due to o-Ps in the void regions of the powder.

In this chapter the formation, thermalization, and quenching of o-Ps in SiO_2 powder with and without O_2 are discussed. This is relevent to experimental results in Chapter III on the conversion quenching of o-Ps with O_2 in an SiO_2 moderator.

II·1 Ps Formation

There are at least three models that may be used to explain Ps formation in oxide powders---- the Ore gap model, the spur model, and the surface formation model. These models are not very useful in making quantitative predictions of the Ps fraction, especially in such a complex medium as a powder. The purpose of stating them here is simply to provide a qualitative understanding of the various processes which may lead to Ps formation.

According to the Ore gap model (Ore 1949b), first proposed for gases and and then extended to molecular solids (Wallace 1960), Ps formation occurs epithermally via charge exchange with

atom (or molecule) A

$$e^+ + A \rightarrow Ps + A^+ \qquad \text{Equation II·1}$$

in the energy region $(E_{ion} - E_B) < E < E_{ex}$ (termed the Ore gap) where E_{ion} is the ionization energy of atom, E_{ex} is the first excitation energy, and E_B (6.8eV) is the binding energy of Ps. Below $E_{ion} - E_B$, Ps formation is energetically forbidden and above E_{ex} excitation and ionization are thought to dominate the dE/dx.

In the spur model (Mogensen 1974) a thermalized e^+ is attracted to, and eventually combines with, a free electron from its own radiation track (composed of small branches called spurs). This model has been particularly successful in explaining experimental results in liquids.

In the surface formation model positrons capture an electron at the surface where it may be energetically favourable. Such surface formation has been observed with low energy positrons incident on metal or oxide coated metal surfaces (Canter 1974). Previous to these results Brandt had proposed on the basis of positron lifetime spectra in SiO_2, MgO and Al_2O_3 powders that o-Ps is formed within the powder grains and then diffuses to the surface where it is ejected into the voids, presumably because of a negative work function at the surface (Brandt 1968). The evidence presented for this ambient temperature thermal diffusion (ATTD) model is that the 2-3 ns component (attributed to o-Ps inside the powder grains) increases at the expense of the 140 ns component (attributed to o-Ps in the voids) as the temperature is lowered or the particle

size increases. However the lifetime spectra may also be consistent with surface formation so that the role of surfaces in Ps formation in oxide powders remains unclear.

II·2 Ps Thermalization in SiO_2 Powder

Whether it formed at the surface or in the bulk the o-Ps appears to be ejected from the oxide surface with a kinetic energy of order 1eV (Ford 1976). For example the kinetic energy of o-Ps ejected from MgO powder has been measured to be 0.25 ± 0.10 eV (Curry 1971). The Ps atom is very light, so that the mean energy loss per collision with the oxide surface is much smaller than for a heavier atom such as Mu. In a purely classical estimate, in which the Ps imparts momentum to individual surface atoms, Ford (1976) estimates the thermalization time in lightly packed SiO_2 powder to be ~140 ns. A slightly more rigorous treatment of the problem employing the one dimensional Devonshire quantum theory of gas-surface interaction is developed in Appendix I. We find that in SiO_2 powder (35 Å radius, density of 0.056 gcm^{-3}) at 121°K the calculation yields ~30 ns for Ps of 1eV to reach 0.0125eV (145°K) with most of that time (25 ns) spent below 0.03eV. This calculation uses the Debye temperature of bulk SiO_2 (470°K) (Zemansky 1968) and a purely repulsive Morse potential at the surface with range parameter $a=0.5$ $Å^{-1}$. The result is not sensitive to the potential parameters and agrees roughly with the purely classical estimate of Ford (1976).

It should be pointed out that it is assumed in these calculations that the Ps atom samples the entire surface area

with equal probability. It does not take into account the aggregate structure of the powder which may have drastic effects on the mean free path and thermalization time. Thus the above result must be considered a lower limit on the thermalization time. In fact the experimental results presented in Chapter III indicate that the Ps has a thermalization time much larger than this in SiO_2 powder below 450 K.

II·3 Effect of O_2 on Ps Thermalization

O_2 introduced into the void regions of a powder should tend to decrease the thermalization time. Low energy o-Ps (< 5eV) may lose energy through collisions with O_2 via elastic scattering, hyperfine transitions, rotational excitation and vibrational excitation. However, we find that below ~0.03 eV the major contribution is from elastic scattering which most likely is insufficient to cause thermalization at low O_2 densities (less than 10^{-19} cm^{-3}).

II·3·1 Vibrational Excitation

The energy loss rate of Ps due to vibrational excitation can be written

$$\left(\frac{dE}{dt}\right)_{vib} = n v \sum_{\nu\nu'} P_\nu \sigma_{\nu\nu'} \Delta E_{\nu\nu'} \qquad \text{Equation II·2}$$

where n is the O_2 concentration, v is the Ps velocity, $\sigma_{\nu\nu'}$ is the cross section for scattering from vibrational state ν to ν', $\Delta E_{\nu\nu'} = E_{\nu'} - E_\nu$ is the energy difference between states and $P_\nu = e^{-E_\nu/kT} / \sum_{\nu''} e^{-E_{\nu''}/kT}$ is the probability that

vibrational state ν is occupied. The energy of vibrational state ν is approximately

$$E_\nu = A_\nu (\nu + \tfrac{1}{2}) hc \qquad \text{Equation II·3}$$

where A_ν = 1580 cm^{-1} for O_2 molecules (Levine 1975). At room temperature $P_0 \sim 1$ and Equation II·2 can be simplified to

$$\left(\frac{dE}{dt}\right)_{vib} = n v \sigma_{0\nu'} \Delta E_{0\nu'} \qquad \text{Equation II·4}$$

If it is assumed $\sigma_{01} \sim 10^{-16}$ cm^2 and $\sigma_{0\nu'} = 0$ for $\nu > 1$, then Ps of energy 1eV in O_2 gas at a density of 10^{19} cm^{-3} will lose energy at a rate of 4.8 KeV/ns. However, below the threshold energy (ΔE_{01} = .19eV) this channel is closed.

II·3·2 Rotational Excitation Below 0.19eV

Only odd rotational states of $^{16}O_2$ ($^3\Sigma_g^-$) are allowed as a consequence of the spatial symmetry of the electrons and permutation symmetry of the ^{16}O nuclei (Tinkham 1964). In first order (ignoring the effect of O_2 spin) the rotational energies are (Levine 1975):

$$E_j = B\, j(j+1) \qquad B = 1.44\ cm^{-1} \qquad \text{Equation II·5}$$

The rate of energy loss can be written

$$\left(\frac{dE}{dt}\right)_{rot} = n v \sum_{j\,j'} P_j \sigma_{jj'} \Delta E_{jj'} \qquad \text{Equation II·6}$$

where $P_j = (2j+1) e^{-E_j/kT} \Big/ \sum_{j''} (2j''+1) e^{-E_{j''}/kT}$ is the probability that the O_2 molecule is in rotational state j (ν = 0), $\sigma_{jj'}$ is the scattering cross section for j --> j′ transitions and $\Delta E_{jj'}$

is the energy loss (gain) per transition.

A rough estimate on $dE/dt)_{rot}$ for Ps of energy 0.1eV in O_2 at 300°K can be made by assuming $P_7 = 1$ (since j = 7 is the most likely occupied state at 300 °K) and $\sigma_{7,9} = 10^{-16}$ cm² (with all other $\sigma_{jj'} = 0$). The estimate yields dE/dt ~ 0.6eV/ns. The threshold for pure rotational excitation (ΔE_{13}) is ~0.014eV. However, it is severely inhibited at energies below ~0.03eV because of the s wave nature of low energy Ps scattering coupled with total angular momentum conservation (see Section AII.9)

II·3·3 Oxygen Hyperfine Transitions Below 0.03eV

Even when rotational excitation is prohibited, the Ps may lose energy inelastically through hyperfine transitions between the states of total angular momentum J = j + s where s is the O_2 spin and j is the rotational angular momentum of the molecule. The splitting between J states corresponding to the same j is 2.5×10^{-4}eV and only weakly dependent on j (Townes 1955). The rate of energy loss can be written

$$\frac{dE}{dt}\Big)_{hyp} = nv \sum_{JJj} P_{jJ}\, \sigma_{jJj'J}\, \Delta E_{jJj'J'} \qquad \text{Equation II·7}$$

In the approximation where total electron spin is conserved, JJ′ transitions at low energy must originate from spin exchange(or s_z changing collisions), since j, j_z and s are conserved (see Appendix II). A very crude estimate of the energy loss rate due to JJ′ transitions can be made by assuming the energies and cross sections are independent of j and that $\sigma_{JJ'} = \sigma_{J'J} = \sigma_{ex}$ (the spin exchange cross section for Ps scattering off O_2). Then it

follows:

$$\left(\frac{dE}{dt}\right)_{hyp} \sim n v \left[1 - e^{-\Delta E/kT}\right] \Delta E \, \sigma_{ex} \qquad \text{Equation II·8}$$

Substituting $n = 10^{19} cm^{-3}$, $\sigma_{ex} = 4 \times 10^{-19}$ cm^2 (the spin exchange cross-section defined as $(28/7)\sigma_c$ (See Equation AII.20) where σ_c is the measured spin conversion cross section (Klobuchar 1980)), T = 300°K, and $\Delta E = 2.5 \times 10^{-4}$eV yields $(dE/dt)_{hyp} \sim 10^{-7}$ eV/ns. Thus it can be neglected in comparison to the rate of energy loss due to surface collisions.

II·3·4 Elastic Scattering

The energy loss rate due to elastic s wave scattering at incident energy E can be written (Mobley 1967)

$$\left(\frac{dE}{dt}\right)_{el} = \sigma_{el} n v \, 2Em/M \qquad \text{Equation II·9}$$

where σ_{el} is the elastic s wave scattering cross section and 2Em/M is the mean energy loss per collision for Ps of mass n scattering off O_2 of mass M. There is considerable uncertainty in the value chosen for σ_{el} since the scattering at low energies involves only one partial wave (see Appenix II). Thus the elastic cross section can vary tremendously depending upon only the s-wave electron spin quartet and doublet phase shifts(see Appendix II). For example the spin conversion cross section is only 10^{-19} cm^2 -- about four orders of magnitude smaller the phyical cross section. However for the purpose of illustration we chose $\sigma_{el} = 10^{-16}$ cm^2 and $n = 10^{19}$ cm^{-3}. One then finds $(dE/dt)_{el} \sim 1.5 \times 10^{-5}$ eV/ns which is the largest contribution to

the energy loss rate due to O_2 but considerably smaller than the energy loss rate due to the SiO_2 powder.

II·3·5 Conclusion

The presence of O_2 gas decreases the time required to reach ~ 0.03eV due to inelastic scattering processes, but has likely has little effect at lower energies where s wave elastic scattering dominates (provided the elastic cross section is not much greater than 10^{-16} cm^2). Since the "thermalization" time in SiO_2 powder at 121°K is primarily due to scattering below 0.03eV it is unlikely that the presence of O_2 has a substantial effect on this time.

II·4 Quenching of o-Ps in SiO_2 Powder

Consider an ensemble of o-Ps in a powder at temperature T with surface area A and free volume $V_F \equiv (V - V_{solid})$. In the most general case, there exist both bound (binding energy B) and free states. Let λ_F and λ_B be the annihilation rates for o-Ps in the bound and free states. These can be written

$$\lambda_F = \nu_c P_a + \lambda_o$$

$$\lambda_B = \lambda_P + \lambda_o \qquad \text{Equation II·10}$$

where ν_c is the collision frequency with the surface, P_a is the probability for pickoff annihilation per collision, λ_P is the pickoff rate from the bound state, and λ_o is the free annihilation rate (7.056 μs^{-1}). The bound state quenching rate, λ_P, can be estimated from the lifetime of o-Ps adsorbed on

surfaces of silica gel. The observed lifetime of 30 ns (Chuang 1973)at 300°K corresponds to a quenching rate of $\lambda_q \sim 26\ \mu s^{-1}$. P_a can be estimated from the o-Ps quenching in Ar gas (due to pickoff) as

$$P_a = \sigma_p / \sigma$$

Equation II·11

where σ_p is the cross section for pickoff annihilation (1.3×10^{-5} Å^2) (Celitans 1964) and σ is the area of an Ar atom over which the electron density is appreciable (assumed to be 10 Å^2). In completely dispersed SiO_2 powder at 300°K (35 Å radius, density = 0.056 g cm^{-3}) where the entire surface area is equally accessable to the Ps, $\nu_c = 6 \times 10^{-11}$s (according to Equation AI.24). This yields $\nu_c P_a$ of order 0.8 μs^{-1} but must be considered an upper limit on since clumping of the powder grains into aggregates may increase the mean free path and decrease ν_c. This possibility will be discussed further in Chapter III.

The form of the o-Ps lifetime spectrum depends on how $\lambda_B \bar{t}$ compares with unity, where $\bar{t}$ is the mean surface dwell time, evaluated in Appendix IV. If the surface bound Ps behaves as a 2 dimensional gas then $\bar{t}$ can be written:

$$\bar{t} = \frac{4\Lambda e^{B/kT}}{P_t v}$$

Equation II·12

where Λ is the thermal wavelength of the o-Ps, v is the mean o-Ps velocity, and P_t is sticking probability on the surface. The two limiting cases $\lambda_B \bar{t} >> 1$ and $\lambda_B \bar{t} << 1$ can easily be evaluated, whereas the intermediate case $\lambda_B \bar{t} \sim 1$ is more complicated and will in general not yield a decay spectrum which is tractable.

II·4·1 Special Case $\lambda_B \bar{t} << 1$ (Adiabatic Approximation)

This is the only possibility considered in the literature (Ford 1976). It implies that the Ps adsorbs and desorbs many times before decay, leading to a single exponential decay spectrum. The decay rate λ_A is then an average of λ_B and λ_F weighted by the fraction of time spent in each state.

$$\lambda_A = \alpha \lambda_B + (1-\alpha) \lambda_F \qquad \text{Equation II·13}$$

where α is the fraction of time spent in the bound state. In thermal equilibrium α can be expressed (according to Equation AIV.15):

$$\alpha = \frac{1}{1 + e^{-\epsilon_0/kT} V_F / A\Lambda} \qquad \text{Equation II·14}$$

II·4·2 Special Case $\lambda_B \bar{t} >> 1$ (Strong Collision Approximation)

This case has not been considered previously, but the ensuing rate equations are well known from the trapping model for positrons in metals (Brandt 1967). The assumption $\lambda_B \bar{t} >> 1$ implies there is no desorbing from the surface before decay and this leads to a decay spectrum which is a sum or difference of two exponentials. This can be seen as follows.

Define $n_F(t)$ and $n_B(t)$ to be the number of o-Ps atoms in the free and bound states respectively. The trapping rate on the surface can be written $\nu_c P_t$, where ν_c is the collision rate with the surface and P_t is the probability for trapping (or

adsorption) per collision. It is assumed that the coupling between a light atom such as Ps and the phonons at the surface is weak so that $P_t << 1$. This corresponds to trapping which is transition rate rather than diffusion rate limited. n_F and n_B then satisfy the following rate equations.

$$\dot{n}_F = -\lambda_F n_F - \nu_c P_t n_F \qquad \text{Equation II·15}$$

$$\dot{n}_B = -\lambda_B n_B + \nu_c P_t n_F \qquad \text{Equation II·16}$$

The initial conditions $n_F(t=0) = n_0$ and $n_B(t=0) = 0$ lead to solutions

$$n_F(t) = n_0 e^{-(\lambda_F + \nu_c P_t)t} \qquad \text{Equation II·17}$$

$$n_B(t) = \frac{\nu_c P_t n_0}{\lambda_F - \lambda_B + P_t \nu_c}\left[e^{-\lambda_B t} - e^{-(\lambda_F + \nu_c P_t)t}\right] \qquad \text{Equation II·18}$$

The decay spectrum will then be of the form

$$n(t) = n_0\left\{\frac{\nu_c P_t}{\lambda_F - \lambda_B + \nu_c P_t} e^{-\lambda_B t} + \left[1 - \frac{\nu_c P_t}{\lambda_F - \lambda_B + \nu_c P_t}\right] e^{-(\lambda_F + P_t \nu_c)t}\right\} \qquad \text{Equation II·19}$$

This is the familiar two component solution derived by Brandt (1967) for positron trapping in defects, except that in this case $\lambda_B > \lambda_F + \nu_c P_t$ leads to a difference of exponentials rather than a sum.

In highly dispersed powders where $\nu_c P_t << |\lambda_B - \lambda_F|$

$$n(t) \sim n_0 e^{-[\nu_c P_t + \lambda_F]t}$$
$$= n_0 e^{-[\nu_c (P_t + P_a) + \lambda_0]t}$$

Equation II·20

Alternatively in highly compacted powders such as silica gel where $\nu_c P_t >> |\lambda_B - \lambda_F|$

$$n(t) \sim n_0 e^{-\lambda_B t}$$

Equation II·21

The assumption $\lambda_B \bar{t} >> 1$ and the consequences discussed above agree qualitatively with experiments on silica gel and SiO_2 powder. In light SiO_2 powder, the quenching rate of o-Ps is a linear function of ν_c (Gidley 1976) as given in Equation II·20, whereas in silica gel the quenching rate of o-Ps is independent of pore size (Chuang 1972) or equivalently, ν_c, as suggested by Equation II·21.

II·5 Effect of O_2 on the Quenching of o-Ps in SiO_2 Powder

O_2 molecules in the gas phase are paramagnetic, possessing two unpaired electrons. The conversion quenching of o-Ps with O_2 can be written

$$o\text{-}Ps + O_2 \rightarrow p\text{-}Ps_0 + O_2$$

Equation II·22

Since p-Ps has a lifetime of only 0.125 ns, spin conversion quenching is easily observable in the lifetime spectrum. At low energy, the o-Ps --> p-Ps conversion cross section can be written (see Appendix II)

$$\sigma_c = \frac{8}{27}\frac{\pi}{k^2}\sin^2\left[\delta_0^{3/2} - \delta_0^{\frac{1}{2}}\right]$$

Equation II·23

where δ_o^S is the scattering phase shift for total electron spin S and orbital angular momentum 0, independent of the rotational state of the molecule. The most recent room temperature value of σ_c is $1.0 \pm 0.1 \times 10^{-19}$ cm^2 (Klobuchar 1980). The pickoff cross section with O_2 is of order 10^{-21} cm^2 (estimated from quenching in pure N_2 gas, Celitans 1964) and can thus be neglected in comparison with spin conversion cross section.

When O_2 gas is admitted into SiO_2 powder, a certain fraction will adsorb onto the surface. The adsorption of O_2 on SiO_2 surfaces has been studied previously. The binding energy is roughly 1100°K estimated from a BET (Brunauer-Emmett-Teller) plot (Brunauer 1938) of the adsorption data. ESR data of H atoms on the SiO_2 surface in the presence of adsorbed O_2 indicate that the O_2 remains paramagnetic on such a surface at temperatures at least as low as 100°K (Surin 1973). Furthermore, O_2 adsorbed onto the pores of silica gel at 300°K has been shown to be an effective conversion quenching agent of o-Ps (Chuang 1974).

Thus when O_2 gas is admitted into the voids of SiO_2, the free and bound annihilation rates of o-Ps must be modified from those given in Equation II·10 to

$$\lambda_F^{O_2} = \nu_c P_a + \nu_c \sigma_{sg}^c n_s + \sigma_{gg} n_g v_g + \lambda_o$$

Equation II·24

$$\lambda_B^{O_2} = \lambda_P + \nu_s \sigma_{ss}^c n_s + \frac{1}{4} n_g v_g^{O_2} \sigma_{gs}^c + \lambda_o$$

Equation II·25

where σ_{sg}^{c} is the conversion cross section of free o-Ps with adsorbed O_2 (surface density n_s), σ_{gg}^{c} is the conversion cross section for free o-Ps with free O_2 (gas density n_g), v_g is the velocity of free o-Ps, v_s is the 2 dimensional velocity of adsorbed o-Ps, σ_{ss}^{c} is the 2 dimensional conversion cross section for bound o-Ps with bound O_2 ($\sim\sigma_{gg}^{1/2}$), $v_g^{O_2}$ is the velocity of free O_2 and σ_{gs}^{c} is the conversion cross section for free O_2 with bound o-Ps. When n is much less than the monolayer coverage,

$$n_s \sim n_g \left(\frac{h^2}{2\pi kT}\right)^{1/2} e^{b/kT} \qquad \text{Equation II·26}$$

where b = 1100°K is the O_2 binding energy on SiO_2 (see Equation AIV·9). Equations II·13, II·20 and II·21 still hold as limiting cases. For example, in highly dispersed powders where $\lambda_B \bar{t} >> 1$ and $\nu_c P_t << |\lambda_B - \lambda_F|$ Equation II·20 yields

$$n(t) = n_o e^{-[\nu_c (P_a + P_t + \sigma_{sg}^{c} n_s) + \sigma_{gg}^{s} n_g v_g + \lambda_o] t}$$

Equation II·27

CHAPTER III : TEMPERATURE DEPENDENCE OF CONVERSION QUENCHING OF o-Ps BY O_2 IN SiO_2 POWDER

Conversion quenching of o-Ps by paramagnetic O_2 in gas moderators at 300°K has been well studied experimentally. [See for example (Klobuchar 1980)]. At 300°K the spin exchange cross section for o-Ps + O_2 (defined in Appendix II as 27/8 times the spin conversion cross section) is 2 x 10^3 times smaller than the spin exchange cross sections for Mu + O_2 (Fleming 1981a) and H + O_2 (Gordon 1981). The o-Ps spin exchange cross section with O_2 (4×10^{-19} cm^2) is considered to be be anomolously low in comparison with the physical cross section, being roughly 1000 times smaller. In fact, some early authors (Celitans 1964)were convinced that quenching was not due to spin exchange because it was so small. However, angular correlation measurements (Chuang 1974) and doppler broadening measurements (Kiefl 1978) discussed in Section I·4 provide clear evidence that the quenching by O_2 in the gas phase is dominated by spin conversion. The temperature dependence of the spin conversion rate may help improve our understanding of this very interesting isotope effect.

In this chapter a positron lifetime experiment is described in which the o-Ps + O_2 --> p-Ps + O_2 conversion rate has been measured from 121°K to 630°K using an SiO_2 powder moderator. The results are pertinent to both conversion quenching of o-Ps with O_2 and to the behaviour of o-Ps in SiO_2 powder.

III·1 Experimental

A 3 μCi ^{22}Na positron source, prepared from a NaCl solution, was dried and sandwiched between 1 μm nickel foil. The source was embedded in SiO_2 powder (mean particle radius 35Å and density 0.056 gcm^{-3}), sealed with a copper o-ring in a welded stainless steel vacuum chamber (Figure III·1) and outgassed at 10^{-5} torr for a period of 12 hours. This removes most of the adsorbed H_2O from the surface (Cabot).

Provisions were made to input extra dry grade O_2 gas (99.65% O_2, 0.03% Ar, 0.05% N_2, 2 ppm CO_2, 20 ppm hydrocarbons) via a gas handling system constructed from 1/4 inch stainless steel tubing and stainless steel bellows valves. The O_2 pressure within the vacuum chamber was measured with a Matheson absolute pressure gauge accurate to ±5 torr.

Two copper constantan thermocouples, inserted in stainless steel wells (see Figure III·1), were used to monitor the temperature and its uniformity (±2°K over the chamber volume). The temperature was controlled to within ±2°K over the range of study (121°K to 630°K). The target chamber was cooled below 300°K by circulating cold N_2 gas around the vessel held in a styrofoam cryostat, whereas higher temperatures were achieved with heating tape.

The positron lifetime measurements were made at TRIUMF using the μ^+SR data acquisition system (see Section VI·1·2). The time delay between the nuclear gamma (1274 KeV) from ^{22}Na (see Section I·3·1) and the subsequent positron annihilation radiation was measured with two 4 inch diameter by 4 inch long NaI detectors using a standard fast-slow coincidence circuit

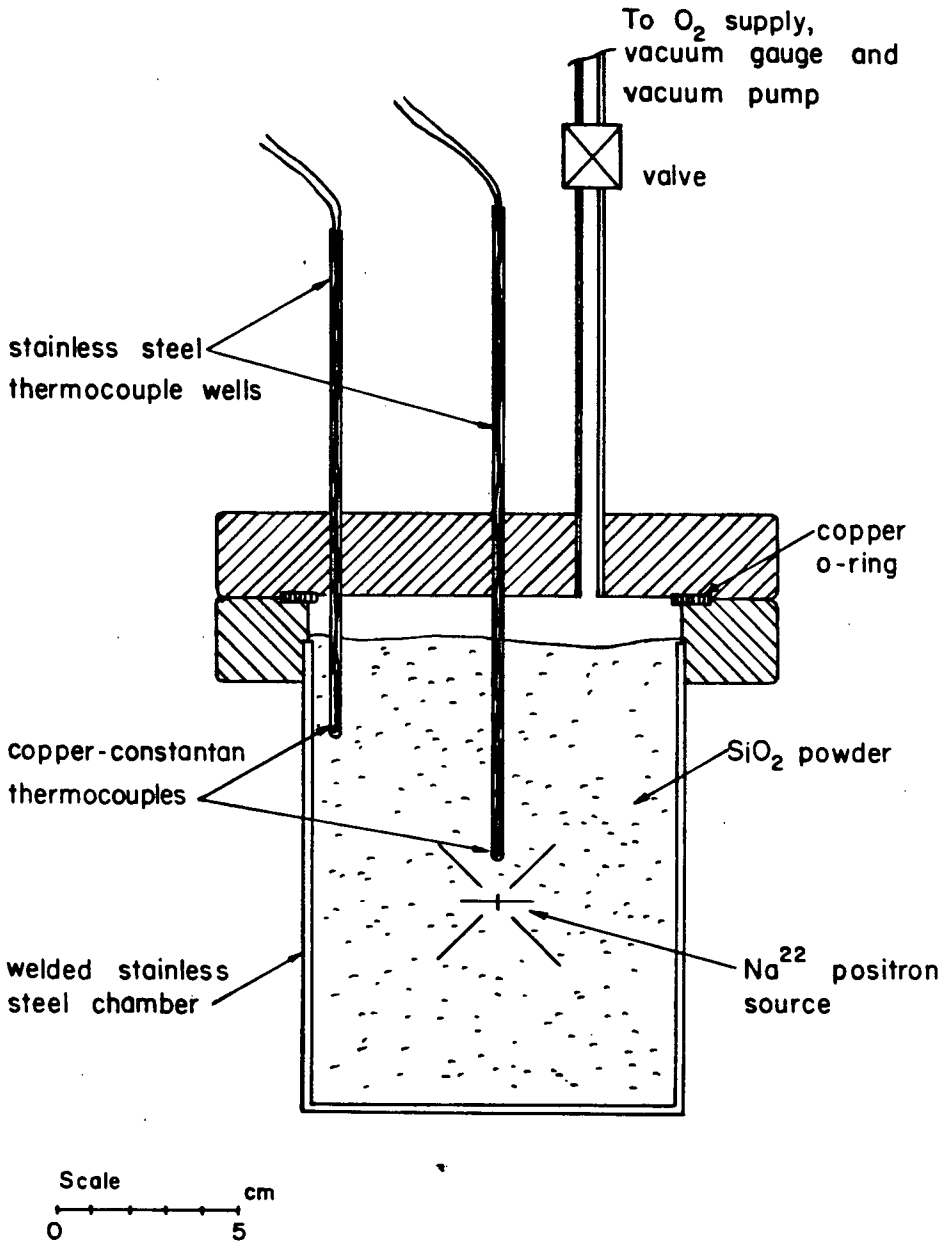

Figure III·1 Apparatus for measuring o-Ps lifetime in SiO_2 powder in an O_2 atmosphere.

(see Figure III·2). Timing information was obtained from the anode output via constant fraction discrimination, whereas energy (pulse height) information was derived from the dynode output by passing the pulse through a spectroscopy amplifier and single channel analyzer. The energy resolution of these

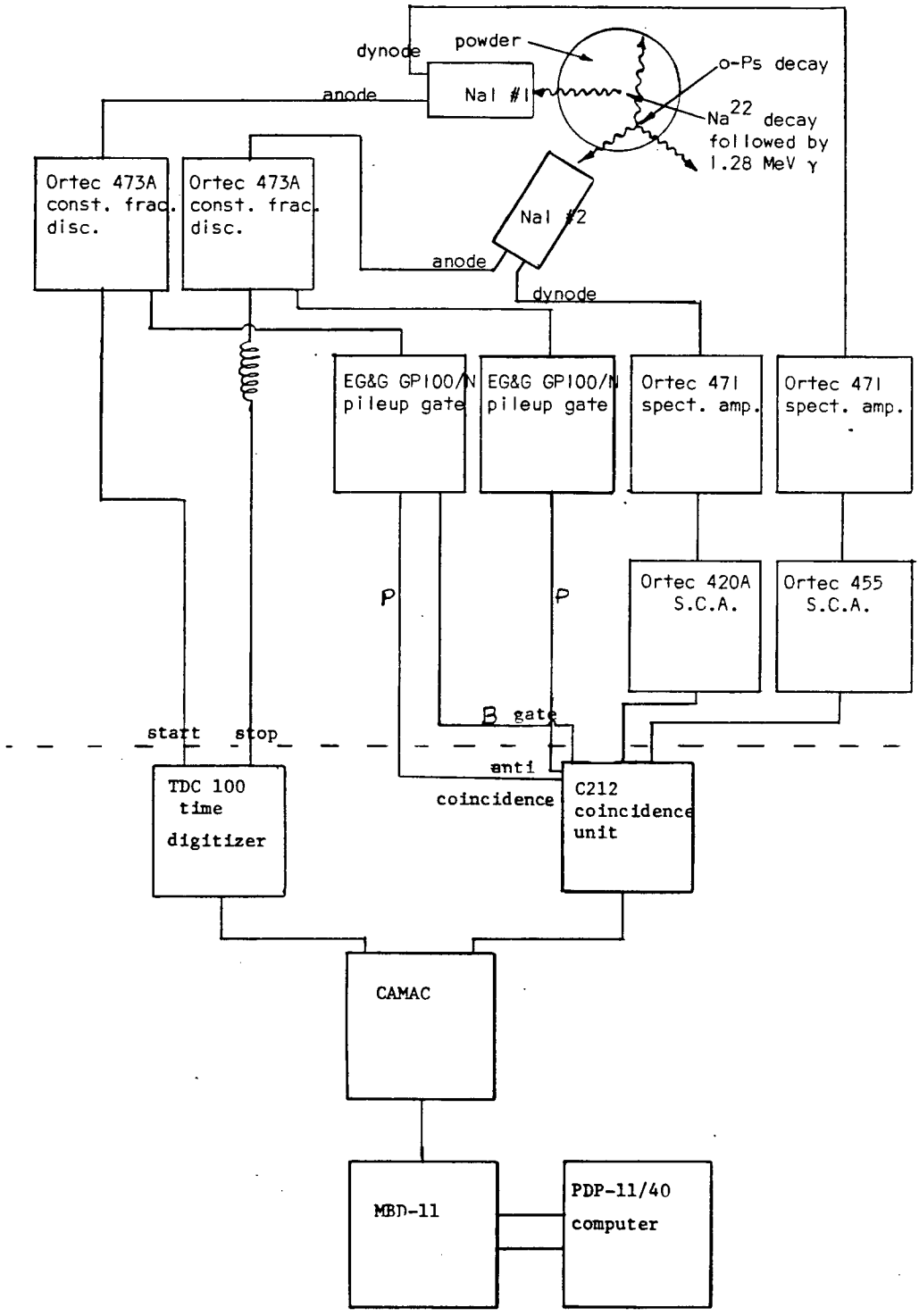

Figure III·2 Electronics and data acquisition system for measuring o-Ps lifetimes.

detectors was 14% FWHM at 1274 KeV. A good event consisted of a single start pulse consistent with a 1274 KeV γ ray and a single

stop pulse in the energy window 400 to 450 KeV, both within a 2 μs gate. The time interval between the start and stop pulses was digitized with an EG&G TDC100 clock. The overall timing resolution was 5 ns FWHM as determined with a ^{60}Co source (which produces two virtually simultaneous γ rays at 1170 and 1330 KeV). The energy window for a good stop was chosen below the 511 KeV photopeak (due to 2γ annihilation) in order to increase the sensitivity to o-Ps decay which has a continuous annihilation spectrum by virtue of its 3γ decay (see Figure I·1). However, due to the poor energy resolution of these detectors and the Compton scattering of 511 keV gammas, the stop detector was still sensitive to some 2 gamma annihilations.

III·2 Procedure and Results

Lifetime spectra consisting of 100,000 events were collected for at least five O_2 pressures at each temperature. Figures III·3 (a) & (b) show the effect of O_2 on the lifetime spectrum of o-Ps in SiO_2 powder. The prompt annihilation is due to free e^+, p-Ps and o-Ps within the powder grains, whereas the long lived component is due to o-Ps in the void regions of the powder. Good fits were obtained assuming a single exponential decay rate

$$N(t) = N_0 e^{-\lambda t} + Bg \qquad \text{Equation III·1}$$

over the fitting range 30-500 ns, where N_0 is the normalization, λ is the o-Ps decay rate, and Bg is a time independent background. Figure III·4 shows two sample plots of λ as a function of O_2 concentration (in the gas phase) determined from

(a)

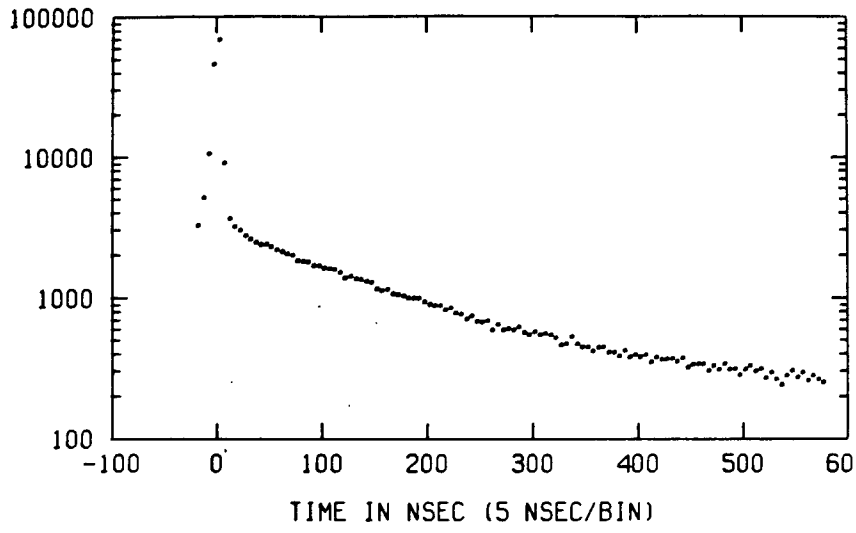

(b)

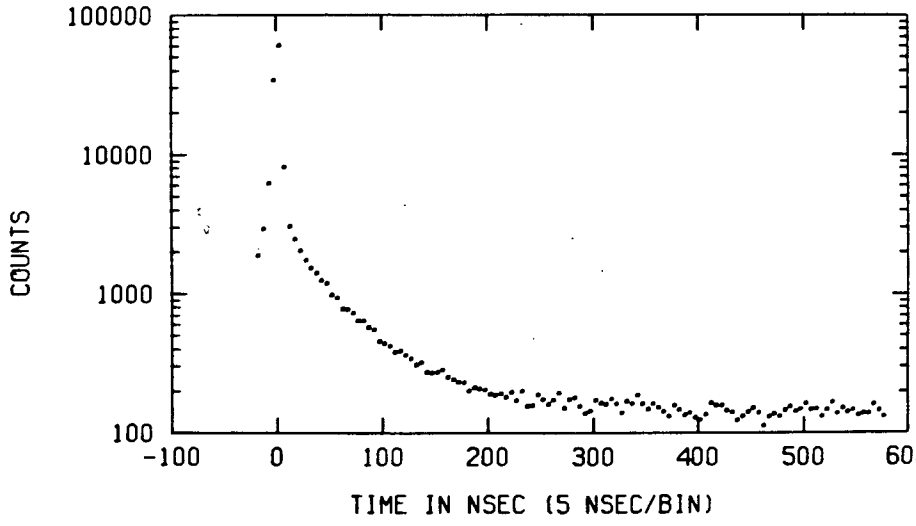

Figure III·3 (a) Positron lifetime spectrum in evacuated SiO_2 powder at 295 °K. (b) Same with O_2 gas density of $10^{19} cm^{-3}$.

the pressure. Good fits were obtained at all temperatues assuming a linear dependence. The slope of each line gives the total conversion rate constant k^c defined from

$$\lambda = k^c n_g + \lambda(n_g=0) \qquad \text{Equation III·2}$$

This rate constant k^c is plotted in Figure III·5 as a function

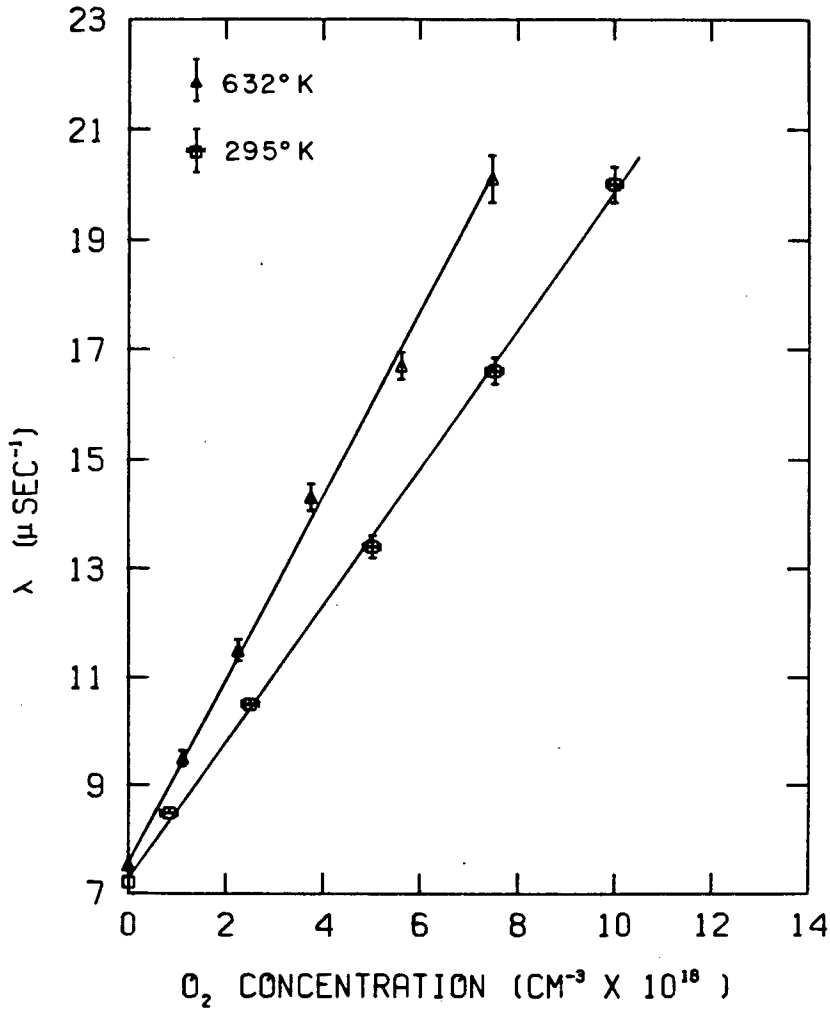

Figure III·4 Decay rate of o-Ps versus O_2 concentration (n_g) at 295°K and 632°K.

of temperature. The data points are given in Table III·1.

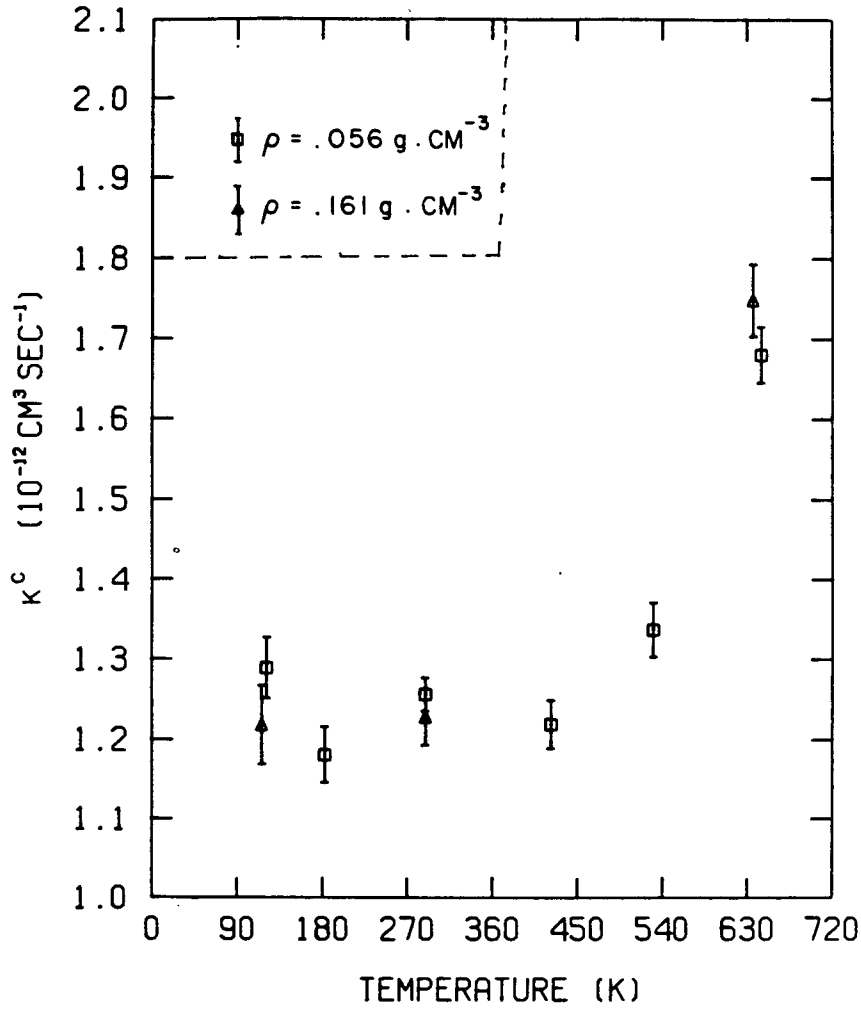

Figure III·5 Conversion rate constant versus temperature in an SiO_2 powder moderator. Note there is no observable dependence on powder density.

III·3 Discussion

It is clear from Figure III·5 that the rate constant, k^c, is independent of temperature below 450°K. This may seem surprising if one expects the adsorbed O_2 to play a role in the quenching since there is a large variation in adsorbed O_2 in the range 121 to 450°K. For example, at a gas density $n_g = 10^{19}$ cm^{-3}, the density of adsorbed O_2, (according to Equation II·26) varies from 2×10^{11} cm^{-2} at 450°K to 2.5×10^{14} cm^{-2} at 121°K. If one assumes that a o-Ps adsorbed on the surface behaves as a

Table III·1. O_2 Conversion Rate Constant Versus Temperature

Temperature (°K)±2	Conversion Rate Constant (10^{-12} cm^3 s^{-1})	Powder Density (g/cc)
645	1.68±0.04	0.056
636	1.75±0.05	0.161
530	1.34±0.04	0.056
422	1.22±0.05	0.056
290	1.26±0.05	0.056
290	1.23±0.04	0.161
183	1.18±0.04	0.056
121	1.29±0.05	0.056
116	1.22±0.05	0.161

2 dimensional gas atom with surface velocity $v_s = (\pi kT/2m)^{1/2}$ and that the 2 dimensional conversion cross section scales with the 3 dimensional conversion cross section ($\sigma^c_{ss} \sim \sigma^{c\,\frac{1}{2}}_{gg}$), then the above O_2 surface concentrations correspond to $\lambda_B(\sigma_{ss} v_s n_s)$ of order $10^2\ \mu s^{-1}$ and $10^5\ \mu s^{-1}$ at 450°K and 121°K respectively. The observed quenching rate at $n_g = 10^{19}$ cm^{-3} is only 13 μs^{-1} and independent of temperature.

However, the data are totally consistent with the "strong collision" model assumptions $\lambda_B \bar{t} >> 1$ and $\nu_c P_t << |\lambda_B - \lambda_F|$, described in Section II·5, which lead to a single exponential decay rate

$$\lambda = \sigma^c_{gg} v_g n_g + \sigma^c_{sg} \nu_c n_s + \nu_c (P_t + P_a) + \lambda_o$$

$$= \left[\sigma^c_{gg} v_g + \sigma^c_{sg} \nu_c \left(\frac{h^2}{2\pi kT}\right)^{\frac{1}{2}} e^{b/kT}\right] n_g + \nu_c (P_t + P_a) + \lambda_o$$

Equation III·3

Note that in this limiting case λ is linearly dependent on n_g at low surface coverage and independent of λ_B(the bound state

annihilation rate), as observed. The essential point is that λ_B is sufficiently large that once the o-Ps is adsorbed on the surface it is lost from the Ps ensemble, independent of precisely how large λ_B is.

The third term in Equation III·3, $\nu_c (P_q + P_t)$, due to quenching by the SiO_2 alone, is much less than 1 μs^{-1}, since the decay rate with no O_2 is close to the free decay rate at all temperatures (see for example Figure III.4). The first term ($\sigma^c_{gg} v_g n_g$) is the conversion rate in the gas phase, whereas the second term ($\sigma^c_{sg} \nu_c n_s$) is the conversion rate due to free o-Ps colliding with adsorbed O_2. The total conversion rate constant, k^c, (the term in square brackets) was observed to be independent of powder density for the two densities studied (0.056 gcm^{-3} and 0.161 gcm^{-3}). Since ν_c differs in these two powders by a factor of approximately 2.5 (see Appendix I), this implies that the conversion rate of unbound o-Ps by gas phase O_2 is much larger than the conversion rate of unbound o-Ps by adsorbed O_2 (i.e.: $\sigma^c_{sg} \nu_c n_s << \sigma^c_{gg} v_g n_g$). If one sets $\sigma^c_{sg} \sim \sigma^c_{gg}$ then at 121°K this reduces to

$$d >> n_s / n_g = 2.5 \times 10^{-5} cm$$

Equation III·4

where $d = v_g / \nu_c$ is the mean free path between surface collisions. While not in accord with $d = 0.6 \times 10^{-5}$ cm, calculated from Equation AI·24 in Appendix I for the higher density powder, the above limit is still quite reasonable since Equation AI·24 is based on the assumption of spherical particles evenly distributed in space, and therefore represents only a lower limit on d.

III·3·1 Thermalization

There are at least two factors which indicate that the o-Ps is not thermalized below 450°K.

1. The rate constant $k^c \sim \sigma_{gg}^c v_g$ is independent of T below 450°K. This is easily explained if v does not change below 450°K. The alternative explanation is that σ_{gg}^c varies as $1/(T)^{1/2}$ below 450°K. There is no theoretical justification for this. Calculations of the spin conversion cross section of o-Ps by H atoms (Hara 1975)indicate that the conversion cross section is only weakly dependent on energy below thermal energies. This would give rise to a conversion rate constant proportional to $(T)^{1/2}$ if the o-Ps is thermalized.

2. The rate constant $\sigma_{gg}^c v_g$ at 300°K ($1.2 \pm 0.1 \times 10^{-12}$ cm^3s^{-1}) is substantially higher than the rate constant of $0.8 \pm 0.1 \times 10^{-12}$ cm^3s^{-1} measured at 300°K in an Ar moderator. It is worth pointing out that the spin exchange cross section of $Mu+O_2$ is the same in Ar gas and powder moderators (Marshall 1978). In these experiments the Mu is known to be thermalized (see Section V·2).

A possible explanation of why the o-Ps may not thermalize as indicated in Section II·2 has to do with the assumption that the entire surface area is equally accessible to the Ps. According to the manufacturer (Cabot), the primary particles (35Å radius spheres) are fused irreversibly into large aggregrate structures with dimensions as large as 20000Å. These aggregrate structures are mechanically entangled into agglomerates, which support the large free volume associated with the powder. A very light atom such as Ps has a thermal wavelength of 60Å at 450°K, which is of the same order as the spacing of the primary particles in the aggregrates. It is conceivable that at lower temperatures the Ps scatters primarily off the surfaces of the aggregrates, thus increasing the mean free path and thus the thermalization time by a large factor

($\sim 10^2$ or more). This large increase in the mean free path could also help explain the independence of the rate constant on powder density. One implication of this hypothesis is that the observed quenching rate in evacuated SiO_2 is not purely due to pickoff annihilation as previously suggested (Ford 1976), since decreasing ν_c by a factor of 100 implies this rate is only of order 0.008 μs^{-1} (see Section II·4). The observed quenching rate would then correspond primarily to the trapping rate on the surface (see Equation II·20). This might be tested at low temperatures by depositing a film of He on the surface. This would most likely eliminate the possibility of trapping since Ps is not likely bound to such a surface. Such a medium might be ideal for determining the vacuum decay rate of o-Ps, a subject of great interest since it provides a test of quantum electrodynamics.

III·3·2 Anomolous Spin Exchange in o-Ps + O_2 Scattering

At low energy, the spin exchange cross section of o-Ps off a 2 electron molecule can be written (see Appendix II)

$$\sigma_{ex} = \frac{\pi}{k^2} \sin^2 [\, \delta_0^{3/2} - \delta_0^{1/2} \,] \qquad \text{Equation III·5}$$

where $\delta_0^{3/2}$ and $\delta_0^{1/2}$ are the spin quartet and spin doublet phase shifts for elastic s wave scattering off the isotropic part of the molecule-atom interaction and independent of the molecular rotational state. The small spin exchange cross section for Ps + O_2 compared with the physical cross section and those of Mu + O_2 and H + O_2 at 300°K can be explained qualitively as follows. In

the case of Mu + O_2 and H + O_2 at 300°K there are many partial waves which contribute to both elastic and inelastic scattering involving rotational excitation. In the case of Ps + O_2 at 300°K, these inelastic channels are closed along with any non-s-wave scattering. Thus only in the case of Ps + O_2 scattering does the spin exchange cross section depend on only two phase shifts. This may lead to a small spin exchange when $\delta_o^{3/2} - \delta_o^{1/2} \sim n\pi$. This is somewhat analogous to the Ramsauer Townsend effect in low energy positron (electron)-atom scattering, where a cancellation in the s wave contribution leads to a very small eleastic cross section.

The increase in the conversion rate constant above 450°K may partly be due to the increase in the mean thermal velocity. There is also indication that σ_{gg}^c increases with temperature. The room temperature value of σ_{gg}^c (1.0 ± 0.1 x 10^{-19} cm^2), obtained using an Ar moderator (Klobuchar 1980), is slightly lower than σ_{gg}^c at 540°K (1.3 ± 0.1 x 10^{-19} cm^2) and σ_{gg}^c at 630°K (1.5 ± 0.1 x 10^{-19} cm^2), obtained from the present data using an SiO_2 powder moderator. This increase in σ_{gg}^c could be the result of a small p-wave contribution expected at higher temperatures, or possibly a weakening of the interference between quartet and doublet s-wave scattering.

III·4 Summary and Conclusions

1. The conversion rate constant with O_2 in SiO_2 powder has been measured over the temperature range from 121°K to 630°K. Below 450°K, the conversion rate was observed to be independent of T. There are indications that the o-Ps does not thermalize at lower temperatures, possibly because of large mean free path resulting from clumping of the powder grains. The conversion cross section measured at 530°K and 630°K is slightly higher than previously measured at 300°K in gas moderators.
2. The anamolously low spin exchange cross section of o-Ps in O_2 is explainable in terms of the s-wave nature of low energy Ps scattering caused by the isotropic part of the Ps - O_2 interaction.

CHAPTER IV : MUONS, MUONIUM AND μ^+SR

Unlike the positron, the existence of the muon was not predicted theoretically. It was discovered in cosmic ray experiments (Anderson 1937, Street 1937) in a search for the pion, a particle predicted by Yukawa to explain the nuclear force. Muons can be considered heavy electrons, having a mass of 103 MeV/c^2, roughly 200 times that of an electron. They are spin 1/2 particles, and come in both positive and negative charges. As in the case of electrons, they do not participate in strong interactions. The magnetic moment of the muon is very close to $e\hbar/m_\mu c$, as predicted by the Dirac equation.

Muon decay was one of the first experiments to show that parity is violated in weak interactions (Garwin 1957, Friedman 1957). Not unexpectedly, the positive muon may capture an electron to form the H-like atom called muonium or Mu. The first observation of Mu was made by Hughes et al. (Hughes 1960). The properties of muons and Mu atoms are of tremendous importance in physics since they provide an almost ideal testing ground for electromagnetic and weak interaction theories (Hughes 1977).

The advent of the "meson factory" in the 1970's has revolutionized muon physics by providing intense beams of polarized muons for experimental study. Apart from its fundamental role in particle physics, the muon has become a useful probe in nuclear physics, solid state physics and physical chemistry. Negative muons can be used to probe nuclear structure because their atomic orbits overlap the nucleus. Positive muons have been employed primarily as magnetic probes

in solid state physics. The Mu atom (μ^+e^-) is of special interest in physical chemistry because it can be considered a light isotope of H, the muon having 1/9 the proton mass.

A description of the Muon Spin Rotation (μ^+SR) technique would be incomplete without first discussing the source of polarized muons and the properties of muon decay. These are briefly presented in the first two sections of this chapter. The μ^+SR technique is then explained with emphasis on the transverse field technique. The basic types of spin relaxation for Mu are then introduced. Finally, the form of the μ^+SR spectrum is derived.

IV·1 Source of Polarized Muons

Intense beams of medium energy protons (~100 μA at 500 MeV), incident on a suitable production target, are currently being used at meson facilities such as TRIUMF, SIN and LAMF as a source of π mesons -- the "nuclear glue" particles. The most common source of polarized muons is from weak decay of π's

$$\pi^+ \longrightarrow \mu^+ + \nu_\mu$$
$$\pi^- \longrightarrow \mu^- + \bar{\nu}_\mu$$

Equation IV·1

which have a free lifetime of 26 ns. The massless neutrino obeys a two component Weyl equation

$$-\bar{\sigma}\cdot\bar{p}\,|\nu_\mu\rangle = |\bar{p}|c\,|\nu_\mu\rangle$$
$$\bar{\sigma}\cdot\bar{p}\,|\bar{\nu}_\mu\rangle = |\bar{p}|c\,|\bar{\nu}_\mu\rangle$$

Equation IV·2

and is thus an helicity eigenstate. Conservation of energy,

total angular momentum, and linear momentum require that the $\mu^{\pm}$ is an helicity eigenstate and monoenergetic at 4.2 MeV in the rest frame of the $\pi^{\pm}$. A secondary beamline, consisting of large dipole magnets(for momentum selection) and quadrupole magnets (for focussing), is used to transmit charged particles from the production target to the experimental area. The muon helicity remains virtually unchanged during passage through this beamline since the cyclotron frequency for a muon in a magnetic field of strength B ($qB/(m_{\mu}c)$) and the precession frequency ($qg_{\mu}B/(2m_{\mu}c)$) are almost the same ($g_{\mu} \sim 2$). The first stopping muon channels were designed to collect backward decaying muons from pions in flight. These types of channels result in a relatively high energy muon beam, ~50 MeV, with polarization ~0.8. Recently, it was discovered (Pifer 1976) that a flux of μ^{+} can be obtained from π^{+} decay on or near the surface of the production target. The technique of producing highly polarized intense fluxes of these surface muons was subsequently developed and exploited at TRIUMF (Oram 1981). The muons have energy 4.2 MeV and are almost completely polarized because the pions are at rest in the lab frame. Surface muons are particularly useful in μ^{+}SR experiments because of their low energy and high polarization.

IV·2 Muon Decay

Muons decay via weak interaction into an electron and two neutrinos with a lifetime of 2199.4 ns (Wu 1966).

$$\mu^+ \rightarrow e^+ + \nu_e + \bar{\nu}_\mu$$
$$\mu^- \rightarrow e^- + \bar{\nu}_e + \nu_\mu \qquad \text{Equation IV·3}$$

The decay properties of muons are described well by a current-current interaction of the following form

$$H_I = \frac{g_\mu}{2^{\frac{1}{2}}}\left[\bar{\Psi}_{\nu_\mu}\gamma^\rho(1-\gamma_5)\Psi_\mu\right]\left[\bar{\Psi}_e\gamma_\rho(1-\gamma_5)\Psi_{\nu_e}\right] + \text{hermitian conjugate}$$

Equation IV·4

(Williams 1971), where g_μ is a constant, the $\bar{\Psi}_\ell$ and the Ψ_ℓ are the field operators for lepton ℓ, γ^ρ are the Dirac matrices, and ρ is a summation index. Each term in square brackets has a vector - axial vector (V-A) form. The product terms involving vector and axial vector components are pseudo-scalars, and thus connect states of opposite parity. Non conservation of parity, simultaneously discovered by Wu (1957) in the beta decay of nuclei and by other groups (Garwin 1957, Friedman 1957) in the very muon decay process now being discussed, leads to an asymmetric muon decay, depending on the pseudo-scalar $\langle\vec{\sigma}^\mu\rangle\cdot\hat{n}_e$, where $\langle\vec{\sigma}^\mu\rangle$ is the muon polarization vector and $\hat{n}_e$ is the positron momentum direction. More specifically, the energy angular distribution of the e^+ can be written

$$\frac{dN}{d\omega\, d\Omega} = C(\omega)\left[1 \pm D(\omega)\langle\vec{\sigma}^\mu\rangle\cdot\hat{n}_e(\Omega)\right]$$

Equation IV·5

where $\omega = E/E_{max}$ is the positron energy in units of $E_{max} = m_\mu/2$.

Figure IV·1 shows the decay parameter C(w) and D(w). Note that

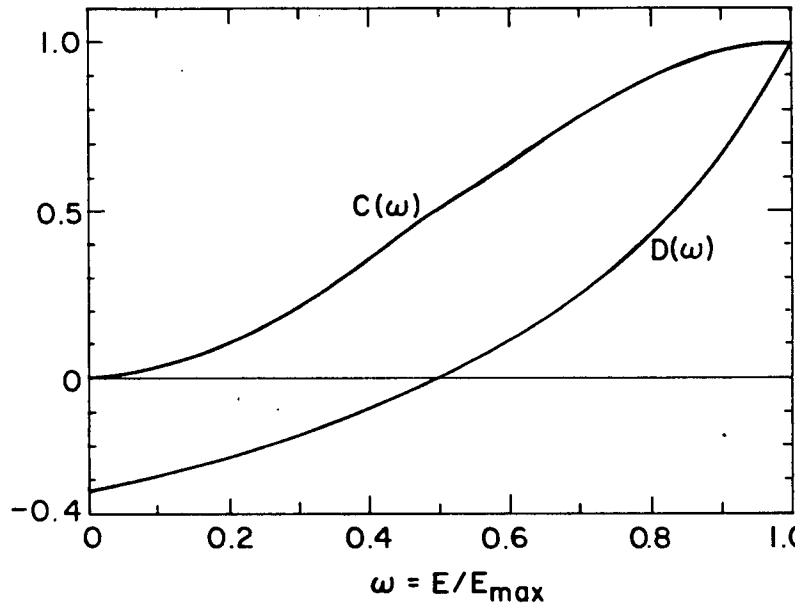

Figure IV·1 Muon decay parameters C(ω) and D(ω).

the asymmetry changes sign with energy and that the distribution of positron energies, C(ω), is weighted towards E_{max}. The average of C(ω)·D(ω) is theoretically 1/3 and has been measured to be 0.324 ± 0.004 (Cronin 1968).

IV·3 Muon Spin Rotation

The techniques of muon spin rotation (μ^+SR) involve measuring the decay rate of the muon in a particular direction as a function of time after the muon arrival in the target. In a typical μ^+SR experiment, the muon arrival is signalled by one or more scintillation counters and its decay by the passage of a high energy positron through a positron telescope, consisting of two or three scintillation counters with some absorber acting as a range filter. The histogram of time delays between these

events (the μ^+SR spectrum) has the following form (for μ^+ decay)

$$N_{\Omega'}(t) = N_{4\pi}(t) \int_0^1 d\omega\, \epsilon(\omega) \int_{\Omega'} \frac{d\Omega}{4\pi} c(\omega)\left[1 + D(\omega)\langle \vec{\sigma}^{\mu}(t)\rangle \cdot \hat{n}_e(\Omega)\right] + Bg$$

Equation IV·6

where $N_{4\pi}(t) = N\, e^{-t/\tau_\mu}$ is the total number of muons in the ensemble at time t, τ_μ is the μ^+ lifetime, $\epsilon(\omega)$ is the efficiency of the positron telescope for detecting a positron of energy ω, Ω' is the solid angle subtended by the positron telescope, Bg is a time independent background, and $\langle\vec{\sigma}^{\mu}(t)\rangle$ is the muon polarization vector (which, in general, is time dependent). Carrying out the integration yields a spectrum of the form

$$N_{\Omega}(t) = N_0\, e^{-t/\tau_\mu}\left[1 + A\langle \vec{\sigma}^{\mu}(t)\rangle \cdot \hat{m}\right] + Bg \qquad \text{Equation IV·7}$$

where $\hat{m}$ is the direction of the positron telescope, N_0 is the normalization, and A_0 is the maximum possible asymmetry. In a typical μ^+SR apparatus, $A_0 \sim 0.3$ and $N_0/N \sim 0.03$. It is clear from Equation IV·7 that the μ^+SR spectrum allows the experimenter to measure the time evolution of the muon polarization vector $\langle\vec{\sigma}^{\mu}(t)\rangle$ -- both its magnitude and direction.

In transverse field μ^+SR , a magnetic field is applied perpendicular to the initial muon polarization $\langle\vec{\sigma}^{\mu}(0)\rangle$, and the positron telescope direction $\hat{m}$. As might be expected, the muon polarization precesses about the applied field direction, giving rise to oscillations in the μ^+SR spectrum. The time evolution of $\langle\vec{\sigma}^{\mu}(t)\rangle$ for free muons and Mu in a transverse field will now be derived.

IV·3·1 Free Muons in a Transverse Magnetic Field

The spin Hamiltonian for an isolated muon in a magnetic field B along the $\hat{z}$ direction is

$$\hat{H}^{\mu} = \frac{\hbar}{2}\,\bar{\omega}^{\mu}\cdot\bar{\sigma}^{\mu} = \frac{\hbar}{2}\,\omega^{\mu}\sigma_z^{\mu} \qquad \text{Equation IV·8}$$

where $\bar{\omega}^{\mu} = g_{\mu} e\bar{B}/2m_{\mu}c$, $g_{\mu} \sim 2$, m_{μ} is the muon mass, and $\bar{\sigma}^{\mu}$ are Pauli spin matrices. The energy eigenstates are then $|\epsilon_1\rangle = |\sigma_z = 1\rangle$ and $|\epsilon_2\rangle = |\sigma_z = -1\rangle$ with eigenvalues $\pm\hbar\omega^{\mu}/2$ respectively.

If the muons are initially in a pure state

$$|\psi(0)\rangle = |\sigma_x = 1\rangle = \frac{1}{\sqrt{2}}\left[\,|\epsilon_1\rangle + |\epsilon_2\rangle\,\right] \qquad \text{Equation IV·9}$$

then the corresponding density matrix at t=0 is

$$\rho(0) = |\psi(0)\rangle\langle\psi(0)| = \frac{1}{2}\left[|\epsilon_1\rangle\langle\epsilon_1| + |\epsilon_2\rangle\langle\epsilon_2| + |\epsilon_1\rangle\langle\epsilon_2| + |\epsilon_2\rangle\langle\epsilon_1|\,\right] \qquad \text{Equation IV·10}$$

In matrix notation

$$\rho_{ij} = \begin{bmatrix} \frac{1}{2} & \frac{1}{2} \\ \frac{1}{2} & \frac{1}{2} \end{bmatrix} \qquad \text{Equation IV·11}$$

The density matrix at a later time t is given as

$$\rho_{ij}(t) = \langle\epsilon_i|\, e^{-\frac{i}{\hbar}\hat{H}^{\mu}t}\, \rho(0)\, e^{\frac{i}{\hbar}\hat{H}^{\mu}t}\, |\epsilon_j\rangle$$

$$= e^{\frac{i}{\hbar}(\epsilon_j - \epsilon_i)t}$$

$$= \begin{bmatrix} \frac{1}{2} & \frac{1}{2}e^{-i\omega^{\mu}t} \\ \frac{1}{2}e^{i\omega^{\mu}t} & \frac{1}{2} \end{bmatrix} \qquad \text{Equation IV·12}$$

The time evolution of muon polarization vector is most easily evaluated in terms of the expectation value of $\sigma^{\mu+} = \sigma_x^\mu + i\sigma_y^\mu$, twice the muon spin raising operator. It is clear $\langle\sigma_x^\mu\rangle = \mathrm{Re}\langle\sigma^{\mu+}\rangle$, $\langle\sigma_y^\mu\rangle = \mathrm{Im}\langle\sigma^{\mu+}\rangle$ and $\langle\sigma_z^\mu\rangle = 0$. In matrix notation,

$$\sigma_{ij}^{\mu+} = \begin{bmatrix} 0 & 2 \\ 0 & 0 \end{bmatrix} \qquad \text{Equation IV·13}$$

It immediately follows from

$$\langle\sigma^{\mu+}\rangle = \mathrm{Tr}\left[\rho(t)\,\sigma^{\mu+}\right] = e^{i\omega t} \qquad \text{Equation IV·14}$$

that

$$\langle\sigma_x^\mu(t)\rangle = \cos\omega^\mu t$$
$$\langle\sigma_y^\mu(t)\rangle = \sin\omega^\mu t \qquad \text{Equation IV·15}$$

Thus the polarization vector rotates about the applied field direction at a single frequency, ω^μ, as expected classically.

IV·3·2 Free Muonium in a Transverse Magnetic Field

The spin Hamiltonian for an isolated Mu atom in a magnetic field along the $\hat{z}$ direction can be written

$$H^{Mu} = \frac{\hbar\omega_0}{4}\,\bar{\sigma}^\mu\cdot\bar{\sigma}^e + \frac{\hbar\bar{\omega}^\mu\cdot\bar{\sigma}^\mu}{2} + \frac{\hbar\bar{\omega}^e\cdot\bar{\sigma}^e}{2} \qquad \text{Equation IV·16}$$

The first term is the hyperfine coupling between the muon and electron. In the ground state, $\omega_0/2\pi$ = 4463.302 MHz (Casperson 1975). The last two terms are muon and electron Zeeman interactions with the applied field. In the $|\sigma_z^\mu\ \sigma_z^e\rangle$ basis, where α and β refer to ±1 respectively,

$$|\epsilon_1\rangle = |\alpha\,\alpha\rangle$$
$$|\epsilon_2\rangle = \sin\varphi\,|\alpha\,\beta\rangle + \cos\varphi\,|\beta\,\alpha\rangle$$
$$|\epsilon_3\rangle = |\beta\,\beta\rangle$$
$$|\epsilon_4\rangle = \cos\varphi\,|\alpha\,\beta\rangle - \sin\varphi\,|\beta\,\alpha\rangle$$

Equation IV·17

with corresponding eigenvalues

$$\epsilon_1/\hbar = \omega_- + \frac{\omega_0}{4}$$
$$\epsilon_2/\hbar = -\frac{\omega_0}{4} + \left(\omega_+^2 + \frac{\omega_0^2}{4}\right)^{\frac{1}{2}}$$
$$\epsilon_3/\hbar = -\omega_- + \frac{\omega_0}{4}$$
$$\epsilon_4/\hbar = -\frac{\omega_0}{4} - \left(\omega_+^2 + \frac{\omega_0^2}{4}\right)^{\frac{1}{2}}$$

Equation IV·18

where

$$\sin\varphi = \frac{1}{\sqrt{2}}\left[1 - \frac{x}{(1+x^2)^{\frac{1}{2}}}\right]^{\frac{1}{2}}$$

Equation IV·19

$$x = 2\frac{\omega_+}{\omega_0} = B/B_0$$

Equation IV·20

where B_0=1585G and

$$\omega_\pm = \frac{Be}{4c}\left(\frac{g_\mu}{m_\mu} \pm \frac{g_e}{m_e}\right)$$

Equation IV·21

These are the familiar Breit-Rabi energy eigenvalues for the H atom(see for example Brewer 1976).

Consider a muon initially polarized along the $\hat{x}$ direction, which captures an unpolarized electron at t=0. The resulting Mu state is a mixture of the two states .

$$\psi_A(0) = \frac{1}{\sqrt{2}}\left[|\alpha\alpha\rangle + |\beta\alpha\rangle\right]$$

$$= \frac{1}{\sqrt{2}}\left[|\epsilon_1\rangle + \cos\varphi\,|\epsilon_2\rangle - \sin\varphi\,|\epsilon_1\rangle\right]$$

$$\psi_B(0) = \frac{1}{\sqrt{2}}\left[|\alpha\beta\rangle + |\beta\beta\rangle\right]$$

$$= \frac{1}{\sqrt{2}}\left[|\epsilon_3\rangle + \sin\varphi\,|\epsilon_3\rangle + \cos\varphi\,|\epsilon_4\rangle\right]$$

Equation IV·22

The corresponding density matrix at t=0 can then be written

$$\rho(0) = \frac{1}{2}|\psi_A(0)\rangle\langle\psi_A(0)| + \frac{1}{2}|\psi_B(0)\rangle\langle\psi_B(0)|$$

Equation IV·23

In matrix notation,

$$\rho_{ij}(0) = \langle\epsilon_i|\rho(0)|\epsilon_j\rangle$$

$$= \begin{bmatrix} \frac{1}{4} & \frac{\cos\varphi}{4} & 0 & -\frac{\sin\varphi}{4} \\ \frac{\cos\varphi}{4} & \frac{1}{4} & \frac{\sin\varphi}{4} & 0 \\ 0 & \frac{\sin\varphi}{4} & \frac{1}{4} & \frac{\cos\varphi}{4} \\ -\frac{\sin\varphi}{4} & 0 & \frac{\cos\varphi}{4} & \frac{1}{4} \end{bmatrix}$$

Equation IV·24

The time evolved density matrix

$$\rho_{ij}(t) = \langle\epsilon_i|e^{-\frac{i}{\hbar}H^{M_4}t}\,\rho(0)\,e^{\frac{i}{\hbar}H^{M_4}t}|\epsilon_j\rangle$$

$$= e^{i\omega_{ij}t}\,\rho_{ij}(0)$$

$$= \begin{bmatrix} \frac{1}{4} & \frac{\cos\varphi}{4} e^{i\omega_{12}t} & 0 & -\frac{\sin\varphi}{4} e^{i\omega_{14}t} \\ \frac{\cos\varphi}{4} e^{-i\omega_{12}t} & \frac{1}{4} & \frac{\sin\varphi}{4} e^{i\omega_{23}t} & 0 \\ 0 & \frac{\sin\varphi}{4} e^{-i\omega_{23}t} & \frac{1}{4} & \frac{\cos\varphi}{4} e^{i\omega_{34}t} \\ -\frac{\sin\varphi}{4} e^{-i\omega_{14}t} & 0 & \frac{\cos\varphi}{4} e^{-i\omega_{34}t} & \frac{1}{4} \end{bmatrix}$$

Equation IV·25

where $\hbar\omega_{ij} = \epsilon_i - \epsilon_j$.

As in the case of the free muon, it is sufficient to evaluate the expectation value of $\sigma^{\mu+}$, twice the muon spin raising operator. It is easy to show

$$\sigma^{\mu+}_{ij} = \langle \epsilon_i | \sigma^{\mu+} | \epsilon_j \rangle$$

$$= \begin{bmatrix} 0 & 0 & 0 & 0 \\ 2\cos\varphi & 0 & 0 & 0 \\ 0 & 2\cos\varphi & 0 & 2\cos\varphi \\ -2\cos\varphi & 0 & 0 & 0 \end{bmatrix}$$

Equation IV·26

It follows immediately from

$$\langle \sigma^{\mu+} \rangle = Tr[\rho(t)\,\sigma^{\mu+}]$$
$$= \tfrac{1}{2}[\cos^2\varphi\, e^{i\omega_{12}t} + \sin^2\varphi\, e^{i\omega_{23}t} + \sin^2\varphi\, e^{i\omega_{14}t} + \cos^2\varphi\, e^{-i\omega_{34}t}]$$

Equation IV·27

that

$$\langle \sigma_x^{\mu} \rangle = \tfrac{1}{2}[\cos^2\varphi \cos\omega_{12}t + \sin^2\varphi \cos\omega_{23}t + \sin^2\varphi \cos\omega_{14}t + \cos^2\varphi \cos\omega_{34}t]$$

$$\langle \sigma_y^{\mu} \rangle = \tfrac{1}{2}[\cos^2\varphi \sin\omega_{12}t + \sin^2\varphi \sin\omega_{23}t + \sin^2\varphi \sin\omega_{14}t - \cos^2\varphi \sin\omega_{34}t]$$

Equation IV·28

In low fields $x \ll 1$ or $B \ll 1585$ G, the period of the ω_{14} and ω_{34} frequencies is of order 0.225 ns and is usually not observable with a typical μ^+SR apparatus, where timing resolution is ~1 ns. Thus half the muon polarization in Mu is not observed, and the remaining two terms in $\langle \sigma_x^{\mu} \rangle$ can be expressed

$$\langle \sigma_x^{\mu} \rangle = \tfrac{1}{2}\left\{\left(1 + \frac{x}{(1+x^2)^{\frac{1}{2}}}\right)\cos[(\omega_- - \Omega)t - \tfrac{\pi}{2}] + \left(1 - \frac{x}{(1+x^2)^{\frac{1}{2}}}\right)\cos[(\omega_- + \Omega)t - \tfrac{\pi}{2}]\right\}$$

Equation IV·29

$$\Omega = \frac{\omega_{12} - \omega_{23}}{2} = \frac{\omega_0}{2}[(1+x^2)^{\frac{1}{2}} - 1]$$

Equation IV·30

In very low fields, < 10G, where $\Omega\tau_{\mu} \ll 1$ (τ_{μ} =2.2 μs is the

muon lifetime) the splitting is negligible and the expression simplifies to

$$\langle \sigma_x \rangle = \frac{1}{2} \cos \omega_- t \qquad \text{Equation IV·31}$$

where $\omega_- = B \cdot 1.40\ \text{MHz} \cdot \text{G}^{-1}$ from equation IV.21.

IV·4 Mu Spin Relaxation

When muons are stopped in matter as bare muons or Mu, the free Hamiltonian is perturbed by the surrounding medium in various ways which lead to decay of the muon polarization $\langle \vec{\sigma}^{\mu} \rangle$. Much of the interest in μ^+SR is focussed on the spin relaxation of muons (Mu), since this yields information on muon (Mu) + host state. So far as spin relaxation is concerned the bare muon is a pure magnetic probe, sensitive to the local magnetic environment. The muon in a Mu atom is strongly coupled to the electron, whose magnetic moment is 200 times larger. Its response to the local magnetic environment are indirect but in general 103 times faster than the bare muon (due to the faster precession frequency). Muons in Mu atoms are also sensitive to electric fields since in general these will alter the muon electron coupling and thus the precession frequencies of Mu. The information obtained from μ^+SR of Mu atoms is similar to that obtained from ESR of H atoms. There are four basic mechanisms by which $\langle \vec{\sigma}^{\mu}(t) \rangle$ of Mu decays in a host.

1. Random local magnetic fields.
2. Random anisotropic distortion.
3. Spin Exchange reactions.
4. Chemical reactions.

IV·4·1 Random Local Magnetic Fields (RLMF)

Consider a Mu atom at position $\bar{r}_M$ in a host containing magnetic moments at positions $\bar{r}_1$, $\bar{r}_2$ ... $\bar{r}_N$. The free spin Hamiltonian for Mu must be modified to include the dipole-dipole coupling between the Mu and the host moments. The perturbing interaction can be written

$$H^{dip} = \sum_i \bar{B}_i(\bar{r}_i) \cdot \left\{ \frac{g_\mu e\hbar}{4 m_\mu c} \bar{\sigma}^\mu - \frac{g_e e\hbar}{4 m_e c} \bar{\sigma}^e \right\}$$

Equation IV·32

where

$$\bar{B}_i = \frac{g_i e\hbar}{4 m_i c} \frac{1}{r_{iM}^3} \left(\bar{\sigma}^i - 3 \frac{\bar{r}_{iM} \bar{\sigma}^i \cdot \bar{r}_{iM}}{r_{iM}^2} \right)$$

$$\bar{r}_{iM} = \bar{r}_i - \bar{r}_M$$

Equation IV·33

is the magnetic field at the Mu site due to the moment at r_i (Abragam 1961). Thus the effective field at the site of Mu atom

$$\bar{B}_{eff} = \bar{B}_{applied} + \Delta \bar{B}_{dip}$$

Equation IV·34

where $\Delta B_{dip} = \sum_i \bar{B}_i$

In a lattice where the host moments are fixed and unpolarized, $\Delta \bar{B}_{dip}$ is randomly distributed about zero, giving rise to a broadening in the Mu frequencies, or (equivalently) a decay of the muon polarization amplitude. A specific example of this will be given in Section V·4. If $\Delta \bar{B}_{dip}$ is flucuating quickly due to motion of the Mu or the host moments, this tends to average the perturbing field so the Mu atom sees the average field. This phenomenon is commonly referred to as motional narrowing.

IV·4·2 Random Anisotropic Distortion

Consider a Mu atom localized at a site $\bar{r}$ in a lattice. The ground state wavefunction may be perturbed by the lattice, altering the hyperfine interaction between the muon and electron. This perturbing interaction can be expressed

$$H^{hyp} = \bar{\sigma}^{\mu} \cdot \hat{A} \cdot \bar{\sigma}^{e} \qquad \text{Equation IV·35}$$

where $\hat{A}$ is a 4 x 4 tensor. In the case of an isotropic perturbation (i.e.: $\hat{A} = \hbar\Delta\omega_0 I$), the energy eigenvalues and eigenstates are identical to those obtained in the free Mu case, except that the hyperfine splitting is modified to $\hbar(\omega_0+\Delta\omega_0)$. In the general case the perturbation is anisotropic and $\langle\bar{\sigma}_x^{\mu}(t)\rangle$ has six frequencies corresponding to all possible ω_{ij}, even in zero applied field. Three of these (of order ω_0) are not normally observed because of their high frequency. All of them may depend on the orientation of the lattice with respect to the muon polarization. Zero field oscillations of Mu have recently been observed in single crystal SiO_2 below 50°K (Brewer 1981). In fused SiO_2, the orientation of the lattice with respect to the initial muon polarization is random the anisotropic distortion causes spin relaxation. As in the case of random local magnetic fields, rapid motion of the Mu atom leads to an averaging of the distortion over many sites, and a subsequent weakening of the relaxation.

IV·4·3 Chemical Reaction

A Mu atom may react chemically with a molecule to form a Mu compound. The magnetic environment of the muon changes dramatically at the instant of formation (except if the Mu compound is a radical in which the muon electron coupling is almost the same as for Mu), so that the muon spin vector quickly falls out of phase with the remaining members of the Mu ensemble. In the gas phase the Mu relaxation rate can be written $\sigma_{ch} v n$, where σ_{ch} is the cross section for the reaction, v is the mean thermal velocity of Mu and n is the concentration of reactant.

IV·4·4 Spin Exchange

As in the case of Ps, the z component of the Mu electron spin is not a conserved quantity in collisions with paramagnetic molecules such as NO (s=1/2) or O_2 (s=1). This leads to hyperfine transitions of Mu which result in a loss of coherence of muon spins. The relaxation rate for Mu due to spin exchange can be written

$$\lambda = f \sigma_{ex} v n / 2 \qquad \text{Equation IV·36}$$

where σ_{ex} is the spin exchange cross section defined in Appendix II and f is a constant depending on the spin of the paramagnetic molecule (f = 3/4 for NO and 8/9 for O_2, Fleming 1981a).

IV·5 The μ^+SR Spectrum in a Transverse Field

It is clear that the precession amplitudes $A_{\mu+}$ and A_{Mu} for muons and Mu in matter have some time dependence due to interaction with host. Let the time dependence be represented by the functions $R_{\mu+}(t)$ and $R_{Mu}(t)$ with $R_{\mu+}(0) = R_{Mu}(0) = 1$. Then the μ^+SR spectrum in a moderate transverse field for a positron telescope in the $\hat{x}$ direction can be written, using Equations IV·7 and IV·29,

$$N(t) = N_0 e^{-t/\tau_\mu} [1 + S_\mu(t) + S_{Mu}(t)]$$

Equation IV·37

where

$$S_\mu(t) = A_{\mu+} R_{\mu+}(t) \cos \omega_\mu t$$

$$S_{Mu}(t) = \frac{A_{Mu}}{2} R_{Mu}(t) \{\cos^2\varphi \cos[(\omega_- - \Omega)t - \tfrac{\pi}{2}] + \sin^2\varphi \cos[(\omega_- + \Omega)t - \tfrac{\pi}{2}]\}$$

Equation IV·38

The spectrum for a telescope in any direction in the plane of precession differs only by a phase factor. In very weak fields (< 10G) one may use Equation IV·31 instead of Equation IV·29 so that

$$S_{Mu}(t) = \frac{A_{Mu}}{2} R_{Mu}(t) \cos \omega_- t$$

Equation IV·39

CHAPTER V : MUONIUM IN INSULATING POWDERS

Mu precession has previously been observed in several oxide powders such as SiO_2, Al_2O_3 and MgO (Marshall 1978, Kiefl 1979). As in the case of Ps, a fraction of the Mu emerges into the void regions of the powder. This has been verified through the introduction of paramagnetic O_2 gas, which rapidly relaxes the Mu in the voids through spin exchange at a rate consistent with that measured in an Ar or N_2 gas moderator.

As a prelude to the experimental results on Mu in these oxides at low temperature, this chapter deals with the formation, thermalization, and spin relaxation of Mu in these highly dispersed media. The form of the relaxation function $R_{Mu}(t)$ will be derived under various experimental conditions.

V·1 Mu Formation

The thermalization and neutralization of energetic positive muons is a complicated process, especially in condensed matter or a powder. As in the case of Ps, epithermal,spur and surface processes can result in Mu formation. However, recently it has been shown that Mu formation is unaffected by the application of an electric field in bulk SiO_2 and several hydrocarbon liquids (Ito 1981). This is in contrast to the case of Ps, where such a field inhibits combination of e^+ and spur e^- (Ito 1979). These results weaken the spur model hypothesis for Mu formation, at least in these cases.

The problem of epithermal Mu formation can be formulated as

follows. Define $f_i(E\ t)$ to be the fraction of muon ensemble in charge state i at energy E and time t. Ignoring double charge exchange [valid below 10KeV for protons (Tawara 1973)] the f_i's obey the following coupled integro-differential equations

$$\frac{\partial f_1}{\partial t} = -f_1(E,t)\int_0^\infty [t_{11}(E E') + t_{10}(E E')]\,dE' + \int_0^\infty [t_{11}(E'E) f_1(E' t) + t_{01}(E'E) f_0(E' t)]\,dE'$$

Equation V·1

$$\frac{\partial f_0}{\partial t} = -f_0(E t)\int_0^\infty [t_{00}(E E') + t_{01}(E E') + t_{0-1}(E E')]\,dE$$
$$+ \int_0^\infty [t_{00}(E'E) f_0(E' t) + t_{10}(E'E) f_1(E' t) + t_{-10}(E'E) f_{-1}(E' t)]\,dE'$$

Equation V·2

$$\frac{\partial f_{-1}}{\partial t} = -f_{-1}(E t)\int_0^\infty [t_{-1-1}(E E') + t_{-10}(E E')]\,dE' +$$
$$\int_0^\infty [t_{-1-1}(E'E) f_{-1}(E' t) + t_{0-1}(E'E) f_0(E' t)]\,dE'$$

Equation V·3

where $t_{ij}(EE')$ is the transition rate between a muon in an initial state of energy E, charge i and a final state of energy E′ and charge j. It is generally accepted that most of the charge exchange occurs in the 2 KeV to 20 eV region, where the muon has a velocity comparable with the valence electrons in most atoms (Fleming 1981b). At thermal energies, charge exchange may be energetically forbidden. Since the thermalization time in condensed matter is estimated to be of order 10^{-11}s (Brewer 1975), all the charge exchange occurs much too fast to be observable via the μ^+SR technique (timing resolution 10^{-9} s). The observable quantities in a μ^+SR experiment are the Mu

fraction $F_{Mu}(t)$ and the diamagnetic fraction $F_{\mu^+}(t)$ where

$$F_{Mu}(t) = \int_0^\infty f_0(Et)\, dE$$

Equation V·4

$$F_{\mu^+}(t) = \int_0^\infty [f_1(Et) + f_{-1}(Et)]\, dE$$

Equation V·5

The Mu^- ion is difficult to distinguish from a bare muon with the μ^+SR technique, since the time evolution of the muon polarization is virtually the same in both cases and thus contributes to the diamagnetic fraction.

In principle, if the transition rates $t_{ij}(EE')$ are known, one can solve equations V·1, V·2 and V·3 and predict F_{Mu} and F_{μ^+}. However, in general, they are not easily measurable or calculable. This is why Mu formation in condensed matter has remained somewhat of a mystery.

Mu precession has also been observed in bulk samples of MgO and SiO_2. Longitudinal field measurements indicate that it is also present in bulk Al_2O_3 (Minaichev 1970). The Mu formation probability is not positively correlated to the degree of aggregation of the oxide, suggesting that Mu formation is a bulk rather than a surface phenomenon.

V·2 Mu Thermalization

Below the lowest electron excitation energy of a non-metallic medium (or of Mu, whichever is smaller), Mu must lose energy through excitation of lattice vibrations (phonons). Once thermalized, it diffuses through the lattice at a rate which is, in general, strongly temperature dependent. At very low temperatures, the Mu atom may become trapped in the lattice for times greater than the muon lifetime. Trapping of H atoms in bulk insulators has been observed in many ESR experiments (Foner 1960, Weil 1981).

The process by which Mu eventually reaches the interstices of oxide powders is not clearly understood. In the thermal diffusion model, Mu thermalizes within the grain and then proceeds to diffuse to the surface where it is ejected into the voids, presumably because of a negative work function at the surface. (Such a work function might arise from the lattice distortion induced by an interstitial Mu atom). This model has been used to explain μ^+SR results from SiO_2 powder (70Å and 140Å mean diameter) at 300°K. (Marshall 1978). There is no indication that the Mu reenters the powder grains, suggesting that the work function at the surface is much greater than 300°K. However, the assumption that all the Mu initially thermalizes within the grains may not be valid at all temperatures and under all conditions. A large work function at the surface, the small particle size and the presence of a buffer gas in the interstices may favour direct thermalization in the voids. The motivation for introducing this model is provided in Chapter VI in light of the experimental data on SiO_2, Al_2O_3 and MgO powders

in a He atmosphere at 6 °K. Its feasibility is qualitativey demonstrated in Appendix III.

Once the Mu reaches the voids with an energy less than the work function at the surface, it will thermalize via phonon excitation during collisions with the surface or by scattering off a buffer gas, if present.

The thermalization of an atom in a powder is treated in Appendix I, using the 1-dimensional Devonshire theory for gas-surface interactions. In this approximation, the time required for 1eV Mu (8600°K) to reach 35°K in Al_2O_3 at 7°K (SA = 220 m^2/g, ρ =0.56 $g \cdot cm^{-3}$, θ_D = 880°K and Morse surface potential parameters a =0.5 $Å^{-1}$, D=0) is 40 ns, with most of the time being spent below 300°K.

The presence of a small amount of monatomic buffer gas in the interstices reduces the thermalization time substantially. In the case of s-wave scattering, the time required to go from energy E_i to E_f is roughly (Mobley 1966).

$$t = \frac{M}{2^{\frac{1}{2}} \sigma n m^{\frac{1}{2}}} \left(\frac{1}{E_i^{\frac{1}{2}}} - \frac{1}{E_f^{\frac{1}{2}}} \right) \qquad \text{Equation V·6}$$

where

m is the Mu mass
M is the mass of the buffer atom
σ is the s wave cross section ($\sim 10Å^2$)
n is the number density of the buffer gas.

The time required to go from 8600°K to 35°K is only 32 ns in 1 torr of He.

We may conclude that the information obtained from μ^+SR experiments on such powders will pertain to thermalized muonium.

V·3 Mu Bound States on Oxide Surfaces

H atoms have been stabilized on silica and alumina surfaces below 120°K (Golubev 1965). The activation energy on the surface ranges from 500°K to 1500°K (in units of k). This represents a rough estimate of the binding energy to the surface.

From the H atom results, it is possible to estimate the binding energy of Mu to a similar surface. The surface-atom interaction is assumed to be represented by a Morse Potential

$$V(z) = D\left(e^{-2az} - 2e^{-az}\right) \qquad \text{Equation V·7}$$

The binding energy of the deepest bound state can be written (Morse, loc. cit.)

$$\epsilon_o^{Mu} = \left(d - \frac{1}{2}\right)^2 \frac{\hbar^2 a^2}{2 m_{Mu}}$$

$$= \left[\epsilon_o^{H\,\frac{1}{2}} - \frac{\hbar a}{2^{3/2} m_{Mu}^{\frac{1}{2}}}\left\{1 - \left(\frac{m_{Mu}}{m_H}\right)^{\frac{1}{2}}\right\}\right]^2 \qquad \text{Equation V·8}$$

where $d = (2m_{Mu}\,D)^{\frac{1}{2}}/\hbar a$ and ϵ_o^H is the corresponding binding energy of the H atom. For example, if ϵ_o^H = 1000°K and a =0.5Å, then ϵ_o^{Mu} = 850°K. This serves to illustrate the isotope dependence one may expect between Mu and H bound on such surfaces.

It is of some interest to consider the fraction of time a Mu atom will spend in a bound state on the powder surface at 300 °K, given that the binding energy is of order 850 °K. This fraction may be estimated by applying some simple thermodynamics given in Appendix IV. One finds, for example in 70 Å SiO_2 at a powder density of 0.04 g cm^3, that the Mu spends only 7.7 % of its time on the surface. It is clear that to trap Mu on the surface of such powder for any appreciable amount of time, one

must experiment at temperatures much less than the binding energy.

V·4 Mechanisms for Mu Spin Relaxation in a Powder

The mechanisms for Mu spin relaxation in a powder (discussed in general in Section IV·4) depends on whether the Mu is bound to the surface or colliding freely with it. Spin relaxation of Mu adsorbed on an unreactive surface has three basic origins:

1. Dipole-dipole interaction with nuclear moments or distant paramagnetic impurities. This is particularly effective when the Mu is static on the surface.

2. Random anisotropic distortion of the Mu atom due to the atom-surface interaction. Again, this is most effective when the Mu is stationary on the surface.

3. Spin exchange with unpaired free electrons on the surface. This, on the other hand, is most effective when the Mu is mobile on the surface.

If the Mu is colliding freely with the surface, the effects of the first two are diminished considerably due to motional narrowing. The situation is analogous to spin relaxation in a gas since the powder grains in this case act as large gas molecules. Thus spin exchange is expected to be dominant in the case of desorbed Mu.

V·4·1 Nuclear Magnetic Moments

If Mu is adsorbed on a surface which possesses nuclear magnetic moments the dipole-dipole coupling between the Mu and the moments leads to a broadening in the precession frequency distribution or equivalently, spin relaxation. The expectation value of the $\hat{z}$ component of magnetic field produced at the Mu site by a moment at position $\bar{r}$ and z component of spin I_z can be written

$$\Delta B_z^{dip} = \langle I_z | B_z | I_z \rangle = \frac{\gamma_I I_z}{r^3}(1 - 3\cos^2\theta) \qquad \text{Equation V·9}$$

where $\bar{B}_z$ is given in Equation IV·33, θ is the angle between $\bar{r}$ and the $\hat{z}$ axis and $\gamma_I = ge/4m_p c$. The shift in the Mu precession frequency about the $\hat{z}$ axis can then be written in first order

$$\Delta\omega = \gamma_{Mu}\,\Delta B_z^{dip}$$

where

$$\gamma_{Mu} = 2\pi \cdot 1.4\ MHz\ G^{-1}$$

Equation V·10

provided that $\Delta B_z^{dip} \ll B_{applied}$. If this condition is not satisfied, proper account must be taken of ΔB_x^{dip} and ΔB_y^{dip}. If one assumes that on a surface only the nearest neighbour contributes to ΔB_z^{dip}, then the mean squared frequency shift is

$$\overline{\Delta\omega^2} = \gamma_I^2 \gamma_M^2 \frac{(1 - 3\cos^2\theta)^2}{r^6} \frac{1}{2I+1} \sum_{I_z=-I}^{I} I_z^2$$

$$= \frac{I(I+1)}{3} \gamma_I^2 \gamma_M^2 \frac{(1 - 3\cos^2\theta)}{r^6} \qquad \text{Equation V·11}$$

This is the second moment due to dipolar broadening by unlike spins (Abragam 1961). In a powder, θ may be averaged to obtain

$$\overline{\Delta\omega^2} = \frac{4}{15} \frac{I(I+1)\gamma_I^2 \gamma_{Mu}^2}{r^6} \qquad \text{Equation V·12}$$

or

$$\overline{(\Delta B^{dip})^2} = \frac{4}{15} \frac{I(I+1)\gamma_I^2}{r^6}$$

Equation V·13

For example, in the case of Mu adsorbed on Al_2O_3 at a distance of 1.5Å from an ^{27}Al nucleus, $2[(\Delta B_z^{dip})^2] = 3.9G$. This agrees reasonably well with the ESR linewidth (4.27 G) of H atoms stabilized on an Al_2O_3 surface (Golubev 1965). For comparison, the ESR linewidth on SiO_2 is only 0.87 G, and is probably due to a random anisotropic distortion, since only 2% of natural Si has nuclear moments. Thus the relaxation rate for Mu atoms frozen on an Al_2O_3 surface is estimated at $2\pi\gamma_{Mu}\left[\overline{\Delta B_z^{dip}}^2\right]^{\frac{1}{2}} = 19\ \mu s^{-1}$.

V·4·2 Paramagnetic Impurities

If the Mu is frozen on the surface of a lattice, the dipole-dipole interaction between Mu and an impurity at position $\bar{r}_i$ leads to a shift in the precession frequency.

$$\Delta\omega^i = \frac{\gamma_I^i \gamma_{Mu}}{r_i^3}(1 - 3\cos^2\theta) I_z^i$$

Equation V·14

If there are N impurities, then the total shift $\omega = \sum_{i=1}^{N} \Delta\omega^i$. In a statistical model (Anderson 1951, Abragam 1961), the frequency distribution $x(\omega)d\omega$ is proportional to the volume of phase space, such that $\omega < \Sigma\, \Delta\omega^i < \omega + d\omega$.

$$\chi(\omega) = \int_V \sum_{I_z\, i} \delta\left(\omega - \sum_i \Delta\omega^i\right) \prod_i d\bar{r}^i$$

$$= \frac{1}{2\pi} \int_{-\infty}^{\infty} dt\, e^{-i\omega t} \left[\frac{1}{V(2I+1)} \sum_{I_z=-I}^{I} \int_V e^{-itB}\, d\bar{r}\right]^N$$

Equation V·15

where

$$B = I_z \gamma_{Mu} \gamma_I \frac{(1 - 3\cos^2\theta)}{r^3}$$

Equation V·16

and where V is the half space associated with the solid. Following (Abragam 1961)

$$= \frac{1}{V(2I+1)} \sum_{I_z} \int_V e^{itB} d\bar{r} = 1 - \sum_{I_z} \frac{1}{V(2I+1)} \int_{\Omega'} \int_0^{\infty} dr[1 - e^{-itB}] r^2$$

where Ω' is 2π steradians associated with the solid.

$$= 1 - \frac{1}{2} \sum_{I_z} \frac{1}{V(2I+1)} \int_{\Omega'} d\Omega \int_{-\infty}^{\infty} dr[1 - e^{-itB'}] r^2$$

where $B' = |I_z| \gamma_I \gamma_S (1 - 3\cos^2\theta)/r^3$

$$= 1 - \frac{\pi \gamma_I \gamma_S |t|}{6V(2I+1)} \sum_{I_z} |I_z| \int_{\Omega'} d\Omega \, |3\cos^2\theta - 1|$$

$$= 1 - \frac{\pi^2 \gamma_I \gamma_S |t|}{6V(2I+1)} \frac{8}{3\sqrt{3}} Tr[|I_z|]$$

$$= 1 - \frac{4\pi^2}{9\sqrt{3}} \gamma_I \gamma_S |t| \frac{Tr[|I_z|]}{2I+1} \frac{n}{N}$$

Equation V·17

where n = density of impurities. Define

$$\lambda = \frac{4}{9}\frac{\pi^2}{\sqrt{3}}\gamma_I\gamma_s\frac{Tr[|I_z|]}{2I+1}n$$

Equation V·18

Substituting Equation V·17 into Equation V·16 yields

$$\chi(\omega) = \frac{1}{2\pi}\int_{-\infty}^{\infty} dt\, e^{-i\omega t}\left(1-\frac{\lambda t}{N}\right)^N$$

$$= \frac{1}{2\pi}\int_{-\infty}^{\infty} dt\, e^{-i\omega t}\, e^{-\lambda t} \quad ; \; N \text{ large}$$

Equation V·19

For example, a 2% Fe^{+3} impurity in Al_2O_3 relaxes Mu on a surface at a rate $\lambda \sim 400 \mu s^{-1}$

If the Mu is moving on the surface, or colliding freely with the surface, then the Mu may undergo spin exchange with paramagnetic impurities. The relaxation rate in a free Mu state can be written

$$\lambda = \frac{f}{2} m \nu_c \sigma_{ex}$$

Equation V·20

where ν_c is the collision frequency with the surface, m is the concentration of paramagnetic impurity on the surface, σ_{ex} is the spin exchange cross section, and f a constant of order unity, depending on the spin of the impurity (see Section IV·4·4). For example, in 70 Å SiO_2 powder at a density of 0.04 g cm^{-3} at 6 °K with σ_{ex} =9.2 $Å^2$ and m=4 x $10^{-3} Å^{-2}$, the relaxation rate of Mu should be of order 120 μs^{-1}.

V·4·3 Motional Narrowing

In the preceding sections, it has been assumed that there are no fluctuations in the random local magnetic field experienced by the Mu atom. However, a very light atom such as Mu may be extremely mobile on a surface, and this may lead to a motional narrowing of the precession frequency distribution, or, equivalently, a reduction in spin relaxation rate. If the local magnetic field in the reference frame of the Mu atom is fluctuating randomly, characterized by some relaxation time τ_c, and if $(\Delta\omega^2)^{\frac{1}{2}}\tau \ll 1$ (the limit of fast fluctuations), then the observed relaxation will be reduced to

$$\lambda \sim \overline{\Delta\omega^2}\,\tau_c$$

Equation V·21

V·4·4 Random Anisotropic Distortion

It is difficult to predict what effect the surface will have on the hyperfine interaction of Mu. If the ESR linewidth of H on SiO_2 is due to this effect, then one might assume that the relaxation of Mu on an SiO_2 surface to be of order $\pi\gamma_{Mu}$ 0.87G = 4.2 μs^{-1}. Note that the relaxation rate of Mu trapped in fused SiO_2 (3.9 μs^{-1}) (Brewer 1981) is thought to be due to this effect.

V·5 The Relaxation Function $R_{Mu}(t)$ for Mu in a Powder

The derivation of the form of the Mu relaxation function $R_{Mu}(t)$ in a powder is completely analogous to the derivation of the lifetime spectrum for o-Ps in a powder (see Section II·4). Consider an ensemble of Mu atoms in a powder at temperature T, where there exists a bound state with binding energy B. Define λ_F and λ_B to be the spin relaxation rates for Mu in the free and adsorbed states. The form of $R_{Mu}(t)$ (which describes how the muon spin in Mu relaxes with time) depends on how $\lambda_B \bar{t}$ compares with unity, where, as before, $\bar{t}$ is the mean surface dwell time for Mu on the surface (see Appendix IV).

V·5·1 Special Case $\lambda_B \bar{t} \ll 1$ (Adiabatic Approximation)

As in the case of Ps, this corresponds to a situation where the Mu adsorbs and desorbs many times while still polarized. The polarization amplitude decays according to a single exponential decay rate -- the average over free and bound states, weighted by the fraction of time spent in each state. Thus

$$R_{Mu}(t) = e^{-\lambda_A t}$$

Equation V·22

with

$$\lambda_A = \alpha \lambda_B + (1-\alpha) \lambda_F$$

Equation V·23

where α is the fraction of time spent in the bound state (see Equation AIV·15). It is assumed that the Mu atom hops many times on the surface before desorbing, so that the desorbing-adsorbing process does not significantly contribute to any motional narrowing. Combining equations AIV·15 and V·23 yields

$$\lambda_A = \left[\frac{1}{1 + e^{-B/kT} \frac{V_E}{A\Lambda}} \right] \lambda_B + \left[\frac{1}{e^{B/kT} \frac{A\Lambda}{V_F} + 1} \right] \lambda_F$$

Equation V·24

In the limit of $\frac{A\Lambda}{V_F} e^{B/kT} << 1$ this reduces to

$$\lambda_A = \frac{A\Lambda}{V_F} e^{B/kT} \lambda_B + \lambda_F$$

Equation V·25

V·5·2 Special Case $\lambda_B \bar{t} >> 1$ (Strong Collision Approximation)

The derivation is identical to that contained in Section II·4·2. The resulting Mu relaxation function is a sum or difference of exponentials.

$$R_{Mu}(t) = \frac{\gamma_e P_t}{\lambda_F + \gamma_e P_t - \lambda_B} e^{-\lambda_B t} + \left[1 - \frac{\gamma_e P_t}{\lambda_F + \gamma_e P_t - \lambda_B} \right] e^{-(\lambda_F + \gamma_e P_t)t}$$

Equation V·26

The limiting forms are as before

$$R_{Mu}(t) \sim e^{-(\gamma_e P_t + \lambda_F)t} \quad ; \quad \gamma_e P_t << |\lambda_B - \lambda_F|$$

Equation V·27

and

$$R_{Mu}(t) \sim e^{-\lambda_B t} \quad ; \quad \gamma_e P_t >> |\lambda_B - \lambda_F|$$

Equation V·28

V·6 Effect of Adsorbed Inert Gas on the Spin Relaxation

If an inert gas such as He or Ne is admitted into the vessel, a fraction of the gas adsorbs on the bare surface, thus decreasing the collision frequency of the Mu with the bare surface according to

$$\nu_c(n_1) = \nu_c(0)\left[1 - \sigma_A^{Mu} n_1\right] \qquad \text{Equation V·29}$$

where n_1 is the density of adsorbed atoms and σ_A^{Mu} is the elastic cross section for Mu scattering off an adsorbed atom. Also the available surface area for adsorption decreases to

$$A(n) = A(0)\left[1 - \sigma_A^{Mu} n_1\right] \qquad \text{Equation V·30}$$

Equation V·23 must then be rewritten with

$$\lambda_A = \left[A(0)\frac{\Lambda}{V_F} e^{B/kT} \lambda_B + \frac{f\sigma_{ex}}{2} m \nu_c(0)\left[1 - \sigma_A^{Mu} n_1\right]\right] \qquad \text{Equation V·31}$$

valid when $\lambda_B \bar{t} \ll 1$ and $\frac{A(n_1)\Lambda e^{B/kT}}{V_F} \ll 1$. Similarly, Equations V·27 and V·28 must be rewritten

$$R_{Mu}(t) = e^{-\nu_c(0)\left[1 - \sigma_A^{Mu} n_1\right]\left[P_t + \frac{f\sigma_{ex}}{2} m\right] t} \qquad \text{Equation V·32}$$

valid when $\lambda_B \bar{t} \gg 1$, $\nu_c(n_1) P_t \ll |\lambda_B - \lambda_F|$

and

$$R_{Mu}(t) = e^{-\lambda_B t} \qquad \text{Equation V·33}$$

valid when $\lambda_B \bar{t} \gg 1$, $\nu_c(n_1) P_t \gg |\lambda_B - \lambda_F|$.

CHAPTER VI : LOW TEMPERATURE STUDY OF MUONIUM IN Al_2O_3, SiO_2 AND MgO POWDERS

The simplicity of the H atom make it an ideal object of fundamental atom-surface interaction studies. In addition, the chemistry and physics of H atoms on solid surfaces may have industrial applications, especially in the field of catalysis. Since Mu can be considered a light isotope of H, having 1/9 the mass of H, the interest in H naturally extends to Mu. In the past this interest has been confined to studies in the gas, liquid, and solid phases. In this chapter the first experimental study of Mu interacting with solid surfaces is presented.

The present study consists of two experiments in which muons have been injected into high specific surface area oxide powders. In the first experiment, the fraction of muons which emerge into the voids as Mu at an ambient temperature of 6°K was measured. This obviously has important consequences in regard to the feasibility of studying Mu surface phonomena. It also represents a test of the thermal diffusion model (Section V·2), since, at low temperature, the diffusion length before decay is expected to be small in comparison with the particle size. For example, in bulk fused quartz, the Mu is believed to be stabilized at a single site below 50°K (Brewer 1981). The second experiment was undertaken to examine the interaction of Mu with γ-Al_2O_3 (Knozinger 1978) surfaces with varying amounts of adsorbed He and Ne.

VI·1 Mu in the Voids of Oxide Powders at 6°K

VI·1·1 Experimental Details

The μ^+SR apparatus is show in Figure VI·1. A beam of spin

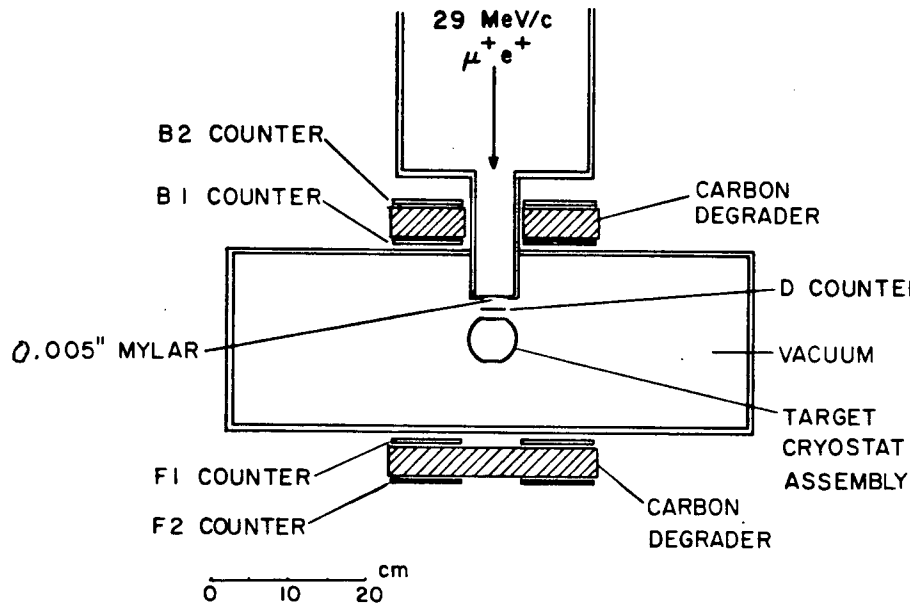

Figure VI·1 The μ^+SR apparatus "Beaver". Note that the positron telescopes are along the beam direction.

polarized positive "surface muons" of momentum 28 MeV/c from the M13 π-μ channel at TRIUMF (μ^+/e^+ ratio $\sim$ 1) was collimated to a 3/4 inch diameter spot, and passed through a thin (0.010 inch) defining counter (D), before entering a He gas flow cryostat. The dE/dx for 28 MeV/c muons is roughly 6 times that for 28 MeV/c positrons, so that surface muons can easily be discriminated from beam positrons. The incident muon rate was typically 10,000 μ^+/s. The target cryostat assembly is shown in Figure VI·2. The Mylar windows (35 mg/cm^2), the thin counter (29.5 mg/cm^2), helium gas (16 mg/cm^2) and aluminized Mylar

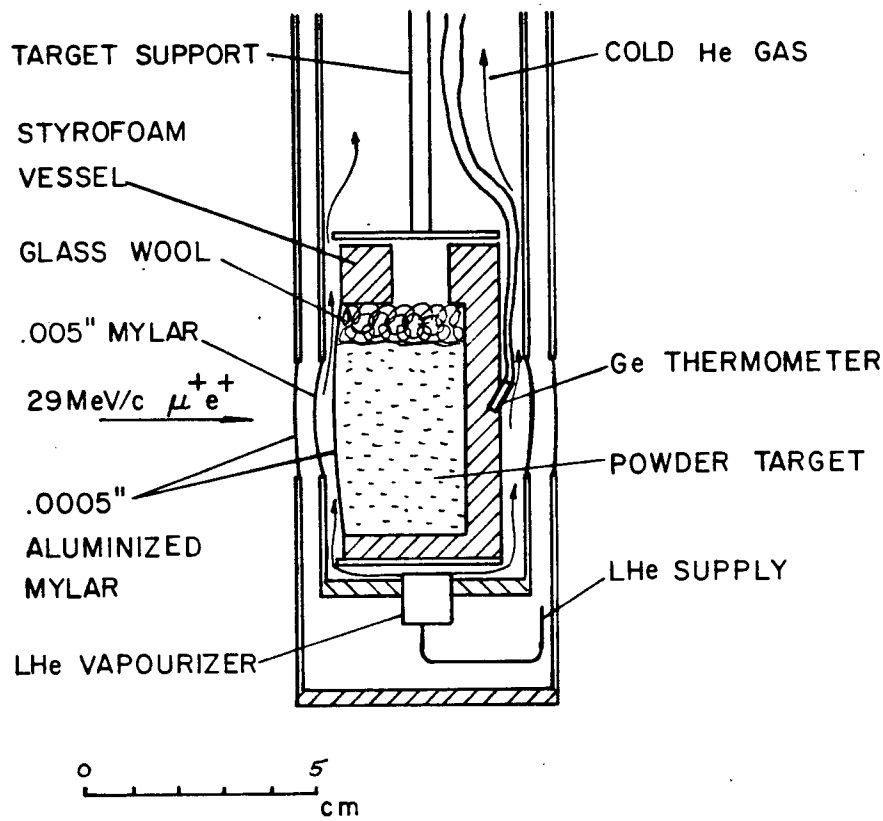

Figure VI·2 The target-cryostat assembly used to study Mu in oxide powders.

windows (3.5 mg/cm²) sum to a total of 84 mg/cm². Since the range of a 28 MeV/c surface muon is only 140 mg/cm² (of Carbon), 56 mg/cm² of target material are sufficient to stop all the muons.

Positrons from muon decay were detected in two telescopes positioned upstream and downstream of the target. Helmholz coils were used to apply a magnetic field perpendicular to the muon polarization direction.

Temperature measurements were made with a CryoCal CR2500H germanium resistor with an absolute accuracy of better than 30 m°K at all temperatures. A very careful human temperature controller maintained the temperature to within ±250 m°K. All

measurements were performed with the powders held in a He atmosphere at a pressure of 760 torr.

VI·1·2 Electronics

Figure VI·3 shows a schematic of the electronics, designed to measure the time interval between a single muon entering the target and its decay. At low incident muon rates ($<< 1/\tau_\mu$) this task is straightforward, but at higher rates precautions must be taken to minimize distortion effects due to pileup (more than one muon in the target at the same time). A "good" event satisfies the following conditions.

1. A muon arrives at t=0 with the microprogrammable branch driver (MBD) not busy and with no μ^+ having entered the target in the time interval $-P < t < 0$ (P is the pileup gate length; $\sim 10\mu s$). This condition starts the time digitizer.

2. A positron event defined by B1·B2 or F1·F2 occurs at $t = \tau$ ($\tau < P$) with no second muon having entered the target in the time interval $0 < t < \tau$. This stops the clock.

3. No second muon or second electron is detected in the time interval $\tau < t < P$.

A histogram of these time delays is termed a μ^+SR spectrum.

The μ^+SR data acquisition system consists of a PDP-11/40 computer and a CAMAC interface, driven by a microprogrammable branch driver (MBD-11). The dead time associated with processing an event is only $20\mu s$. This is made possible by using the relatively fast MBD to process an event and increment the appropriate histogram bin in the PDP-11/40 memory.

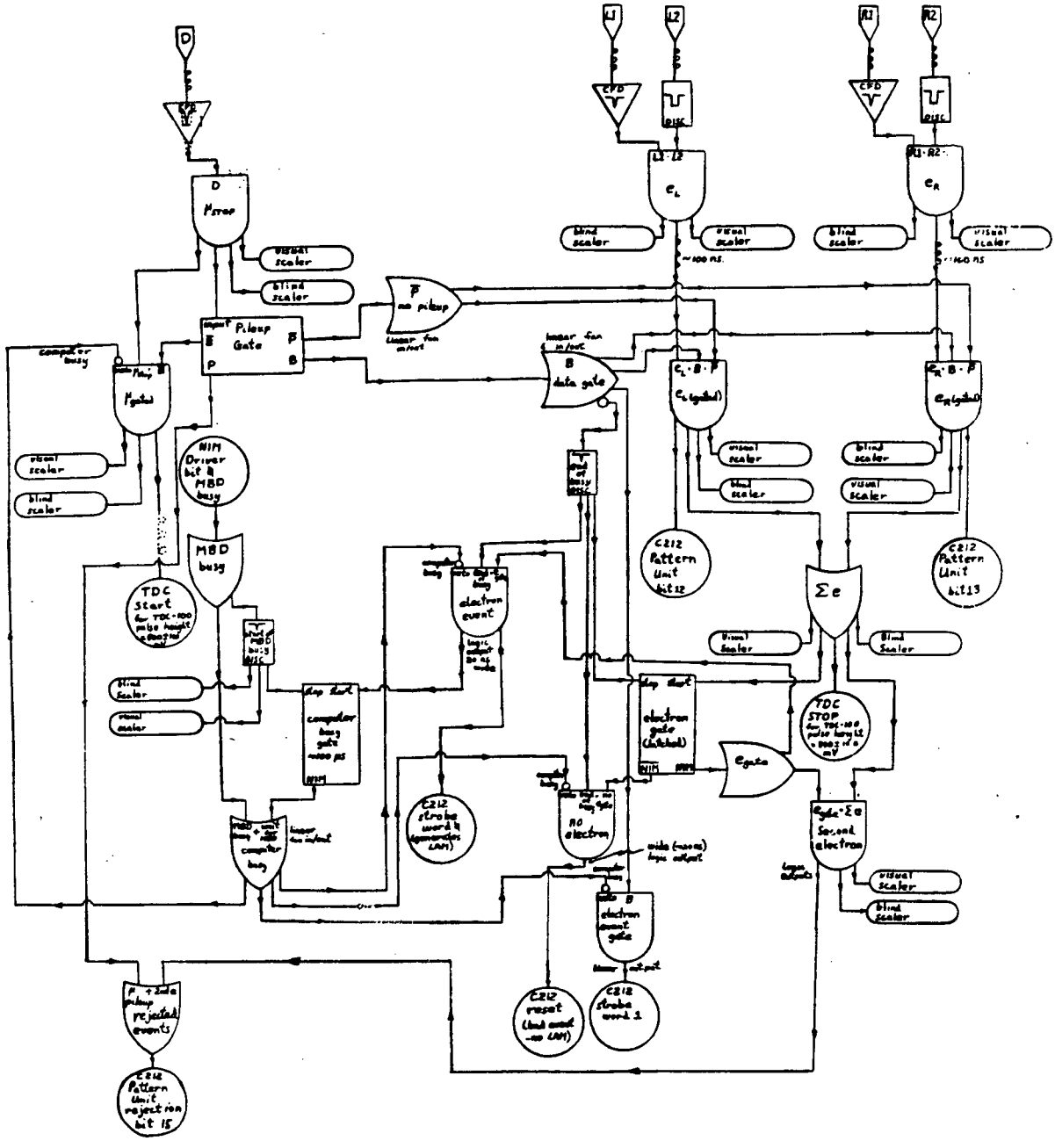

Figure VI·3 μ^+SR electronics that are used to measure the time interval between an incident muon and its decay positron (Garner 1981).

VI·1·3 Analysis and Results

μ^+SR spectra were taken in a transverse magnetic field of 8G in order to evaluate the Mu precession amplitude and its relaxation rate. The data were fitted to the functional form derived in Section IV·5

$$N(t) = N_0 e^{-t/\tau_\mu}[1 + S_\mu(t) + S_{Mu}(t)] + Bg$$

Equation VI·1

with

$$S_\mu(t) = A_\mu R_\mu(t) \cos(\omega_\mu t + \varphi_\mu)$$

$$S_{Mu}(t) = \frac{A_{Mu}}{2} R_{Mu}(t) \cos(\omega_- t + \varphi_{Mu})$$

Equation VI·2

where φ_μ and φ_{Mu} are the initial phases for free muon and Mu precession (determined by the orientation of the telescope relative to the muon polarization vector at t=0). The muon relaxation rates were very small for SiO_2 and MgO ($\sim 0.05\ \mu s^{-1}$), so the fits were insensitive to whether $R_\mu(t)$ was gaussian ($e^{-\beta^2 t^2}$) or exponential ($e^{-\lambda t}$). In the case of Al_2O_3, which has a high concentration of nuclear moments, better fits were obtained with a gaussian form with $\beta \sim 0.2\ \mu s^{-1}$. In theory, one expects the relaxation function for static muons interacting with only nearest neighbor dipoles to be gaussian (Pake 1948). In reality, the presence of paramagnetic impurities and muon mobility complicate the situation. However, since this study focusses on Mu in these targets, it suffices to say that the Mu precession parameters A_{Mu} and λ_{Mu} are only weakly correlated with the free muon relaxation function $R_\mu(t)$, and a gaussian form yielded good fits in all cases.

The general form of the relaxation function $R_{Mu}(t)$ for Mu in the voids of a powder is too complicated to use for fitting. However, the limiting forms consist of a single exponential or a difference of exponentials (Section V·5). If a fraction of the Mu remains inside the powder, then an additional component must be added. In the present experiment, good fits were obtained with a single exponential relaxation function $R_{Mu}(t) = e^{-\lambda t}$, except in the case of 140Å SiO_2 powder (see Figure IV·4). In this

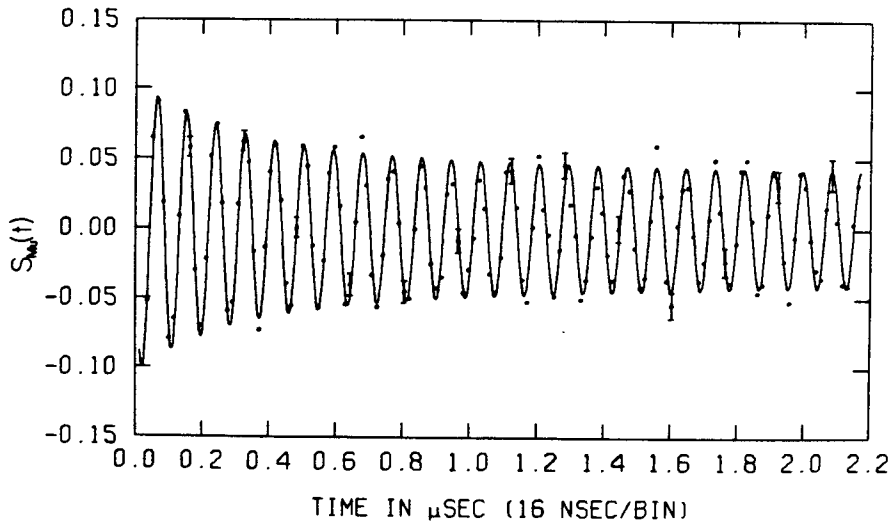

Figure VI·4 The Mu precession signal $S_{Mu}(t)$ (defined in Equation VI.2) for 140Å SiO_2 powder in a He atmosphere at 6°K.

particular case, a sum of exponentials [$R_{Mu}(t) = \alpha \exp(-\lambda_1 t) + (1-\alpha) \exp(-\lambda_2 t)$] gave a substantial improvement in the χ^2 per degree of freedom (315 for 301 degrees of freedom, compared with 401 for 303 degrees of freedom).

The Mu fractions were evaluated from the fitted parameters A_{Mu} by normalizing to the free muon amplitude in Al. It was assumed that all the muons injected into Al precess at the free muon Larmor frequency B·13.55 KHz G^{-1} (B in Gauss). The free muon precession background due to muons stopping in parts of the target vessel other than the powder itself was determined with an antiferromagnetic Fe_2O_3 powder target. Muons in Fe_2O_3 experience very large local magnetic fields and thus do not contribute to the free muon Larmor frequency. The Mu fractions were evaluated as

$$F_{Mu} = \frac{A_{Mu}(sample)}{A_{\mu}(Al) - A_{\mu}(Fe_2O_3)} \qquad \text{Equation VI·3}$$

The values for A_{μ} in Al and Fe_2O_3 were obtained from coarsely packed data taken at 45G, fitted to Equations VI·1 and VI·2 with $S_{Mu}(t)=0$.

Table VI·1 gives the Mu relaxation rates and fractions measured at 6°K in 760 torr of He. For comparison, the low temperature results for bulk oxides and the room temperature results for both bulk and powdered samples are included. The temperature dependence of the Mu relaxation rate in the Al_2O_3 powder is shown in Figure VI·5.

TABLE VI·1. μ^+SR results in bulk and powdered oxides.

Target	Temperature (K)	Mu Fraction (%)	Mu Relaxation Rate (μs^{-1})
SiO_2 bulk fused	6	79 ± 3 [b,g]	3.3 ± 0.5
SiO_2 bulk fused	295	79 ± 3 [b,g]	0.20±0.05
SiO_2 powder (70 Å)	6	49 ± 3	0.46±0.03
SiO_2 powder (70 Å)	295	61 ± 3 [d]	0.18±0.03
SiO_2 powder (140 Å)	6	35 ± 5 (1) [a,b]	4.1 ± 0.7 (1)
		35 ± 5 (2)	0.16±0.05 (2)
SiO_2 powder (140 Å)	295	45 ± 20 [b,f]	0.18±0.03
Al_2O_3 bulk fused	6	>80 [c]	>20
Al_2O_3 bulk fused	295	>80 [c]	>20
Al_2O_3 powder (75 Å)	6	29 ± 3	0.35±0.05
Al_2O_3 powder (75 Å)	295	35 ± 14 [d]	11.3 ± 4.4
MgO single XL	6	35 ± 10 [b]	6.3 ± 1.4
MgO single XL	295	35 ± 10 [b,e]	2.0 ± 0.5
MgO powder (300 Å)	6	12 ± 3	0.22±0.03
MgO powder (300 Å)	295	15 ± 3	1.9 ± 0.5

a The (1) and (2) refer to the two components resolved in the fit.
b Rough estimate using Mu asymmetries only.
c Esitmate based on the missing fraction presuming it to be Mu
d (Kiefl 1979)
e (Spencer 1981)
f (Marshall 1978)
g (Brewer 1981)

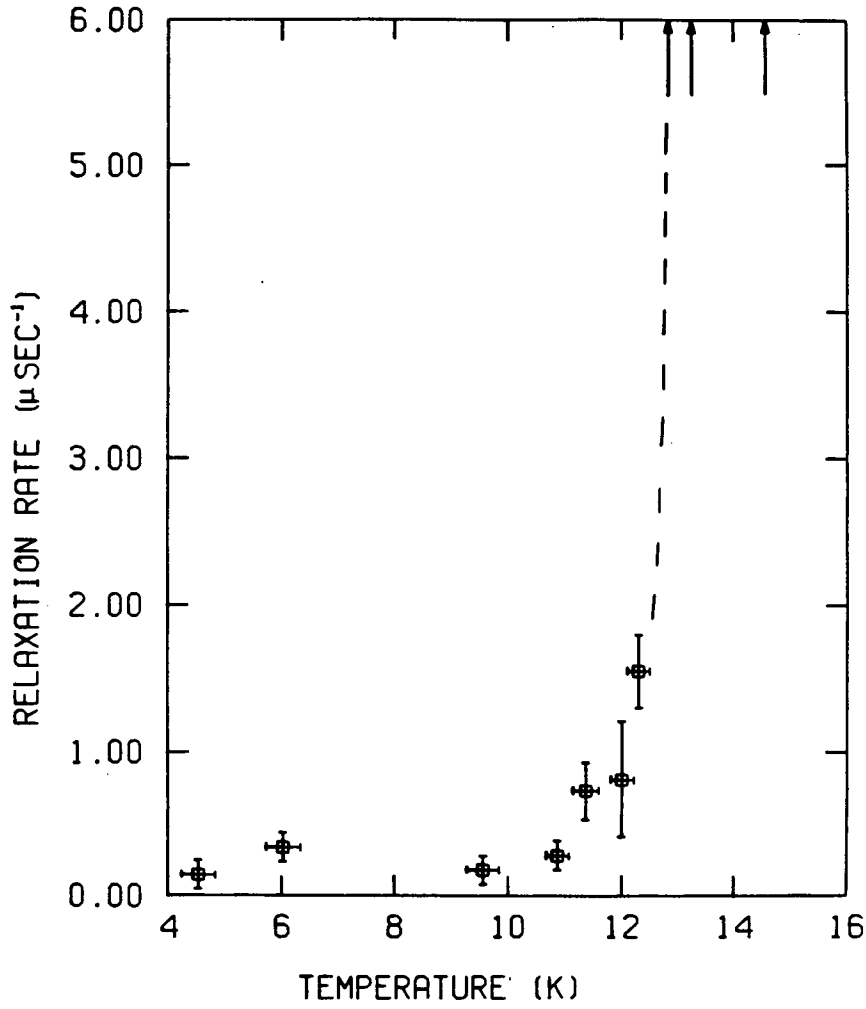

Figure VI·5 The temperature dependence of the Mu spin relaxation rate in Al_2O_3 powder in a He atmosphere. The arrows indicate points that are off scale.

VI·1·4 Discussion

VI·1·4·1 Mu in SiO_2 Powder at 6°K in a He Atmosphere

It is worth while to point out the varying conditions under which the SiO_2 powder targets in Table VI.1 were studied. . The room temperature 70Å and 140Å targets were evacuated to 10^{-6} torr, which effectively removes adsorbed water (see Cabot). The 70Å target at 6°K was admitted into a He gas flow cryostat in an open top vessel without evacuation. Thus it had adsorbed water plus whatever O_2 and N_2 was adsorbed during cooling (4 x 10^{-3} O_2

atoms per Å^2, 1.6 x 10^{-2} N_2 per Å^2, assuming that all the air in the target vessel was adsorbed). The 140Å target at 6°K was evacuated to 10^{-1} torr at 270°K before further cooling and thus had adsorbed water but little O_2 or N_2. Also, the cold runs were made in a dense atmosphere of He (760 torr of He at 6°K corresponds to a density of ~ 0.01 g/cm^3).

In regard to the results taken in a He atmosphere there is no Mu formation in He gas (Fleming 1981), so that the observed Mu originates from the powders. Although there is insufficient information to conclusively state that the surfaces play no role in Mu formation, the large Mu fraction in the bulk oxides(see Table VI.1) is indication that Mu formation is a bulk phenomenon. In some cases the observed Mu fraction in the powder is less than in the bulk. This may partly be explained in terms of a Mu component trapped inside the powder grains where the relaxation is very fast. Another possibility is that a portion of the Mu reacts epithermally with surface groups such as $(OH)^-$ to form a diamagnetic surface state such as $(OMu)^-$.

In both the 70Å powder and 140Å powder, a slowly relaxing Mu component was observed (0.46 ± 0.03 μs^{-1} and 0.157 ± 0.05 μs^{-1}, respectively). This component cannot be due to Mu inside the powder grains, since Mu is static in fused SiO_2 below 50°K and has a relaxation rate of 3.3 ± 0.5 μs^{-1}, attributable to random anisotropic distortion(Section IV·4·2). Therefore, the slowly relaxing component in the SiO_2 powder must be due to Mu which has thermalized in the voids. This is in contradiction to the ambient temperature thermal diffusion model (Section V·2) since, according to this model, no Mu would escape the powder

grains at low temperature where there is little or no diffusion. In fact, a second fast relaxing component (see Figure VI·4) in the 140Å powder (4.1 ± 0.7 μs^{-1}) is most likely due to Mu which is trapped inside the powder grains. The reason that such a component was not observed in the 70Å powder is probably due to the smaller particle size. Also the presence of O_2 on the surface could rapidly relax Mu within 15Å of the surface (essentially the entire powder grain). Such O_2 was not present in the 140Å powder.

It may seem surprising at first that O_2 on the surfaces does not have a more pronounced effect on the relaxation of Mu in the extragranular region. According to Equation V·20 one would expect that such a concentration of O_2 on the surface would lead to a Mu spin relaxation rate of roughly 120 μs^{-1}. However, it is well known that He readily adsorbs on such surfaces at this temperature (6°K) (See for examples Dash 1975). It is likely that a He film shields the Mu from depolarizing effects of the surface. More evidence for this will be given shortly.

VI·1·4·2 Mu in MgO Powder at 6°K

This sample was studied under the same conditions as the 70Å SiO_2, in an open-top non-evacuated vessel, and thus had H_2O, O_2 and N_2 on the surfaces.

A single long lived component was resolved whose amplitude agrees well with the room temperature value. However, the relaxation rate was substantially less at 6°K (0.22 ± 0.03 μs^{-1}) compared with that at 300°K (1.9 ± 0.5 μs^{-1}). Considering the

low purity of the MgO powder (see Table VI·2), it is unlikely that this component is due to Mu inside the powder grains. As in the case of the SiO_2, it is attributed to Mu in the extragranular region shielded from the surface by a He film.

VI·1·4·3 Mu in Al_2O_3 Powder (5°K - 20°K)

This target also had adsorbed H_2O, O_2 and N_2 (3 x 10^{-4} O_2 per Å^2 and 1.2 x 10^{-3} N_2 per Å^2 assuming that all the air was adsorbed on the powder surfaces). In addition, the sample contained an 1.8% paramagnetic Fe^{+3} impurity.(see Table VI.2)

Table VI·2. Properties of oxide powders.

Powder	Density (g/cc)	Surface Area (m^2/g)	Paricle Size(dia.) (Å)	Impurities
SiO_2 Cabot EH5	0.04	400	70	Na(20-40 ppm) P (<300 ppm) All other element less than 30 ppm (see Cabot)
SiO_2 Cabot M5	0.04	200	140	same as above
Al_2O_3 Davison SMR-7-7563	0.56	225	75	Fe^{+3}(1.8%)from (Fe_2O_3) SO_4 (.2%) SiO_2 (.08%) Na_2O (.03%) Cl_2 (<.01%)
MgO Matheson Coleman Bell MX 65-05	0.12	not available	300	Na (.5%) Cl(.01%) Ca (.05%) Ba(.005%) SO_4 (.02%) K (.005%) $NH_4(OH)$ (.02%) Sr(.005%) In (.01%) Heavy Metals(.003%) Mn(5ppm)

The observed long-lived component ($0.35 \pm 0.05\ \mu s^{-1}$) must not be due to Mu in the powder grains or adsorbed directly on the surface, since the Fe^{+3} impurity would relax such Mu at a rate of roughly $400\ \mu s^{-1}$ (see Section V·4·2). As in the case of the 70Å SiO_2, the adsorbed O_2 should relax extragranular Mu colliding directly with the Al_2O_3 surface. Again, the small relaxation is attributed to the presence of a He film on the oxide surface.

Convincing evidence for this He film hypothesis is shown in Figure VI·5, which displays the temperature dependence of λ in Al_2O_3. The sharp increase in λ above $12.5 \pm 0.5°K$ is attributed to vacancies in the film as the first monolayer begins to evaporate. A more detailed examination of this phenomenon is the subject of the following experiment.

VI·1·5 Summary and Conclusion

A slowly relaxing Mu component ($\lambda \sim 0.2\ \mu s^{-1}$) has been observed in Al_2O_3, SiO_2, and MgO powders in a He atmosphere at 6 °K. It is attributed to Mu outside the powder grains colliding freely with He coated oxide surfaces. In the 140 Å SiO_2 powder an additional fast relaxing component was also resolved and attributed to Mu trapped inside the powder grains. The dramatic increase in Mu spin relaxation rate in Al_2O_3 above 12.5 °K is thought to be due to evaporization of the He film.

In conclusion, it appears that a sizeable fraction of the Mu atoms emerge into the void regions of these oxide powders regardless of temperature and that the presence of a He film on the oxide surfaces inhibits Mu spin relaxation.

VI·2 Spin Relaxation of Mu in Al_2O_3 Powder with Adsorbed He/Ne

In this section further evidence is presented which substantiates the above conclusion at least in the case of Al_2O_3 powder. The Mu spin relaxation rate has been measured as a function of adsorbed gas per unit surface area at constant temperature. Both He and Ne gases were used as an adsorbate. Isotherms were measured at 7.3°K and 10.4°K for He and 28.7°K and 30.3°K for Ne. The spin relaxation rate is a steep, linearly decreasing function of adsorbed gas below monolayer completion and is virtually independent of the amount of adsorbed gas at higher coverages.

VI·2·1 Experimental Details

The TRIUMF/Lawrence Berkely Laboratory (LBL) surface muon apparatus, "Eagle" (see Figure VI·6), was used in this experiment. The main difference between this apparatus and that described in Section VI·1 is the additional left and right positron telescopes, which are in general more suited for transverse field μ^+SR since they are less sensitive to scattering of beam positrons.

The TRIUMF M9 π-μ channel equipped with a 3m long Wien filter velocity selector, or "DC separator", set at $\bar{E}$ = 3.9 kV/cm $\hat{x}$, $\bar{B}$ = 48 G $\hat{y}$, was used to obtain a clean beam (e^+ contamination undetectable) of 28 MeV/c "surface muons". An added effect of the separator was to rotate the muon polarization by a small vertical angle (9°) relative to the beam direction. Muons entering the target region were collimated to a

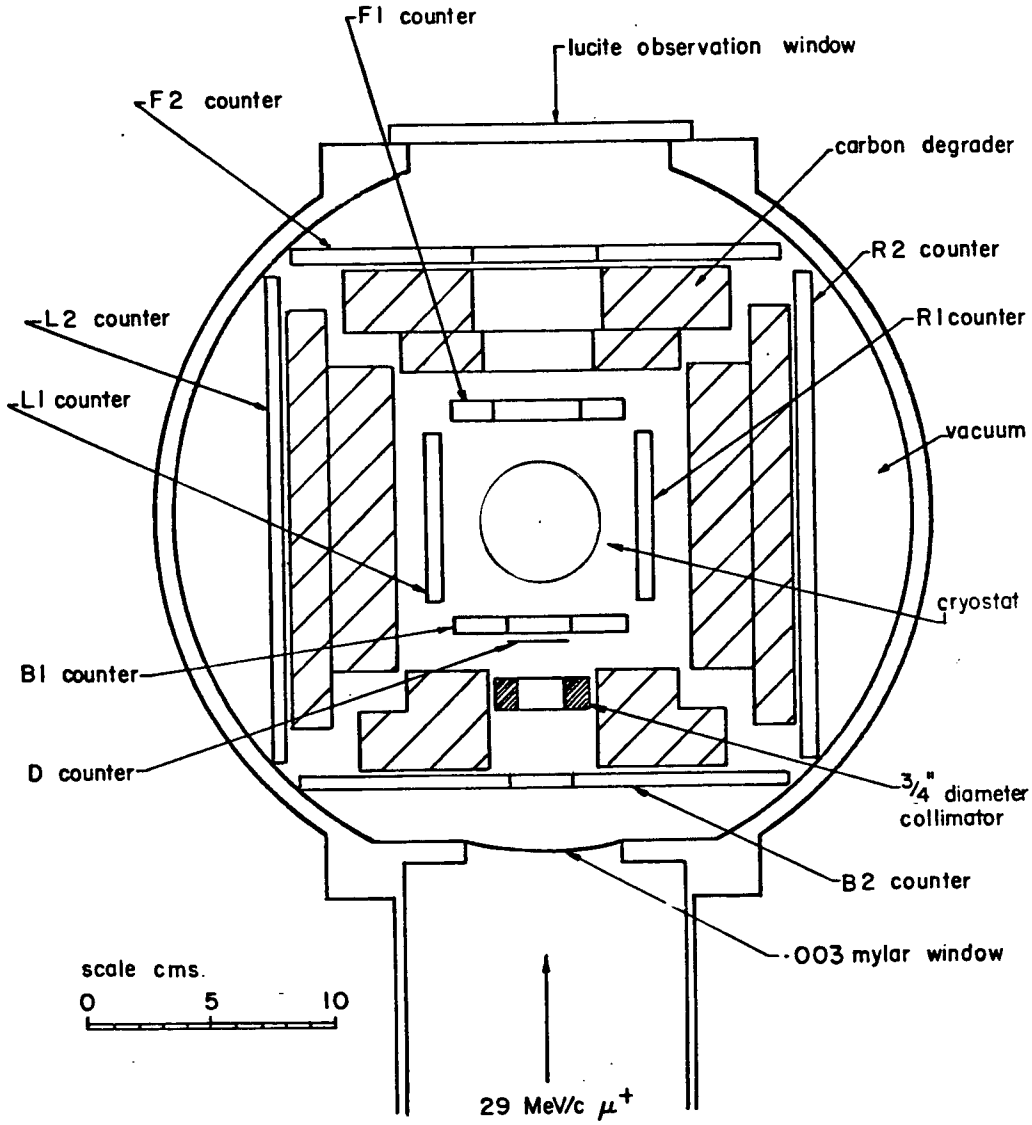

Figure VI·6 The μ^+SR apparatus "Eagle". Note the four positron telescopes.

3/4 inch diameter spot before detection by a thin (0.010 inch) scintillator. Typical incident muon rates were 30,000/s.

The He leak tested target vessel (see Figure VI·7) was constructed from stainless steel with two 1 inch diameter 0.001 inch thick stainless steel windows.

The Al_2O_3 powder sample (weighing 10.5g) was baked at 500°C

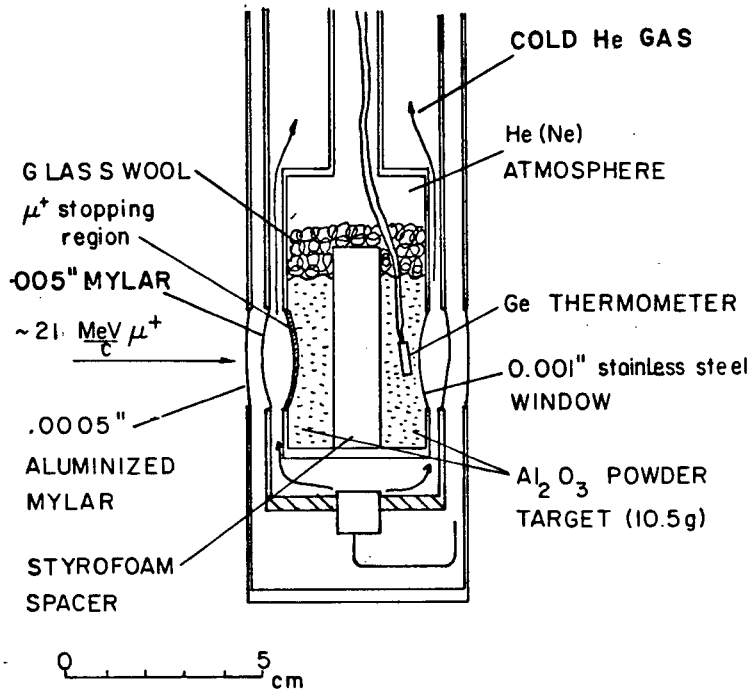

Figure VI·7 The powder target vessel and cryostat used to study Mu relaxation versus He/Ne coverage. Note the target vessel is isolated from the He atmosphere of the cryostat.

for 24 hours in air and cooled in a dessicator before being placed in the target vessel. Adsorbed water on γ-Al_2O_3 forms hydroxyl groups with heated above 100°C, so that the surface was likely terminated by a layer of hydroxyl groups (Knozinger 1976). . The vessel was then soldered to the gas handling system and evacuated to 10^{-5} torr for a period of 24 hours immediately prior to the experiment.

A CryoCal 2500L germanium resistor with an absolute accuracy of better than ± 30 m°K at all temperatures studied was used to monitor the temperature and control it to within ± 60 m°K.

The all-metal (stainless steel and copper) gas handling apparatus (Figure VI·8) was composed primarily from 1/4 inch

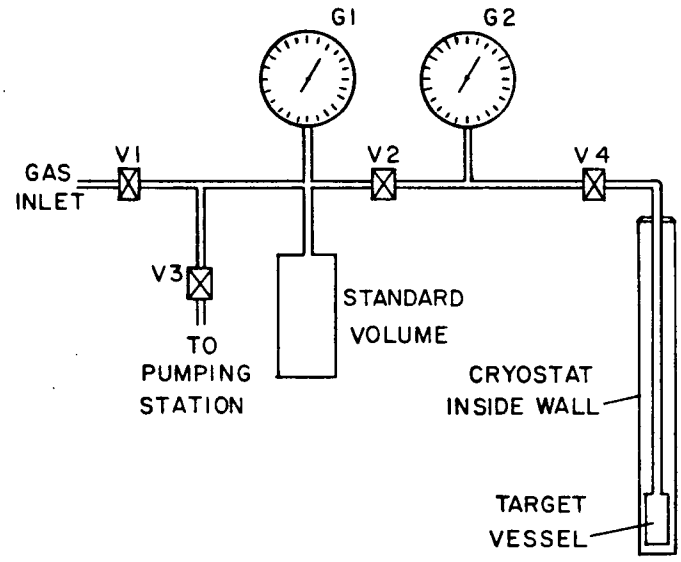

Figure VI·8 The gas handling system used to deposit controlled amounts of He/Ne on γ-Al_2O_3 powder.

tubing, Swagelock fittings and Nupro bellows valves. The vapour pressure measurements in the target vessel were made with a Wallace and Tiernan pressure gauge (0-800 torr)(G2), accurate to ±0.5 torr. The pressure difference measurements were made with a Matheson 6301 stainless steel absolute pressure gauge (0-760 torr)(G1), accurate to ± 2 torr. The system was evacuated to 10^{-4} torr and He leak tested prior to the experiment. High purity grade ^{4}He (99.995%) and purified grade ^{20}Ne (99.99%) were used as adsorbates.

VI·2·2 Electronics

The electronics are as described in Section VI·1 with a minor modification to allow acquisition of four histograms instead of the two used in the first experiment.

VI·2·3 Procedure

The experimental procedure consisted of admitting a controlled amount of adsorbate into the target vessel held at constant temperature, recording the vapour pressure, and collecting a μ^+SR spectrum. The precise steps were as follows (with the system initially under vacuum and all valves closed except V4, which was open for the entire experiment).

1. V1 was opened to pressurize the standard volume (1368 ± 20 cc) bounded by V1, V2, and V3.
2. The pressure on gauge G1 was recorded.
3. V2 was opened and closed to admit a small amount of gas (80 cc at STP) into the target vessel volume bounded by V2.
4. The pressure on G1 was recorded again so that the amount of gas admitted into the target volume could be calculated.
5. The pressure and temperature in the target vessel were stabilized over a 30 minute period and the vapour pressure recorded (G2).
6. An μ^+SR spectrum was taken (4 million events) over a period of about one or two hours.
7. The pressure in the target vessel, G2, was recorded again. The difference from before and after the run was typically 1 or 2 torr, indicating that the system was very close to thermal equilibrium.
8. Steps 3 through 7 were repeated until more than a monolayer of gas was adsorbed.

Afterwards the powder was removed and replaced with a piece of aluminum of volume m / ρ_{bulk}, where m is the mass of powder

(10.5 g) and ρ_{bulk} is the density of bulk Al_2O_3 (3.7 g/cm^3). Steps 1 through 5 were repeated. The pressure in the target vessel was found to be a linear function of the amount of gas admitted for each temperature studied. The amount of gas adsorbed on the Al_2O_3 surfaces(in units of cc at STP) at a given temperature and vapour pressure was determined from the difference between the amount of gas admitted with and without powder. The specific surface area (225m^2/g as specified by Davison Chemicals) and total mass of the powder (10.5 g) were then used to determine the number of adsorbed atoms per unit surface area.

VI·2·4 Analysis and Results

The μ^+SR data analysis was done exactly as described in Section VI·1·3. Good fits were obtained with a single exponential relaxation function for the Mu precession signal. The results from the left and right telescopes were averaged as a last step.

The Mu spin relaxation rate as a function or the number of adsorbed ^{4}He atoms per unit area at 7.3°K and 10.4°K is shown in Figure VI·9. For comparison, the vapour pressure in the vessel at each coverage is also plotted. Similar results for ^{20}Ne adsorbed on Al_2O_3 are shown in Figure VI·10.

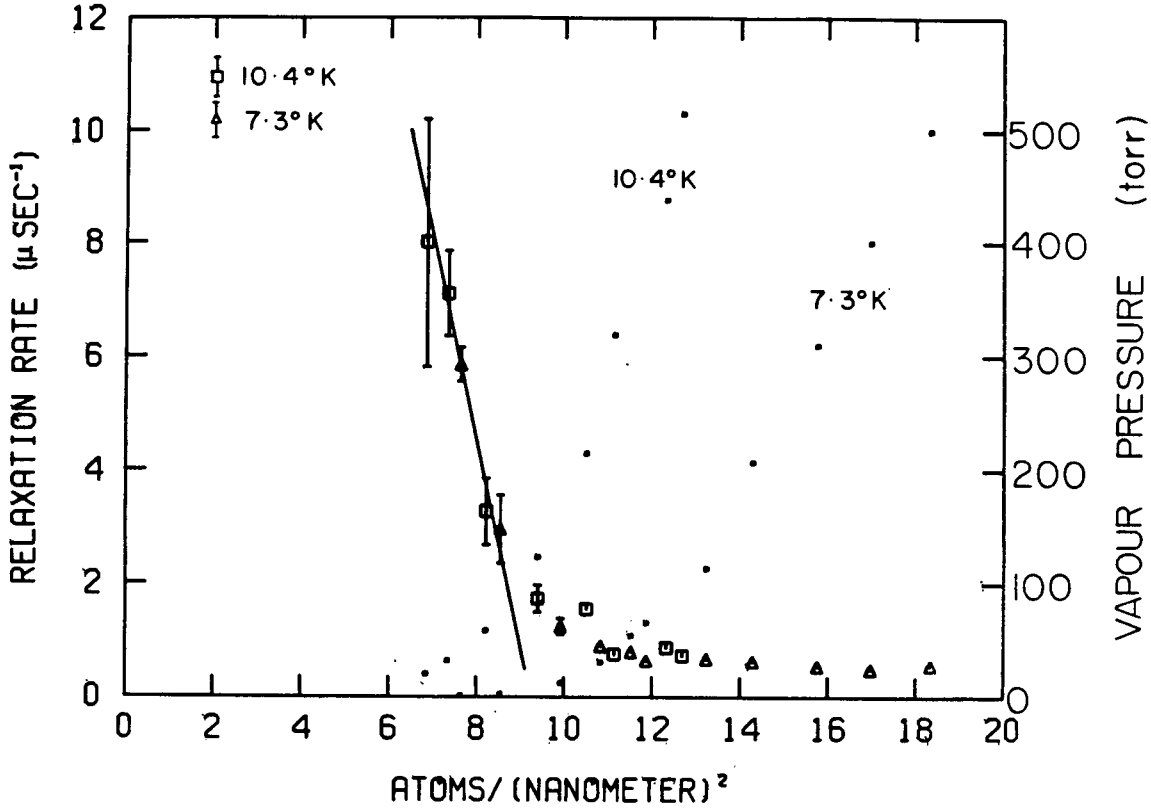

Figure VI·9 The Mu spin relaxation rate in Al_2O_3 powder versus adsorbed He at 7.3°K and 10.4°K. The dots represent the vapour pressure at each coverage.

VI·2·5 Discussion

VI·2·5·1 Adsorption Isotherms of He on Al_2O_3

Vapour pressure isotherms are a common means of determining the amount of gas required to complete a monolayer. The point on the isotherm at which the density of adsorbed atoms becomes a linear function of vapour pressure is a rough indication of the monolayer density (Brunauer 1938). This is referred to as the point B method.

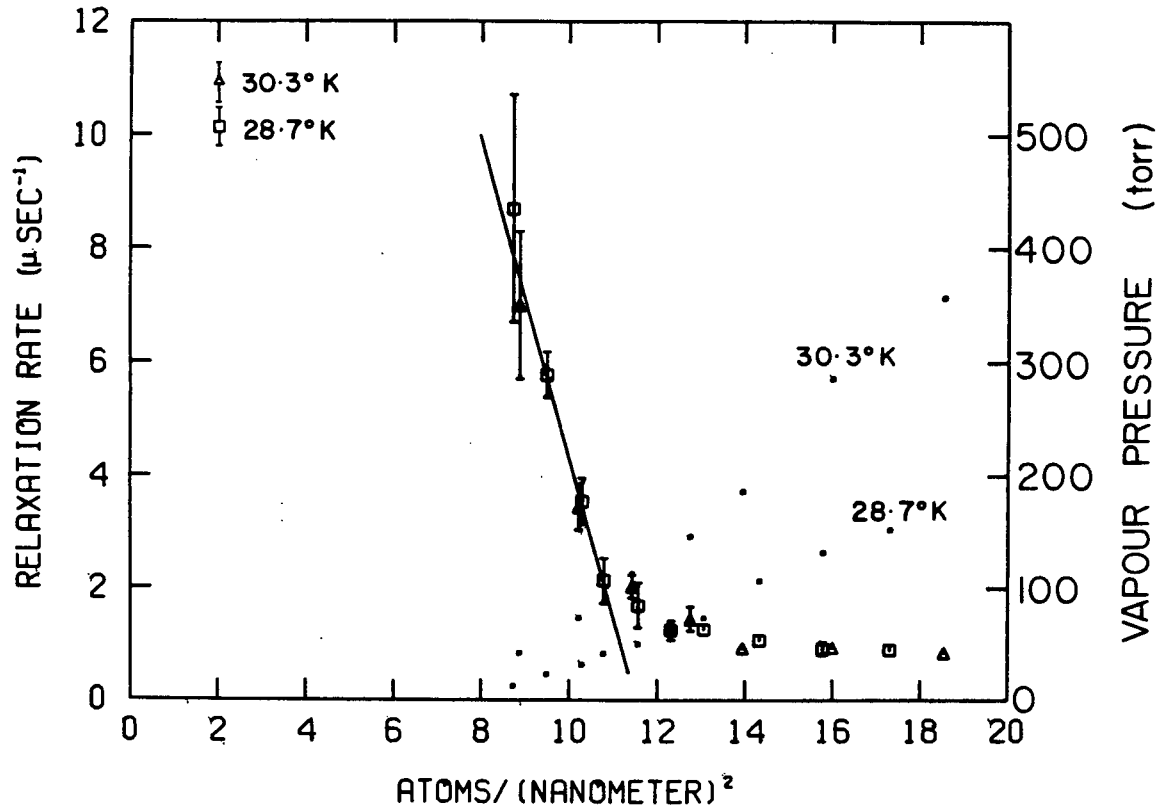

Figure VI·10 The Mu spin relaxation rate in Al_2O_3 powder versus adsorbed Ne at 30.3°K and 28.7°K.

Applying this method to the 7.3°K and 10.4°K ^{4}He adsorption isotherms (see Figure VI·9) yields a monolayer density $n_m(7.3°K) = 0.125 \pm 0.01 Å^{-2}$ and $n_m(10.4°K) = 0.10 \pm 0.01 Å^{-2}$. The effective hard sphere cross section assuming a close packed 2 dimensional array, $\sigma_{He}^{He} = \frac{\pi}{2\sqrt{3}\, n_m}$, is then $8.6 \pm 0.5 Å^2$ at 10.4°K and $7.3 \pm 0.5 Å^2$ at 7.3°K. For comparison the hard sphere cross section of ^{4}He on graphite at 4.2°K, obtained from the monolayer density, 0.123

Å² (Dash 1975), is 7.9 Å², whereas for liquid He at 4.2 °K, assuming a simple cubic packing factor is $\pi\rho^{-2/3}/4) = 10.4$ Å². Aston (1955) has compared the properties of adsorbed He to those of bulk He under an effective pressure. The slight temperature dependence of n_m indicates there may be some thermal expansion of the film between these two temperatures, although the non-uniformity of these surfaces along with the rough nature of the point B method cannot be ruled out as a cause.

VI·2·5·2 Mu Spin Relaxation in Al_2O_3 Powder With Adsorbed He

The μ^+SR data taken on Al_2O_3 with adsorbed He is also shown in Figure VI·9. Below monolayer completion, the Mu spin relaxation rate fits well to a linear function of adsorbed He, independent of temperature. Above monolayer completion, the relaxation rate rapidly levels off at a constant value $\lambda_0 \sim 0.54 \pm 0.05\ \mu s^{-1}$.

The interpretation is quite simple. The Mu relaxation rate is proportional to the fraction of exposed surface area:

$$\lambda(n_1) = \begin{cases} k\left(1 - n_1 \sigma_{He}^{Mu}\right) + \lambda_0 ; & n_1 \leq \dfrac{1}{\sigma_{He}^{Mu}} \\ \lambda_0 ; & n_1 > \dfrac{1}{\sigma_{He}^{Mu}} \end{cases}$$

Equation VI·4

where n_1 is the density of adsorbed atoms in the first layer only, σ_{He}^{Mu} is the total elastic cross section for Mu scattering off an adsorbed He atom, k is a constant (to be discussed shortly) and λ_0 is a constant relaxation rate unrelated to the Mu-Al_2O_3 surface interaction. There are at least three factors which contribute to λ_0.

1. In a transverse field of 8 G, the splitting (Ω) of the Mu precession frequencies is 0.178 μs^{-1}. The effect of fitting these two frequencies to a single component yields an apparent relaxation $\lambda \sim \Omega$.

2. The target vessel was contructed from slightly magnetic stainless steel causing a small field inhomogenity over the effective target volume.

3. The He used in the experiment was 99.995%, so that impurities may have caused a small relaxation.

At low coverage, n_1 is simply the total amount of adsorbed gas (this explains the linear behaviour of $\lambda(n)$ below monolayer completion) whereas at higher coverages, $n_1 \dashrightarrow n_m$, the monolayer density, and thus $\lambda(n) \dashrightarrow \lambda_0$. There was no marked temperature dependence in $\lambda(n)$, and therefore the combined data at 7.3 and 10.4°K were fitted to a linear function at low coverage, yielding $k = 32.9 \pm 0.3\ \mu s^{-1}$ and $\sigma_{He}^{Mu} = 11.0 \pm 0.2\ \text{Å}^2$.

Not surprisingly, the hard sphere cross section of helium, σ_{He}^{He} at 7.3 and at 10.4°K ($7.3 \pm 0.5\text{Å}^2$ and $8.6 \pm 0.5\text{Å}^2$ respectively) determined from the adsorption isotherms is slightly different than σ_{He}^{Mu}. This could easily be explained classically as due the finite size of the Mu atom which also contributes to the He-Mu scattering cross section. Perhaps more correctly this difference can be explained by the fact that σ_{He}^{He} is determined by the by the He-He-surface interaction, whereas σ_{He}^{Mu} is determined by the He-Mu-surface interaction.

The linear dependence of $\lambda(n)$ at low coverage is consistent with two limiting cases discussed in Section V·6. They are:

1. $\lambda_B \bar{t} \ll 1$ $\quad \frac{A(n)}{V_F} \Lambda e^{B/kT} \ll 1$

for which $\quad k = \left[\frac{A(0)}{V_F} \Lambda e^{B/kT} \lambda_B + \frac{f \sigma_{ex} m \nu_c(0)}{2} \right]$

Equation VI·5

2. $\lambda_B \bar{t} \gg 1$ $\quad \nu_c(n) P_t \ll |\lambda_B - \lambda_F|$

for which $\quad k = \nu_c(0) \left[P_t + \frac{f \sigma_{ex} m}{2} \right]$

Equation VI·6

Considering the strong binding of H to the bare surfaces (Section V·3) and the large value of λ_B expected because of the Fe^{+3} impurity (400 μs^{-1} for static Mu, see Section V·4·2) limiting case 2 must be favoured.

It is difficult to extract any more information from the the present results, such as a value for P_t, without making unjustified assumptions. The contribtion to k from spin exchange with the Fe^{+3} on the surface is not known. Further experiments on a paramagnetic free sample would eliminate this unknown. Furthermore only an upper limit on the collision frequency with the surface is known, since Mu at low temperatures may scatter off the aggregate structures rather than off the primary particles just as in the case of Ps (see Section III.3.1). This could cause a significant decrease in ν_c. Despite these uncertainties it is interesting to estimate P_t under the assumptions that the entire surface area is equally accessible to the Mu, in which case $\nu_c(0)$ at 7.3°K is 4.3×10^4 μs^{-1}, and

that the spin exchange rate is negligable. One then finds the trapping probability P_t to be 0.00074. In the future it should be possible to measure P in well characterized samples where ν_c is known.

VI·2·5·3 Adsorption Isotherms of Ne on Al_2O_3

Applying the point B method gives an effective hard sphere cross section for adsorbed Ne, $\sigma_{Ne}^{Ne} = 7.9 \pm 1.0$ Å^2 at 30.3°K and 8.6 ± 1.0 Å^2 at 28.7°K. For comparison, σ_{Ne}^{Ne} on graphite near 20°K is 7.37Å^2 (Huff 1975), whereas a layer of liquid neon at 27.1°K corresponds to $\sigma_{Ne}^{Ne} = 7.23$ Å^2. The agreement between all these methods is indication that Ne atoms are much like hard spheres.

VI·2·5·4 Mu Spin Relaxation in Al_2O_3 Powder With Adsorbed Ne

The shape of the relaxation rate versus density of adsorbed Ne atoms was identical to that observed for He. As in the case of He, no marked temperature dependence was observed between 30.3°K and 28.7°K. Fitting the region below 0.11 atoms Å^{-2} to Equation VI·2 with $\lambda_0 = 0.85 \pm 0.08$ μs^{-1} gives $k = 31.4 \pm .3$ μs^{-1} and $\sigma_{Ne}^{Mu} = 8.9 \pm 0.2$Å^2.

The value of σ_{Ne}^{Mu} obtained from the fit is in fair agreement with σ_{Ne}^{Ne} obtained from the adsorption isotherms. and is substantially lower than σ_{Ne}^{Mu}. This might be due to the stronger attraction the Mu feels toward the Ne, which could enhance the probability of trapping and thus decrease the the elastic cross section.

Surprisingly, the value obtained for k is close to that observed at the lower temperatures (7.3°K and 10.4°K) in the case of He. Unfortunately, since the temperature dependence for the spin relaxation rate and the trapping rate in Equation IV·4 are both unknown, this observation cannot be used to conclusively distinguish one from the other.

The measureably larger value of λ_0 in the case of Ne is probably due to the higher impurity level in the Ne as opposed to the He.

VI·2·6 Status of the ATTD Model

According to the ambient temperature thermal diffusion (ATTD) model the Mu thermalizes at the ambient temperature inside the grains, diffuses to the oxide surface, and is ejected into the voids because of a negative work function. However, since Mu is static in bulk oxides such as SiO_2 below 50 °K (Brewer 1981), the ATTD model fails to explain the copious amount of Mu in the voids of these powders at low temperatures. A simple model that explains why Mu might thermalize directly in the voids is given in Appendix III

VI·2·7 Conclusion

It has been shown that Mu emerges from 75Å Al_2O_3 powder grains below 30°K in low density He and Ne atmospheres (10-760 torr). The Mu spin relaxation rate is linearly dependent on the amount of exposed surface area. This substantiates the conclusions reached in the previous experiment (Section VI.1.5).

The effective cross section for elastic scattering of Mu off adsorbed He (7.3 to 10.4°K) and Ne (28.7 to 30.3°K) have been measured to be 11.1 ± 0.1Å^2 and 8.9 ± 0.2Å^2 respectively.

A new technique for studying the properties of these oxide surfaces and adsorbed atoms on them has been demonstrated.

CHAPTER VII : MUONIUM IN THE CONDENSED PHASES OF Ar, Kr AND Xe

Motivation for studying Mu in the condensed phases of Ar, Kr, and Xe is easy to find. Firstly, when a muon stops in matter it leaves a hot track of excited and ionized species. There has been considerable debate in recent years on the effect of this track on Mu formation and relaxation (Percival 1981, Walker 1981). Since the properties of the track are phase dependent it is of interest to study the effect of phase (gas, liquid and solid) on Mu formation and relaxation. In this chapter the first observations of Mu in the condensed phases of Ar, Kr and Xe are reported. These measurements, along with the existing gas phase data (Fleming 1981b) represent the first complete μ^+SR study of an element in all three phases.

Secondly, H atoms have been stabilized and studied in solid Ar, Kr, and Xe using ESR. The ESR measurements are sensitive to lattice-induced perturbations of the hyperfine contact interactions as well as to the presence of nuclear moments. In principle, isotopic dependence of these effects can be studied using μ^+SR .

Finally, there have been several studies of chemical reactions of H atoms with impurities such as C_4H_{10} deposited in solid Xe (Kinugawa 1978, Iwasaki 1978). In the past μ^+SR has been used very successfully in exploring isotopic effects of H atom chemistry in gas and liquid phases. If there is a large Mu fraction in the solid phase of these elements isotopic effects of the above mentioned H atom reactions in the solid phase could be studied.

VII·1 Experimental

The muon beam has been described in Section VI·1·1. The LBL surface muon apparatus has been shown in Figure VI·5. The target vessel (Figure VII·1) was constructed from copper and stainless

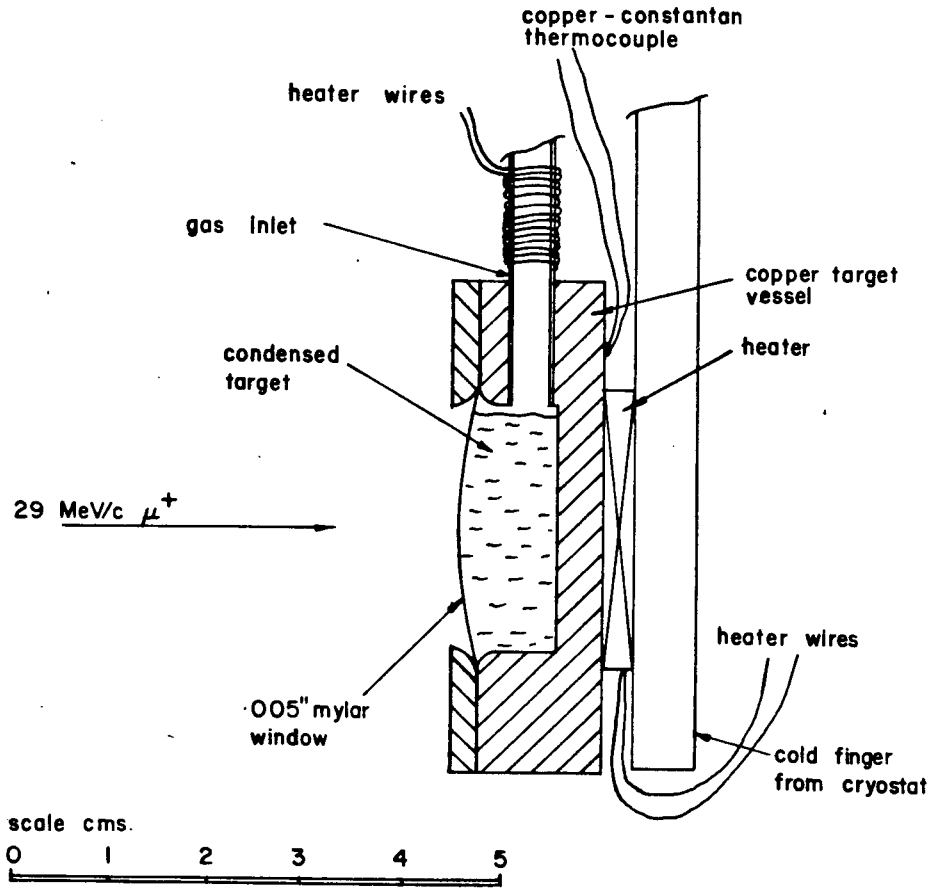

Figure VII·1 The target vessel used to condense noble gases.

steel except for the mylar window. The vessel was mounted on a rotatable LN_2 cryostat such that condensation and solidification of the gas could be observed prior to facing it towards the beam. The target gases (ultra high purity Xe, ultra high purity Kr, and research grade Ar) were admitted via the gas inlet tube (Figure VII·1). The vessel was equipped with two heaters, one on

the gas inlet to prevent blockages, and a second mounted between the copper vessel and the cold finger of the cryostat for temperature control. Two copper constantan thermocouples were used to monitor the temperature (controlled to ±1°K).

The μ^+SR electronics have been described in Section VI·1·3.

VII·2 Data Analysis and Results

μ^+SR spectra were taken in a transverse field of 65G in order to determine the free muon fraction. The data were coarsely binned and fitted to Equation VI·1 with $S_\mu(t)$ given by Equation VI·2 and $S_{Mu}(t) = 0$ The parameter of interest, A_μ, did not depend on whether $R_\mu(t)$ was gaussian or exponential. The free muon fractions in Table VII·1 were determined from

$$F_\mu = \frac{A_\mu(\text{sample}) - A_\mu(Fe_2O_3)}{A_\mu(Cu) - A_\mu(Fe_2O_3)} \qquad \text{Equation VII·1}$$

μ^+SR spectra were also taken in a low transverse field 8 G in order to determine the Mu fraction. The data were fit to Equation V·1 with $S_\mu(t)$ and $S_{Mu}(t)$ given by Equation V·2 and with $R_\mu(t) = e^{-\beta^2 t^2}$. In all cases except liquid Ar and solid Kr, good fits were obtained with a single component Mu relaxation function ($R_{Mu}(t) = e^{-\lambda t}$). There were seven free parameters, N_0, ω_μ, A_{Mu}, ω_{Mu}, ϕ_{Mu}, λ and Bg. The parameters A_μ, β and ϕ_μ were held fixed at the values obtained from the high field data. In the cases of liquid Ar and solid Kr, considerably better fits were obtained with a two component Mu relaxation function [$(R_{Mu}(t) = \alpha e^{-\lambda_1 t} + (1 - \alpha)e^{-\lambda_2 t}$]. The improvement in the χ^2 was significant:

Table VII·1. μ^+SR results in condensed Ar,Kr,and Xe.

Target Substance	Temperature K	Free Muon Fraction[a] %	Mu Fraction(s)[b] %	Missing Fraction %	Mu Relaxation Rate(s) μsec^{-1}	Mu Hyperfine Splitting[c] MHz
Liquid Ar	85	1.6 ± 1.0	(1) 48 ± 6	3 + 29	(1) 0.65 ± 0.12	
			(2) 49 ± 28		(2) 19.0 ± 11.0	
Solid Ar	77	0.8 ± 0.2	91 ± 9	8 ± 9	0.15 ± 0.03	4463.8 ± 6.0
Liquid Xe	162	3.3 ± 0.8	43 ± 9	54 ± 10	2.07 ± 0.21	
Solid Xe	150	5.0 ± 3.3	79 ± 25	16 ± 28	19.0 ± 2.5	
Liquid Kr	120	6.5 ± 0.1	57 ± 10	36 ± 10	3.6 ± 0.9	
Solid Kr	90	1.4 ± 1.8	(1) 71 ± 7	0 ± 10	(1) 6.68 ± 0.20	4462.9 ± 3.7
			(2) 29 ± 7		(2) 0.89 ± 0.04	

[a] These fractions were determined from data at ~70 G.

[b] These fractions were determined from data at ~8 G except for solid Xe where the fraction was from ~70 G data.

[c] The vacuum hyperfine splitting is 4463.302 MHz.

from 164 (145 degrees of freedom) to 126 (143 degrees of freedom) for solid Kr and from 169 (145 degrees of freedom) to 154 (143 degrees of freedom) for liquid Ar. The Mu fractions in Table VII·1 were determined from Equation VI·3. For comparison the results in the gas phase are shown in Table VII·2.

In the case of solid Xe, the relaxation rate of Mu was so fast that a reliable measure of the Mu asymmetry and relaxation rate was not possible in low field. It was necessary to use data taken at 70G(where the precession signal is more complicated) to determine the Mu fraction and relaxation rate. The data were fit to Equation VI·1 with

Table VII·2. Mu Fraction in Gas Phase Ar, Kr, and Xe.[a]

Target	Pressure (atmospheres)	Mu Fraction[b] %	Free Muon Fraction[b] %
Ar	2.5	75	24
Kr	0.9	100	3
Xe	0.65	100	3

[a] from (Fleming 1981b)
[b] error estimate is 5%

$$S_{Mu}(t) = \frac{A_{Mu}}{2}\{\cos^2\varphi\cos[(\omega_- - \Omega)t + \varphi_{Mu}] + \sin^2\varphi\cos[(\omega_- + \Omega)t + \varphi_{Mu}]\}e^{-\lambda t}$$

Equation VII·2

This expression is valid at intermediate transverse fields 65G (see Section IV·5). The parameters A_μ, β, N_0, ω_μ and ϕ_μ were fixed at the values obtained from the coarsely binned data. The parameters ϕ (not to be confused with ϕ_μ and ϕ_{Mu}) and Ω are functions of the applied field (B) and the hyperfine frequency (ω_0) (see Section IV·3·2). In this fit, ω_0 was set to the vacuum value, leaving four free parameters, A_{Mu}, λ, ϕ_{Mu} and B_g.

The relaxation rate of Mu in solid Ar and Kr was sufficiently small so that the two normal Mu frequencies could be resolved at an intermediate field of 66G (See Section IV.3.2). The difference between these frequencies is a function of B and ω_0 (Equation IV.31) and thus provides a measurement of ω_0. The two frequency precession of Mu in solid Ar at 66 G is shown in Figure VII·2. The hyperfine splitting determined in

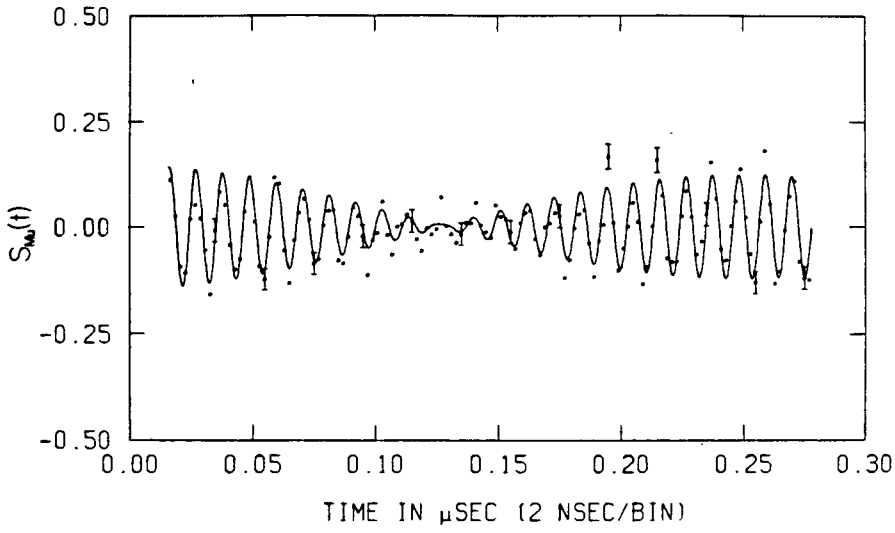

Figure VII·2 Two freqency Mu precession signal in solid Ar at 77°K in high field (66 G).

this way is also given in Table VII·1.

VII·3 Discussion

VII·3·1 Mu in Liquid and Solid Ar

The free muon component in both liquid and solid Ar is extremely small (<2%). This is a strong indication that most of the muons form Mu, since there are no strong local fields to relax free muon polarization. In fact, there is no source of even weak local magnetic fields, since there are no significant amounts of naturally occuring isotopes of Ar with nuclear moments.

In solid Ar, a large Mu precession signal (F_{Mu} = 91 ± 9%)

was observed with a small relaxation rate (λ=0.15 ± 0.03 μs^{-1}). The Mu precession signals in solid and liquid argon are shown in Figure VII·3. In liquid Ar, there is a slowly relaxing component

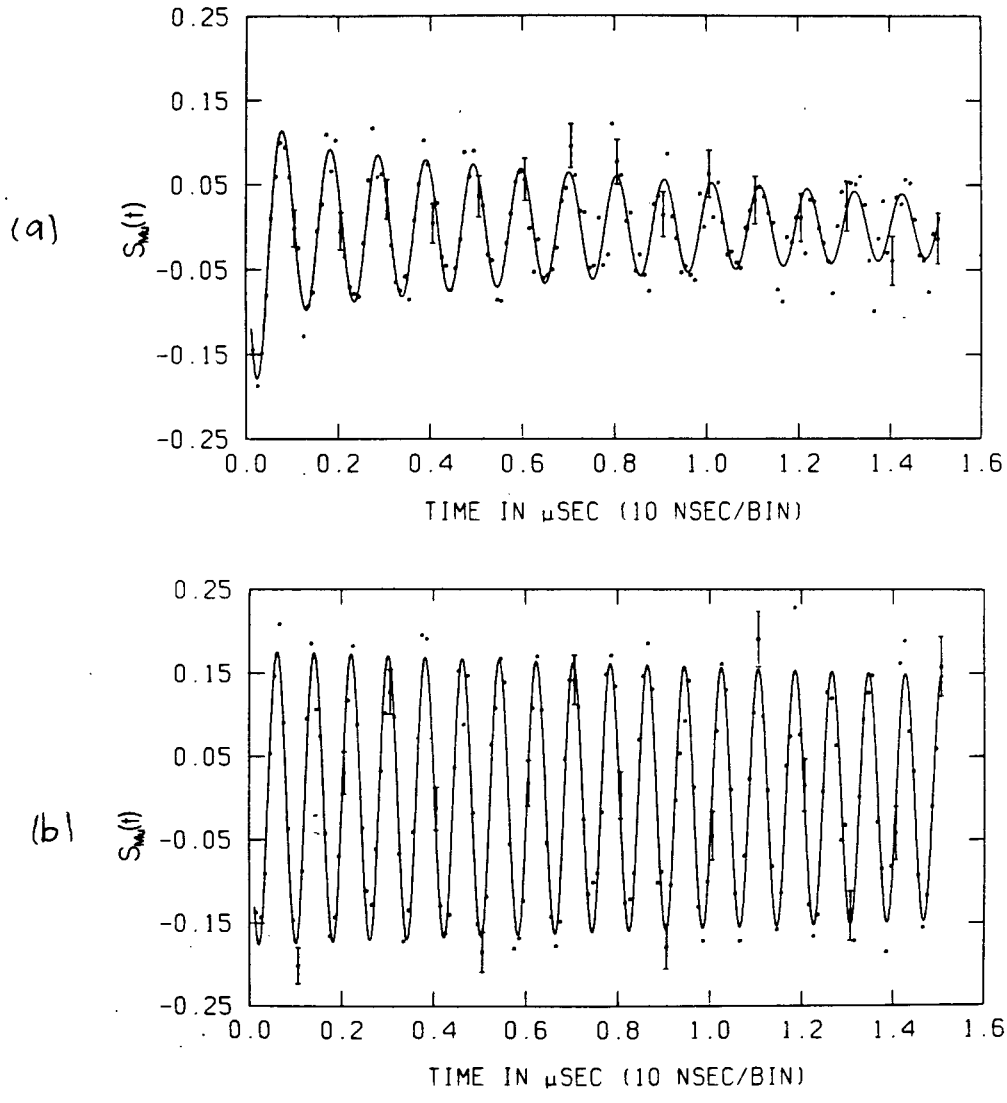

Figure VII·3 (a) Single frequency Mu precession in liquid Ar at 85°K at low field (8 G); (b) In solid Ar at 77°K.

(λ=0.65 ± 0.17 μs^{-1}) which accounts for only 48 ± 6% of the muon polarization. The relaxation is likely due to a reactive impurity present at a ppm level. In addition, there is

indication of a very fast-relaxing component (λ=19 ± 11 μs^{-1}), accounting for the remaining muon polarization and observable only within the first 100 ns. The long-lived Mu signal demonstrates that the inert liquid or its impurities are not responsible for this relaxation. It is possible that the fast relaxing component is due to Mu interacting with the radiation track consisting of free electrons, ions and excited atoms. This will be discussed further in Section VII·4.

Electron spin resonance experiments on H atoms in a solid Ar lattice at 4.2°K indicate at least two trapping sites (Foner 1960). The major component has a hyperfine splitting shift of -0.46% relative to the vacuum value. At temperatures above 39°K, the H atoms become mobile. In the present experiment, we have measured the mean hyperfine splitting of Mu in solid argon at 77°K to be 4463.8 ± 6MHz, which gives a shift of 0.01 ± 0.13%. Although this does not agree with the H atom results, the two measurements are not directly comparable because in the ESR experiment the H atoms are trapped at fixed lattice sites, whereas in the present μ^+SR experiment the Mu atoms are probably diffusing through the lattice so that the hyperfine perturbation $\bar{\sigma}^{\mu}\cdot\hat{A}\cdot\bar{\sigma}^{e}$ (see Section IV·4·2) is averaged over many sites.

VII·3·2 Mu in Liquid and Solid Xe

As in the case of Ar, the free muon fraction in liquid and solid Xe is small (3.3 ± 8% and 5 ± 3%, respectively). In solid Xe, the Mu component accounts for 79 ± 25% of the muon ensemble. The large error is due to the fast relaxing nature of the signal. In liquid Xe, the Mu component accounts for only 43 ± 9% of the muons. It is possible that there is also a fast relaxing Mu component as in the case of liquid Ar, but it is not resolvable.

The Mu relaxation rate increases sharply from 2.1 ± 0.2 μs^{-1} in the liquid to 19.0 ± 2.5 μs^{-1} in the solid. The nuclear dipole moments of ^{129}Xe and ^{131}Xe , which comprise 26.44% and 21.18% of the naturally occurring Xe, are likely responsible for the fast relaxation in the solid. Motional narrowing (see Section V·4·4), an effect greatly enhanced in the liquid, might cause such a discontinuity between phases. The larger relaxation rate in liquid Xe compared with liquid Ar is likely due to the higher impurity content in the Xe.

The ESR spectrum for H atoms trapped at interstitial sites in the Xe lattice at 4.2°K is multicomponent with an overall spread of 98.2 G. Each frequency corresponds to a particular magnetic environment, determined primarily by the isotopic compositions of its nearest neighbours. Thus, the mean local field experienced by an interstitial H atom is of order 25 G. This corresponds to a Mu relaxation rate of order $2\pi \cdot 1.4$ $MHzG^{-1} \cdot 25G = 220\ \mu s^{-1}$. The observed Mu relaxation rate at 150°K is only 19.0 ± 2.5 μs^{-1}. Thus, it is likely that the Mu is diffusing rapidly at this temperature or possibly trapped in

defects where the local fields are much smaller. It should be noted that H atoms are mobile in solid Xe at temperatures above 20°K (Kinugawa 1978).

VII·3·3 Mu in Liquid and Solid Kr

Again, the free muon fractions in solid and liquid Kr are small (1.4 ± 1.8% and 6.5 ± 0.1%, respectively). As in the case of liquid Xe, the Mu component in liquid Kr accounts for only 57 ± 10% of the muon ensemble, whereas the Mu fraction in solid Kr, 99 ± 10%, is consistent with 100% Mu formation with no missing fraction.

The Mu relaxation in liquid Kr is again likely due to impurities, since motional narrowing is expected to quench any relaxation due to ^{83}Kr , which accounts for 11.48% of the natural Kr.

Perhaps the most interesting μ^+SR spectrum in this experiment is for solid Kr. As mentioned in Section VII·2, a considerably better fit to the data was obtained using a two component Mu relaxation function (see Figure VII·4). The sum of these components accounts for 99 ± 10% of the muon ensemble. One interesting interpretation is that there exist trapping sites due to vacancies or defects. The situation is analogous to the trapping of Mu on a surface described in Section V·5 with $\lambda_B \bar{t} >> 1$. In the present case λ_B corresponds to the relaxation rate of trapped Mu. This is expected to be small, since the RLMF (Section IV·5·1) due to ^{83}Kr (11.48% of natural Kr, possessing a magnetic moment of -0.969 μ_N) falls off rapidly as $1/r^3$. The relaxation rate of interstitial Mu, being much closer to the nuclear moments, is expected to be larger. As in V·5, we define

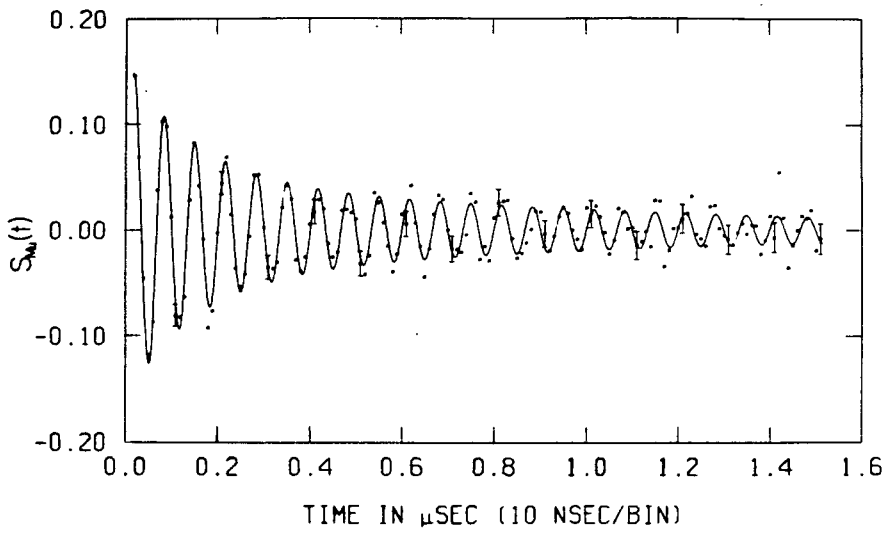

Figure VII·4 The Mu precession signal solid Kr at 90°K in a magnetic field of 10.7G

ν as the trapping rate. Under these conditions, one would expect a relaxation function

$$R_{Mu}(t) = \frac{\nu}{\lambda_F + \nu - \lambda_B} e^{-\lambda_B t} + \left[1 - \frac{\nu}{\lambda_F + \nu - \lambda_B} \right] e^{-(\lambda_F + \nu)t}$$

Equation VII·3

(i.e.: a sum of exponentials as observed). Using the fitted amplitudes and relaxation rates yields $\nu = 1.7 \pm 0.4\ \mu s^{-1}$, $\lambda_F = 5.0 \pm 0.4\ \mu s^{-1}$ and $\lambda_B = 0.89 \pm 0.04\ \mu s^{-1}$.

One may also make a rough estimate on the hopping rate between interstitial sites by comparing λ_F with the calculated static relaxation rate. The interstitial trapping sites in a face centered cubic lattice such as solid Kr have tetrahedral or octahedral symmetry. We will assume that the Mu atoms hop between octahedral sites which have a larger Mu-nucleus

separation (1.418 Å) (Foner 1960). The static relaxation rate of Mu at one of these sites may be calculated from equation V·13, assuming one of the eight nearest neighbours is ^{83}Kr (nuclear moment=-0.969 nuclear magnetons). The result yields $\lambda=15\ \mu s^{-1}$ which is a factor of three larger than the observed relaxation rate. This indicates that the hopping is rather slow-- $45\ \mu s^{-1}$ according to equation V·21 (assuming τ is the mean time between hops). Also the Mu atoms hop only 26 times before trapping.

This model could be tested by studying the effect of annealing and temperature on the μ^+SR spectrum.

VII·3·4 Missing Fractions

It is clear from these results that in solid Ar, Kr and Xe all the muon polarization is accounted for, whereas in the liquids roughly half the muon polarization is missing after 100 ns. Recently, such results have been explained qualitatively (Walker 1981)in terms of an expanding track model. According to this model, the Mu is formed epithermally and begins to diffuse randomly from some point beyond the end of the track. At some time τ, the concentration of track species, also diffusing, overlaps with the Mu for a short period of time, during which the spin exchange relaxation rate is large. Thus, one would expect a fraction of the muon polarization to be lost within time τ. In cold liquids, such as liquid Ar at 85°K, the diffusion rates may be sufficiently small so that the relaxation of the fast component is barely observable. In slightly warmer liquids, such as liquid Xe at 150°K and liquid Kr at 120°K, the diffusion rates are too large, and τ too small, for the fast

relaxing component to be observed. It is argued that in the solid phase the diffusion rates are too small and τ too large ($>> 2.2\ \mu s$) for the fast component to be observed.

VII·4 Conclusions

As in the gas phase, most of the muons in the liquid and solid Ar, Kr and Xe form Mu. The only real discrepency is in the case of Ar gas, where a 25% muon fraction is observed (Fleming 1981). No such free muon fraction was observed in either liquid or solid Ar.

The elements of Ar, Kr and Xe are ideal substances to study Mu-lattice states because of their large ($\sim$100%) Mu formation probability and their simple monatomic structure. It may be possible to make more direct comparisons with existing ESR data of trapped H atoms at lower temperatures where perhaps the Mu also becomes trapped.

There is an indication that the Mu interacts with its own radiation track in the liquid elements, leading to a fast relaxing Mu component.

CONCLUDING REMARKS

It has been demonstrated in the preceding chapters how Ps and Mu studies can provide a unique perspective on atom-molecule, atom-surface and atom-solid interactions.

In the future, it is possible that Mu and Ps could provide a testing ground for fundamental theories dealing with atom-surface interaction. Measurements of such quantities as single atom binding energies, surface diffusion rates and adsorption probabilities are all within the realm of possibility.

Until now, the chemistry of Mu on surfaces and in solids has been neglected. It is hoped that this study will stimulate some interest in this direction.

APPENDIX I THERMALIZATION OF GAS ATOMS IN A POWDER

The mean energy loss per collision for a thermal beam of atoms can be written

$$\Delta E = \frac{1}{kT^{\mathcal{J}}} \int_0^\infty \int_0^\infty d\epsilon_i^{\mathcal{J}}\, d\epsilon_f^{\mathcal{J}}\, P(\epsilon_i^{\mathcal{J}}, \epsilon_f^{\mathcal{J}})(\epsilon_i^{\mathcal{J}} - \epsilon_f^{\mathcal{J}}) e^{-\epsilon_i^{\mathcal{J}}/kT^{\mathcal{J}}}$$

Equation AI·1

where $T^{\mathcal{J}}$ = the temperature of the beam.
$\epsilon_i^{\mathcal{J}}$ = the initial energy of the gas atom.
$\epsilon_f^{\mathcal{J}}$ = the final energy of the gas atom.
$P(\epsilon_i^{\mathcal{J}}, \epsilon_f^{\mathcal{J}})$ = the probability per collision for a transition $\epsilon_i^{\mathcal{J}} \rightarrow \epsilon_f^{\mathcal{J}}$.

$P(\epsilon_i^{\mathcal{J}}, \epsilon_f^{\mathcal{J}})$ can be approximated in a one-dimensional theory for atom surface scattering, first developed by Devonshire (1937) and recently reviewed by Goodman (1971). The effect of using a one-dimensional calculation increases the transition rate by a small factor (2 or 3) in cases where the three-dimensional calculation has been done.

In the Devonshire theory, the surface atom potential is represented by a function

$$V(z-Z) \sim V(z) + Z\,V'(z) \quad ; \; z \text{ small}$$

Equation AI·2

where z and Z are the displacements of the gas atom and surface atom respectively. V(z) is often chosen to be a Morse potential

$$V(z) = D\left(e^{-2az} - 2e^{-az}\right) .$$

Equation AI·3

$$V'(z) = -2Da\left(e^{-2az} - e^{-az}\right)$$

Equation AI·4

D and a^{-1} are the depth and range of the potential, respectively.

The unperturbed gas atom states are solutions to

$$[H_0 + V(z)]\,|\epsilon^g\rangle = \epsilon^g\,|\epsilon^g\rangle$$

Equation AI·5

The transition rate from ϵ_i^g --> ϵ_f^g is given as

$$T_{if} = \frac{2\pi}{\hbar}\,|\langle\epsilon_f^g|\,V(z)\,|\epsilon_i^g\rangle|^2 \sum_f |\langle s_f|\,Z\,|s_i\rangle|^2\,\delta(\epsilon_f^s + \epsilon_f^g - \epsilon_i^s - \epsilon_i^g)$$

Equation AI·6

where $|s_i\rangle$ is the initial state of the solid at temperature T^s with energy ϵ_i^s. The sum is over all final states of the solid, $|s_f\rangle$. The matrix element involving the solid is most easily evaluated by expressing Z in terms of phonon creation and annihilation operators (Ashcroft 1976).

$$Z = \frac{1}{\sqrt{N}} \sum_q \sqrt{\frac{\hbar}{2M\omega_q}}\,(a_q + a_{-q}^+)$$

Equation AI·7

where a_q annihilates a phonon corresponding to normal mode q, a_q^+ creates one of the same, ω_q is the phonon frequency, M is the mass of the solid atoms, and N is the number of atoms in the solid.

$$\sum_f |\langle s_f|Z|s_i\rangle|^2\,\delta(\epsilon_f^s + \epsilon_f^g - \epsilon_i^s - \epsilon_i^g) = \frac{\hbar}{N2M} \sum_q \frac{1}{\omega_q}\{(\bar{n}_q + 1)\,\delta(\epsilon_f^g - \epsilon_i^g + \hbar\omega_q) + \bar{n}_q\,\delta(\epsilon_f^g - \epsilon_i^g - \hbar\omega_q)\}$$

Equation AI·8

where

$$\bar{n}_q + 1 = \frac{1}{1 - e^{-\hbar\omega_q/kT^s}}$$

Equation AI·9

$$\bar{n}_q = \frac{1}{e^{\hbar\omega_q/kT^s} - 1}$$

Equation AI·10

Substituting a three dimensional Debye density of modes,

$$g(\omega) = \frac{3\omega^2 N}{\omega_D^3 \Omega}$$

Equation AI·11

where ω_D is the Debye frequency and Ω is the volume of the solid, into Equation AI·8 yields

$$\text{L·H·S·} = \frac{3\hbar}{2M\omega_D^3} \int_0^{\omega_D} d\omega \left[\omega(\bar{n}_\omega + 1)\delta(\epsilon_f^g - \epsilon_i^g + \hbar\omega) + n_\omega \delta(\epsilon_f^g - \epsilon_i^g - \hbar\omega) \right]$$

Equation AI·12

$$= \begin{cases} \frac{3}{\omega_D^3 2M\hbar} \frac{(\epsilon_f - \epsilon_i)}{\exp[(\epsilon_f - \epsilon_i)/kT^s] - 1} & ; \hbar\omega_D > |\epsilon_f - \epsilon_i| > 0 \\ 0 & ; \text{otherwise} \end{cases}$$

Equation AI·13

where the g superscript has been dropped. [6]

Thus

$$T_{if} = \begin{cases} \frac{3\pi}{\hbar^2 M\omega_D^3} \frac{|\langle\epsilon_f|V'(z)|\epsilon_i\rangle|^2(\epsilon_f - \epsilon_i)}{\exp[(\epsilon_f - \epsilon_i)/kT^s] - 1} & ; \hbar\omega_D > |\epsilon_f - \epsilon_i| > 0 \\ 0 & ; \text{otherwise} \end{cases}$$

Equation AI·14

The probability per collision for scattering into an energy

interval $d\epsilon_f$ is

$$P(\epsilon_f \epsilon_i) = \frac{T_{if}\ \rho(\epsilon_f)}{\dot{n}}$$

Equation AI·15

where $\rho(\epsilon_f) = \frac{L}{2\pi\hbar}\left(\frac{m}{2\epsilon_f}\right)^{\frac{1}{2}}$ is the density of final states in one dimension with normalization L and $\dot{n} = \frac{(2\epsilon_i)^{\frac{1}{2}}}{m} / L$ is the collision frequency.

$$P(\epsilon_f \epsilon_i) = \begin{cases} \dfrac{3mL^2}{4M(\hbar\omega_D)^3(\epsilon_f-\epsilon_i)^{\frac{1}{2}}} \dfrac{|\langle\epsilon_f|V'(z)|\epsilon_i\rangle|^2(\epsilon_f-\epsilon_i)}{\exp[(\epsilon_f-\epsilon_i)/kT^s]-1} \\ \qquad ;\ \text{for } \hbar\omega_D > |\epsilon_f-\epsilon_i| > 0 \\ 0 \quad ;\ \text{otherwise} \end{cases}$$

Equation AI·16

For a Morse potential,

$$|\langle\epsilon_f|V'(z)|\epsilon_i\rangle|^2 = \frac{8m\pi^2(\epsilon_f-\epsilon_i)^2(\epsilon_f\epsilon_i)^{1/2}\sinh 2\pi\mu' \sinh 2\pi\mu}{\hbar^2 a^2 L^2 [\cosh 2\pi\mu' - \cosh\mu]^2}$$

$$\times \left[\left|\frac{\Gamma(\frac{1}{2}-d+i\mu')}{\Gamma(\frac{1}{2}-d+i\mu)}\right| + \left|\frac{\Gamma(\frac{1}{2}-d+i\mu)}{\Gamma(\frac{1}{2}-d+i\mu')}\right|\right]^2$$

Equation AI·17

$$P(\epsilon_f \epsilon_i) = \frac{6\pi^2 w^3 \sinh 2\pi\mu \sinh 2\pi\mu'}{\hbar^2 a^2 w_D^3 (\exp[\hbar w/kT^s]-1)(\cosh 2\pi\mu' - \cosh 2\pi\mu)^2}$$

$$\times \left[\left|\frac{\Gamma(\frac{1}{2}-d+i\mu')}{\Gamma(\frac{1}{2}-d+i\mu)}\right| + \left|\frac{\Gamma(\frac{1}{2}-d+i\mu)}{\Gamma(\frac{1}{2}-d+i\mu')}\right|\right]^2$$

where

$$\mu = (2m\epsilon_i)^{1/2}/\hbar a$$
$$\mu' = (2m\epsilon_f)^{1/2}/\hbar a$$
$$d = (2mD)^{1/2}/\hbar a$$
$$\hbar\omega = \epsilon_f - \epsilon_i$$

Equation AI·18

Substituting Equation AI·18 into Equation AI·1,

$$\Delta E = \frac{\hbar^2}{kT_g}\int_0^\infty d\epsilon_i \int_0^\infty dw\, w\left[P(\epsilon+w,\epsilon)\,e^{-\epsilon/kT_g} - P(\epsilon,\epsilon+w)\,e^{-(\epsilon+\hbar\omega)/kT_g}\right]$$

Equation AI·19

By the principle of microscopic reversibility

$$|\langle\epsilon_f|V'(z)|\epsilon_i\rangle|^2 = |\langle\epsilon_i|V'(z)|\epsilon_f\rangle|^2$$

Equation AI·20

so

$$P(\epsilon,\epsilon+\hbar\omega) = e^{\hbar\omega/kT_s}\,P(\epsilon+\hbar\omega,\epsilon)$$

Equation AI·21

$$\Delta E = \frac{\hbar^2}{kT_s}\int_0^\infty d\epsilon \int_0^{\omega_D} dw\, w\, e^{-\epsilon/kT_s} P(\epsilon+\hbar\omega,\epsilon)\left[1 - e^{\frac{\hbar\omega}{k}\left(\frac{1}{T_s}-\frac{1}{T_g}\right)}\right]$$

Equation AI·22

Thus, in thermal equilibrium, there is no mean energy transfer.

The rate of energy loss can be written

$$\frac{d\epsilon}{dt} = \Delta E\,\nu_c$$

Equation AI·23

where ν_c is the collision frequency with the surface. ν_c can be

estimated as

$$\nu_c = \frac{N\pi R^2 v}{V_F}$$

Equation AI·24

where N is the number of particles per unit mass, V_F is the free volume per unit mass, R is the radius of the powder grains and v is the mean velocity of the atom.

$$\frac{N\pi R^2}{V_F} = \frac{\rho \rho_{solid} SA}{4(\rho_{solid} - \rho)}$$

Equation AI·25

where SA is the specific surface area of the powder, ρ_{solid} is the density of the solid, and ρ is the density of the powder.

The time required for an atom of mean energy E_i to reach E_f is obtained by integrating Equation AI·23

$$t = \frac{4(\rho_{solid} - \rho)}{SA\ \rho \rho_{solid}} \left(\frac{m}{2}\right)^{1/2} \int_{E_i}^{E_f} \frac{d\epsilon}{\Delta E\, \epsilon^{1/2}}$$

Equation AI·26

where ΔE is given by Equations AI·22 and AI·18.

APPENDIX II PS SCATTERING OFF 2 ELECTRON ATOM (MOLECULE)

In this appendix, a theory for low energy scattering of o-Ps off a two-electron atom is developed. It is assumed that the spin (s) of the atom and thus the spacial symmetry of the electrons in the atom is conserved during collisions. When s=0 (e.g., He) there is no spin conversion, but when s=1 (e.g., $He^*(2^3S)$), o-Ps may be converted to p-Ps via spin exchange. The effect of a large magnetic field on the observed quenching rate is considered. Finally, the result is generalized to a 2 electron molecule.

The particle interactions are assumed to be a function of only the spacial coordinates. Thus, effects due to the spin-spin and spin-orbit coupling are neglected. The spin of each particle and the total electron spin are therefore conserved quantities. However, the direction of the electron spin associated with the o-Ps is not necessarily conserved during collisions, because of the exchange degeneracy associated with the electrons (i.e., the electrons may interchange). This is the basic principle behind spin exchange.

A II·1 Total Electron Spin States

States of total electron spin $|SS_z\beta\rangle$ (β the z component of positron spin) span an irreducible sub-space $\mathcal{E}_{spin}^{SS_z\beta}$ with respect to permutation of the electron spin coordinates. Basis vectors for $\mathcal{E}_{spin}^{SS_z\beta}$ generate the irreducible representation Γ^S of the permutation group S_3. The basis vector for $\Gamma^{3/2}$ transforms according to the one dimensional, totally symmetric irreducible representation A_1 of S_3 [using notation of Tinkham (1964)], whereas the basis vectors for $\Gamma^{1/2}$ transform according to the two dimensional irreducible representation E of S_3. For example,

$$|A_1, S_z=-\tfrac{1}{2}\ \beta\rangle = |S=\tfrac{3}{2}\ S_z=-\tfrac{1}{2}\ \beta\rangle = \frac{1}{\sqrt{3}}\{|\downarrow\downarrow\uparrow\beta\rangle+|\downarrow\uparrow\downarrow\beta\rangle+|\uparrow\downarrow\downarrow\beta\rangle$$

Equation AII·1

$$|E\xi_1\ S_z=\tfrac{1}{2}\ \beta\rangle = |S=\tfrac{1}{2}\ S_z=\tfrac{1}{2}\ \beta\ \xi_1\rangle = \frac{1}{\sqrt{6}}\{2|\uparrow\uparrow\downarrow\beta\rangle-|\downarrow\uparrow\uparrow\beta\rangle-|\uparrow\downarrow\uparrow\beta\rangle\}$$

Equation AII·2

$$|E\xi_2\ S=\tfrac{1}{2}\ \beta\rangle = |S=\tfrac{1}{2}\ S_z=\tfrac{1}{2}\ \beta\ \xi_2\rangle = \frac{1}{\sqrt{2}}\{\qquad -|\downarrow\uparrow\uparrow\beta\rangle+|\uparrow\downarrow\uparrow\beta\rangle\}$$

Equation AII·3

where ξ_i is the row index of the irreducible representation $\Gamma^{\frac{1}{2}}=E$.

A II·2 Spacial States

The space of asymptotic states for Ps (momentum k and orbital angular momentum lm) incident on a two electron atom (spin s) are spanned by the three states

$$\psi_\ell^m(\bar{r}_3\,\bar{r}_p)\,\psi^{1-2S}(\bar{r}_1,\bar{r}_2)$$
$$\psi_\ell^m(\bar{r}_1\,\bar{r}_p)\,\psi^{1-2S}(\bar{r}_3,\bar{r}_2)$$
$$\psi_\ell^m(\bar{r}_2\,\bar{r}_p)\,\psi^{1-2S}(\bar{r}_1,\bar{r}_3)$$

where

$$\psi_\ell^m(\bar{r}_3\,\bar{r}_p) = j_\ell[k|\bar{r}_3+\bar{r}_p|]\,Y_\ell^m\left[\frac{\bar{r}_3+\bar{r}_p}{|\bar{r}_3+\bar{r}_p|}\right]\psi^{P_3}(|\bar{r}_3-\bar{r}_p|)$$

and $\psi^{1-2S}(\bar{r}_1,\bar{r}_2)$ is the two electron wavefunction, symmetric for s=0 and antisymmetric for s=1.

There are two irreducible subspaces $\mathcal{E}_{space}^{\Gamma_3}$ associated with each value of s. For s=1, one has A_2 symmetry (totally antisymmetric) and one has E symmetry. For s=0, there is one with A_1 symmetry and one with E symmetry. For example,

$$|k\ell m\,A_2\,s=1\rangle = \frac{1}{\sqrt{3}}\left\{\psi_\ell^m(\bar{r}_3\,\bar{r}_p)\,\psi^-(\bar{r}_2,\bar{r}_1) + \psi_\ell^m(\bar{r}_1\,\bar{r}_p)\,\psi^-(\bar{r}_3,\bar{r}_2) + \psi_\ell^m(\bar{r}_2\,\bar{r}_p)\,\psi^-(\bar{r}_1,\bar{r}_3)\right\}$$

Equation AII·4

$$|k\ell m\,E\,\xi,s=1\rangle = \frac{1}{\sqrt{2}}\left\{-\psi_\ell^m(\bar{r}_1\,\bar{r}_p)\,\psi^-(\bar{r}_3,\bar{r}_2) + \psi_\ell^m(\bar{r}_2\,\bar{r}_p)\,\psi^-(\bar{r}_1,\bar{r}_3)\right\}$$

Equation AII·5

$$|k\ell m E \xi_2 s=1\rangle = \frac{1}{\sqrt{6}}\{-2\psi_\ell^m(\bar{r}_3\bar{r}_p)\psi^-(\bar{r}_2\bar{r}_1) + \psi_\ell^m(\bar{r}_1\bar{r}_p)\psi^-(\bar{r}_3\bar{r}_2) + \psi_\ell^m(\bar{r}_2\bar{r}_p)\psi^-(\bar{r}_1\bar{r}_3)\}$$

Equation AII·6

A II·3 Physical Asymptotic States of Total Electron Spin

These states are found in the direct product space $\mathcal{E}_{space}^{\Gamma_s}$ x $\mathcal{E}_{spin}^{SS_z\beta}$ and must have A_2 symmetry. The value of S uniquely determines the irreducible representation Γ_s^{space} associated with the spacial wave function.

For S=3/2, $\Gamma^{spin} = A_1$ and thus $\Gamma^{space} = A_2$. For S=1/2, $\Gamma^{spin} = E$ and thus $\Gamma^{space} = E$.

$$|k\ell m S=\tfrac{3}{2}\ S_z\ s=1\ \beta\rangle = |k\ell m A_2 s=1\rangle\,|S=\tfrac{3}{2}\ S_z\ \xi_1\beta\rangle$$

Equation AII·7

$$|k\ell m S=\tfrac{1}{2}\ S_z\ s=1\ \beta\rangle = \frac{1}{\sqrt{2}}\{|k\ell m E \xi_1 s=1\rangle\,|S=\tfrac{1}{2}\ S_z\ \xi_2\beta\rangle + |k\ell m E \xi_2 s=1\rangle\,|S=\tfrac{1}{2}\ S_z\ \xi_1\beta\rangle\}$$

Equation AII·8

$$|k\ell m S=\tfrac{1}{2}\ S_z\ s=0\ \beta\rangle = \frac{1}{\sqrt{2}}\{-|k\ell m E \xi_1 s=0\rangle\,|S=\tfrac{1}{2}\ S_z\ \xi_2\beta\rangle + |k\ell m E \xi_2 s=0\rangle\,|S=\tfrac{1}{2}\ S_z\ \xi_1\beta\rangle$$

Equation AII·9

Since the Hamiltonian and thus the T matrix are invariant under the group operations of S_3, the matrix elements of T vanish between states belonging to different irreducible representations of S_3 or to different rows of the same

irreducible representation of S_3, according to a general matrix element theorem (Tinkham 1964). Since we have imposed the condition that s is conserved, the T matrix is diagonal in the above basis. The diagonal elements are

$$T^{1/2\ s}_{k\ell} = \langle k\ell m E\ \xi, s | T | k\ell m E\ \xi, s \rangle$$

Equation AII·10

$$T^{3/2\ 1} = \langle k\ell m A_2\ s=1 | T | k\ell m A_2\ s=1 \rangle$$

Equation AII·11

A II·4 Physical States of Ps spin (II_z)

Consider the Ps spin states:

$$|k\ell m\ II_z\ ss_z\rangle = \frac{1}{\sqrt{3}}\{\psi^m_\ell(\bar{r}_3\bar{r}_p)\psi^{1-2s}(\bar{r}_2\bar{r}_1)\chi^I_{I_z}(p,3)\chi^s_{s_z}(2,1)\psi^m_\ell(\bar{r}_1\bar{r}_p)\psi^{1-2s}(\bar{r}_3\bar{r}_2)\chi^I_{I_z}(p,1)\chi^s_{s_z}(3,2) + \psi^m_\ell(\bar{r}_2\bar{r}_p)\psi^{1-2s}(\bar{r}_1\bar{r}_3) \times \chi^I_{I_z}(p,2)\chi^s_{s_z}(1,3)\}$$

Equation AII·12

These states also have A_2 symmetry, but are not well defined states of total electron spin in general. Thus, the T matrix is not diagonal in this representation.

A II·5 The T matrix in $|klmII_z ss_z>$ Representation

Define

$$T^{s}_{k\ell}(II_z s_z; I'I'_z s'_z) = \langle k\ell m I I_z s s_z | T | k\ell m I' I'_z s s'_z \rangle$$

$$= \sum_{SS_z\beta} \langle k\ell m I I_z s s_z | k\ell m S S_z s\beta \rangle T^{S_s}_{k\ell} \langle k\ell m S S_z s\beta | k\ell m I' I'_z s s'_z \rangle$$

Equation AII·13

The matrix $\langle klmII_z ss_z | klmSS_z s\beta \rangle$ and the T matrix in the $|klmII_z ss_z>$ representation (in terms of $T^{S_s}_{k\ell}$) are given in the following tables.

Table AII.1. The Matrix $\langle klmII_z\, ss_z \mid klmSS_z\, s\beta \rangle$

				s	1	1	1	1	1	1	1	1	1	1	1	1	0	0	0	0	
				S	3/2	3/2	3/2	3/2	3/2	3/2	3/2	3/2	1/2	1/2	1/2	1/2	1/2	1/2	1/2	1/2	
				S_z	3/2	1/2	-1/2	-3/2	3/2	1/2	-1/2	-3/2	1/2	-1/2	1/2	-1/2	1/2	-1/2	1/2	-1/2	
				β	1/2	1/2	1/2	1/2	-1/2	-1/2	-1/2	-1/2	1/2	1/2	-1/2	-1/2	1/2	1/2	-1/2	-1/2	
I	I_z	σ	s_z																		
1	1	1	1		1																
1	0	1	1			$1/\sqrt{6}$			$1/\sqrt{2}$				$-1/\sqrt{3}$								
1	-1	1	1							$1/\sqrt{3}$					$-\sqrt{\frac{2}{3}}$						
0	0	1	1			$-1/\sqrt{6}$			$1/\sqrt{2}$				$1/\sqrt{3}$								
1	1	1	0			$\sqrt{\frac{2}{3}}$							$1/\sqrt{3}$								
1	0	1	0				$1/\sqrt{3}$			$1/\sqrt{3}$				$1/\sqrt{6}$	$1/\sqrt{6}$						
1	-1	1	0								$\sqrt{\frac{2}{3}}$					$1/\sqrt{3}$					
0	0	1	0				$-1/\sqrt{3}$			$1/\sqrt{3}$				$-1/\sqrt{6}$	$1/\sqrt{6}$						
1	1	1	-1				$1/\sqrt{3}$							$-\sqrt{\frac{2}{3}}$							
1	0	1	-1					$1/\sqrt{2}$			$1/\sqrt{6}$					$-1/\sqrt{3}$					
1	-1	1	-1									1									
0	0	1	-1					$-1/\sqrt{2}$			$1/\sqrt{6}$					$-1/\sqrt{3}$					
1	1	0	0														-1				
1	0	0	0															$1/\sqrt{2}$	$-1/\sqrt{2}$		
1	-1	0	0																	-1	
0	0	0	0															$-1/\sqrt{2}$	$-1/\sqrt{2}$		

Table AII.2. The Matrix $\langle klmI I_z s s_z | T | klm'I'_z s's'_z \rangle$

				I'	1	1	1	0	1	1	1	0	1	1	1	0	1	1	1	0	
				I'_z	1	0	-1	0	1	0	-1	0	1	0	-1	0	1	0	-1	0	
				s'	1	1	1	1	1	1	1	1	1	1	1	1	0	0	0	0	
				s'_z	1	1	1	1	0	0	0	0	-1	-1	-1	-1	0	0	0	0	
I	I_z	s	s_z																		
1	1	1	1		a																
1	0	1	1			b		d	d												
1	-1	1	1				c			d		d									
0	0	1	1			d		b	-d												
1	1	1	0			d		-d	b												
1	0	1	0				d			b			d								
1	-1	1	0								b			d		d					
0	0	1	0				d					b	-d								
1	1	1	-1							d		-d	c								
1	0	1	-1								d			b		-d					
1	-1	1	-1												a						
0	0	1	-1								d			-d		b					
1	1	0	0														e				
1	0	0	0															e			
1	-1	0	0																e		
0	0	0	0																	e	

$$a = T^{3/2\,1}_{kl} \qquad b = \frac{2T^{3/2\,1}_{kl} + T^{1/2\,1}_{kl}}{3} \qquad c = \frac{T^{3/2\,1}_{kl} + 2T^{1/2\,1}_{kl}}{3}$$

$$d = \frac{T^{3/2\,1}_{kl} - T^{1/2\,1}_{kl}}{3} \qquad e = T^{1/2\,0}_{kl}$$

A II·6 The Spin Conversion Cross Section for s=1

The scattering amplitude for a given transition $I'I_z's's_z'$ $\rightarrow II_z ss_z$ is given as

$$i\delta(k-k')f_{\bar{k}\bar{k}'}(II_z ss_z; I'I_z's's_z') = \langle \bar{k}\, II_z ss_z \mid T \mid \bar{k}'I'I_z's's_z'\rangle$$

$$= \sum_{l=0}^{\infty} \frac{2l+1}{4\pi k^2} P_l\left(\frac{k\cdot k'}{k^2}\right) T_{kl}(II_z ss_z; I'I_z's's_z')\,\delta(k-k')$$

Equation AII·14

Thus

$$f_{\bar{k}\bar{k}'}(II_z ss_z; I'I_z's's_z') = \frac{1}{2ik}\sum_{l=0}^{\infty}(2l+1)P_l\left(\frac{\bar{k}\cdot\bar{k}'}{k^2}\right) T_{kl}(II_z ss_z; I'I_z's's_z')_{k=k'}$$

Equation AII·15

The total cross section for such a transition

$$\sigma(II_z ss_z; I'I_z's's_z') = \frac{\pi}{k^2}\sum_{l=0}^{\infty}(2l+1)\left| T_{kl}(II_z ss_z; I'I_z's's_z')\right|^2$$

Equation AII·16

The o-Ps-->p-Ps conversion cross section is obtained by averaging over initial states of o-Ps with s=1 and summing over final states of p-Ps

$$\sigma^c = \frac{1}{9}\sum_{I_z s_z s_z'} \sigma(1I_z 1s_z; 001 s_z')$$

$$= \frac{2}{27}\frac{\pi}{k^2}\sum_{l=0}^{\infty}(2l+1)\left| T_{kl}^{3/2\,1} - T_{kl}^{1/2\,1}\right|^2$$

Equation AII·17

Since the scattering matrix is unitary T_{kl}^{Ss} may be parameterized in terms of a single real angle, the scattering phase shift for scattering in a state of Ps orbital angular momentum l, total electron spin S, and atomic spin s.

$$T_{kl}^{Ss} = e^{2i\delta_l^{Ss}} - 1$$

Equation AII·18

Thus the conversion cross section can be rewritten

$$\sigma_k^c = \frac{2}{27}\frac{\pi}{k^2}\sum_{l=0}^{\infty}(2l+1)\left|e^{2i\left[\delta_l^{3/2\,1}-\delta_l^{1/2\,1}\right]}-1\right|^2$$

$$= \frac{8}{27}\frac{\pi}{k^2}\sum_{l=0}^{\infty}(2l+1)\sin^2\left(\delta_l^{3/2\,1}-\delta_l^{1/2\,1}\right)$$

Equation AII·19

The spin exchange cross section is defined as

$$\sigma_{ex} = \frac{\pi}{k^2}\sum_{l=0}^{\infty}(2l+1)\sin^2\left(\delta_l^{3/2\,1}-\delta_l^{1/2\,1}\right)$$

$$= \frac{27}{8}\sigma^c$$

Equation AII·20

In a large magnetic field, where (10) and (00) hyperfine states of Ps are mixed slightly, the relevant conversion rate is from $I_z = \pm 1 \rightarrow I_z = 0$.

$$\sigma_k^c = \frac{1}{6}\sum_{\substack{I_z=\pm 1\\ I' S_z S_z'}}\sigma\left(|I_z|S_z; I'0|S_z\right)$$

$$= \frac{16}{27}\frac{\pi}{k^2}\sum_{l=0}^{\infty}(2l+1)\sin^2\left(\delta_l^{3/2\,1}-\delta_l^{1/2\,1}\right)$$

Equation AII·21

A II·7 The Total Cross Section

The total cross section for s=1

$$\sigma^T = \frac{1}{9}\sum_{\substack{I_z I' I_z'\\ S_z S_z'}}\sigma\left(|I_z|S_z; I'I_z'|S_z'\right)$$

$$= \frac{1}{3}\frac{\pi}{k^2}\sum_{\ell=0}^{\infty}(2\ell+1)\left[\,2\left|T_{k\ell}^{3/2\,1}\right|^2 + \left|T^{1/2\,1}\right|^2\right]$$

$$= \frac{4}{3}\frac{\pi}{k^2}\sum_{\ell=0}^{\infty}(2\ell+1)\left[\,2\sin^2\delta_\ell^{3/2\,1} + \sin^2\delta_\ell^{1/2\,1}\right]$$

Equation AII·22

The total cross cross for s=0 is simply

$$\sigma^T = \frac{4\pi}{k^2}\sum_{\ell=0}^{\infty}(2\ell+1)\sin^2\delta_\ell^{1/2\,0}$$

Equation AII·23

whereas the conversion cross section is zero.

A II·8 Generalization to a 2 Electron Molecule

In the case of Ps of orbital angular momentum l, scattering off a molecule with rotational angular momentum j, invariance under rotations requires only that the total angular momentum, J = j + l, be conserved. This allows for the possibility of inelastic collisions involving rotational excitation. The average cross section for scattering from rotational state j --> j′ (Arthurs 1960) in a total electron spin state S (molecular spin s) can be written

$$\sigma^{Ss}(j;j') = \frac{\pi}{(2j+1)k^2}\sum_{J=0}^{\infty}\sum_{\ell=|J-j|}^{\ell=|J+j|}\sum_{\ell'=|J-j'|}^{\ell'=|J+j'|}(2J+1)\left|T^{JSs}(j\,\ell\,;j'\ell')\right|^2$$

Equation AII·24

where $T^{JSs}(j'l'jl)$ is the T matrix element between initial state

jl and final state j'l'. The average cross section for scattering from initial state $jI I_z\, ss_z \longrightarrow j'I'I_z' ss_z'$ can be written

$$\sigma(j'I'I_z' s_z'; j I I_z s_z) = \frac{\pi}{(2j+1)k^2} \sum_{J=0}^{\infty} \sum_{l=|J-j|}^{l=|J+j|} \sum_{l'=|J-j'|}^{l'=|J+j'|} \times \left| T^J(j'l'I'I_z' s_z'; jl I I_z s_z) \right|^2$$

Equation AII·25

The corresponding spin conversion cross section

$$\sigma^c(j;j') = \frac{2}{27}\frac{\pi}{k^2(2j+1)} \sum_{J=0}^{\infty} \sum_{l=|J-j|}^{l=|J+j|} \sum_{l'=|J-j'|}^{l'=|J+j'|} (2J+1) \left| T^{JS=3/2,\, s=1}(j'l';jl) - T^{JS=\frac{1}{2},\, s=1}(j'l';jl) \right|^2$$

Equation AII·26

As will be shown in the following section

$$T^{JSs}(j'l';jl) \sim \delta_{l0}\,\delta_{jj'}\left(e^{2i\delta_0^{Ss}} - 1\right)$$

Equation AII·27

in the low energy limit kR << 1, where R is the range of the potential. In this limit,

$$\sigma^c(j;j') \sim \delta_{jj'}\frac{8}{27}\frac{\pi}{k^2}\sin^2\left(\delta_0^{3/2\,1} - \delta_0^{1/2\,1}\right)$$

Equation AII·28

Thus the conversion cross section averaged over rotational states of the molecule is simply

$$\sigma^c \sim \frac{8}{27}\frac{\pi}{k^2}\sin^2\left(\delta_0^{3/2\,1} - \delta_0^{1/2\,1}\right)$$

Equation AII·29

Note that the phase shifts are independent of the rotational state of the molecule.

A II·9 Evaluation of $T^{JSs}(j'l'; j\ l)$ in the Limit kR << 1

We assume that the scattering states of total electron spin S and molecular spin s at low energy evolve in time according to some effective Hamiltonian

$$H = \frac{1}{2}\frac{\hbar^2 k^2}{m} + B_0 j(j+1) + V^{Ss} \qquad \text{Equation AII·30}$$

where B_0 is the rotational constant for the molecule and V^{Ss} is an effective local interaction between the Ps and the molecule which depends on the total electron spin S and molecular spin s. Now consider matrix elements of V^{Ss}

$$\langle k J J_z j l | V^{Ss} | k' J J_z j' l' \rangle \qquad k - k' = B_0[(j(j+1) - j'(j'+1)]$$

$$= \int d\bar{r}\, d\hat{\omega} \sum_{\substack{j_z l_z \\ j_z' l_z'}} \langle k J J_z j l | k j j_z l l_z \rangle \langle k j j_z l l_z | \bar{r}\,\hat{\omega} \rangle$$

$$\times V^{Ss}(\bar{r}\,\hat{\omega}) \langle \bar{r}\,\hat{\omega} | k' j' j_z' l' l_z' \rangle \langle k' j' j_z' l' l_z' | k' J J_z j' l' \rangle$$

Equation AII·31

where $\bar{r}$ is the vector from the Ps cm to molecular CM and $\hat{\omega}$ is the molecular axis unit vector. $V^{Ss}(\bar{r},\omega)$ can then be expanded as

$$V^{Ss}(\bar{r}\,\hat{\omega}) = \sum_{\text{even } L} \frac{(2l+1)}{4\pi} U_L^{Ss}(r) P_L(\bar{r}\cdot\hat{\omega}) = \sum_{\text{even } L} U^{Ss}(r) Y_L^{M^*}(\hat{r}) Y_L^{M}(\hat{\omega})$$

Equation AII·32

where we have assumed V^{Ss} to be a real finite function of $\bar{r}$ and $\hat{r}\cdot\hat{\omega}$, invariant under $\hat{\omega} \dashrightarrow -\hat{\omega}$. Using

$$\langle k j j_z l l_z | \bar{r}\,\hat{\omega} \rangle = i^l \sqrt{\frac{2}{\pi}}\, k\, j_l(kr)\, Y_l^{l_z}(\hat{r})\, Y_j^{j_z}(\hat{\omega})$$

Equation AII·33

$$\int d\hat{\omega}\, Y_j^{j_z *}(\hat{\omega})\, Y_L^M(\hat{\omega})\, Y_{j'}^{j_z'}(\hat{\omega}) = \left[\frac{(2j+1)(2L+1)}{4\pi(2j'+1)}\right]^{1/2} C(jLj'000)\, C(jLj'j_z M j_z')$$

Equation AII·34

$$\int d\hat{r}\, Y_\ell^{\ell_z *}(\hat{r})\, Y_L^{M*}(\hat{r})\, Y_{\ell'}^{\ell_z'}(\hat{r}) = (-1)^M \left[\frac{(2\ell+1)(2L+1)}{4\pi(2\ell'+1)}\right]^{1/2} C(\ell L\ell' 000)\, C(\ell L\ell' \ell_z - M \ell_z')$$

Equation AII·35

It follows:

$$\begin{aligned}
&\langle k J J_z\, j\ell \,|\, V^{Ss} \,|\, k' J J_z\, j'\ell' \rangle \\
&= \sum_L \sum_{\substack{\ell_z \ell_z' \\ j_z j_z'}} C(j\ell J\, j_z \ell_z J_z)\, C(j'\ell' J\, j_z' \ell_z' J_z) \\
&\times 8kk' \int dr\, r^2 j_\ell(kr)\, U_L^{Ss}(r)\, j_{\ell'}(kr) \int d\hat{\omega}\, Y_j^{j_z *}(\hat{\omega})\, Y_L^M(\hat{\omega})\, Y_{j'}^{j_z'}(\hat{\omega}) \\
&\times \int d\hat{r}\, Y_\ell^{\ell_z *}(\hat{r})\, Y_L^{M*}(\hat{r})\, Y_{\ell'}^{\ell_z'}(\hat{r}) \\
&= 8kk' \sum_{\text{even } L} \sum_{\substack{\ell_z \ell_z' \\ j_z j_z'}} C(j\ell J\, j_z \ell_z J_z)\, C(j'\ell' J\, \ell_z' j_z' J) \\
&(-1)^M \left[\frac{(2\ell+1)(2L+1)}{4\pi(2\ell'+1)}\right]^{1/2} C(\ell L\ell' 000)\, C(\ell L\ell' \ell_z - M \ell_z') \left[\frac{(2j+1)(2L+1)}{4\pi(2j'+1)}\right]^{1/2} \\
&\times C(jLj' j_z M j_z')\, C(jLj'000) \int dr\, r^2 j_\ell(kr)\, U_L^{Ss}(r)\, j_{\ell'}(k'r)
\end{aligned}$$

Equation AII·36

At 300°K, k for Ps is 0.113Å^{-1}, and at 600°K is still only 0.163Å^{-1}. If we assume that the potential is negligable for R > 3Å, then the integral over r is small for all values of l L l′, except l=L=l′=0. Thus the matrix element of V^{Ss} can be approximated to

$$\sim \delta_{l0}\,\delta_{jj'}\,\delta_{kk'}\,\frac{8}{4\pi}\int_0^{\infty} dr\, v_0^{Ss}(r)$$

Equation AII·37

This implies that the scattering is dominated by the s wave elastic component involving only the isotropic part of the Ps molecule interaction. The corresponding matrix element in the T matrix can therefore be expressed

$$T^{JSs}(jl;j'l') \sim \delta_{l0}\,\delta_{jj'}\left(e^{2i\delta_0^{Ss}} - 1\right)$$

Equation AII·38

where the phase shifts δ_0^{Ss} are independent of j.

This is precisely the conclusion reached by Arthurs and Dalgarno concerning low energy scattering of electrons by a rigid rotor (Arthurs 1960). They found that scattering off a non spherical potential such as

$$V(r,\hat{\omega}) = \begin{cases} \infty & r < 3a_0 \\ -\frac{5.43}{r^4} - \frac{0.774}{r^3} P_2(\hat{\omega}) & r > 3a_0 \end{cases}$$

Equation AII·39

was completely elastic s-wave for electron energies below 0.01 Rydberg, which corresponds to a wave vector k less than 0.187 Å^{-1}.

It is immediately clear from the Clebsh Gordon coefficient $C(jLj'\ j_z\ M\ j_z')$ in Equation AII·36 that j_z is also conserved in this low energy limit.

APPENDIX III DIRECT THERMALIZATION OF MUONIUM IN THE VOIDS OF OXIDE POWDERS

The failure of the ATTD model (see Section VI.2.6) necessitates an alternative explanation for how Mu emerges into the void regions at low temperature. In this appendix, the possibility that Mu thermalizes directly in the voids is examined.

A cross section of the Mu-powder potential can be imagined as in Figure AIII·1. Given that there is a collision of a

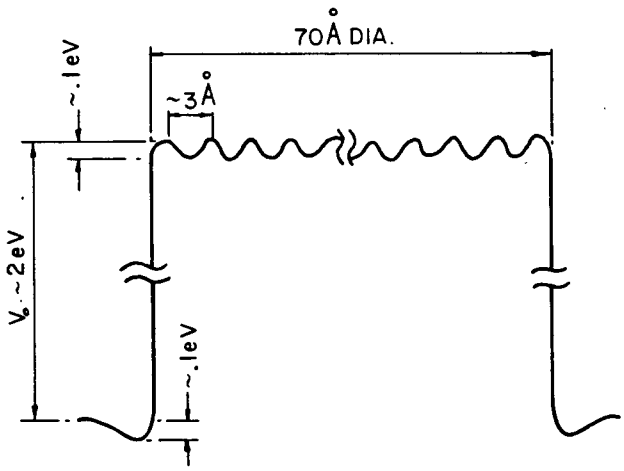

Figure AIII.1. Imagined cross section of the Mu-powder grain potential.

Mu atom (E < 6 eV) with a powder grain there are four possible outcomes.

1. The atom is scattered elastically off the surface, losing a fraction of its energy. Since the thermal wavelength for a 100°K Mu atom is much less than the atomic dimensions, momentum is transferred primarily to individual atoms. Thus the mean energy loss is 3mE/M, where m is the Mu mass and M is the surface atom mass.

2. The atom may be captured in a surface state via phonon interaction. This is only important near thermal energies.

3. The atóm enters the grain with kinetic energy E - V_0, loses energy via phonons, and thermalizes within the grain. In this case, the Mu might become trapped in the lattice at very low temperatures if the diffusion rate is small.

4. The atom enters the grain with kinetic energy E - V_0, loses energy via phonons and is expelled from the surface before thermalization. This can be thought of as a generalization of inelastic scattering.

For $E < V_0$, outcomes 1 and 2 are the only ones allowed energetically. It may be assumed that for Mu energies greater than some threshold energy E_{th} (dependent on the type of powder and the grain radius, R), outcome 4 dominates. Thus there is, in effect, an energy window $V_0 < E < E_{th}$ where thermalization within the powder is most likely.

The probability for a particle of energy, E, to be transmitted into the powder grain can be estimated from the transmission probability for square potential barrier of height $V_0 < E$. In one dimension (Leighton 1959),

$$\mathcal{T}(E) = \frac{4E^{1/2}(E-V_0)^{1/2}}{(E^{1/2}+V_0^{1/2})^2} \qquad \text{Equation AIII·1}$$

Therefore, a sufficient condition for Mu to thermalize directly in the voids is for $(E_{th} - V_0)/V_0 << 1$, since $\mathcal{T}(E)$ is then small over the entire energy window $V_0 < E < E_{th}$.

E_{th} can be estimated by assuming that a Mu atom which enters a grain loses energy through elastic collisions with individual atoms until it reaches a critical kinetic energy, E_c - V_0, at which point it becomes trapped. E_{th} can be approximated as:

$$E_{th} - V_o = (E_c - V_o) e^{R^2 2m/\bar{l}^2 M}$$

Equation AIII·2

where $\bar{l}^2$ is the mean squared distance between collisions and $R^2/\bar{l}^2$ is the mean number of collisions required for a Mu atom to scatter randomly the radius of the grains (R) (Reif 1965), losing an average $2m(E - V_0)/M$ per collision. $\bar{l}^2$ should be on order of the mean atomic spacing squared (10Å^2). Since Mu becomes trapped in SiO_2 below 50°K, a value for $E_c - V_0$ is somewhat arbitrarily chosen to be 100°K. The above parameters, inserted into Equation AIII·2, yield $E_{th} - V_0 \sim 0.033$eV. In other words if a Mu atom is to deposit the last of its kinetic energy within a powder grain and stop, then its kinetic energy inside the grain must not exceed about 0.033 eV.

The work function at the surface is not known, although the barrier height must be much greater than 300°K, since the Mu does not reenter the SiO_2 powder at room temperature. In order to illustrate the feasibility of this model, V_0 is chosen to be 2 eV, which yields $\gamma(E) < 0.13$ over the entire energy window (V_0, E_{th}).

Another important factor which may influence the probability for direct thermalization in the voids is the number of collisions a Mu atom makes with the surface in the sensitive energy window (V_0, E_{th}). In an evacuated powder sample, this may be estimated as $n_c = (E_{th} - V_0)/\Delta E_{th}$, where ΔE is the energy loss per surface collision. Using $\Delta E = 3mE_{th}/M$, $n_c = 1.5$ in the SiO_2 powder. The presence of a buffer gas such as He will tend to reduce n_c due to the additional energy loss between surface

collisions. If the mean distance between collisions with gas atoms is less than that between surface collisions, then $n_c \sim (E_{th} - V_0)/\Delta E^B$. In this equation

$$\Delta E^B = [1 - e^{-z\sigma_g n d m/M_g}] E_{th} \qquad \text{Equation AIII·3}$$

is the mean energy loss through elastic collisions with the buffer gas (of density n, s wave scattering cross section σ_g and mass M_g) after travelling a distance d (the mean free path between surface collisions). Inserting σ_g = 10Å^2, n = 10^{21} cm^{-3} (an ideal gas at 760 torr and 7°K), $M_g = M_{He}$ = 3720 MeV/c^2 and d = 1800Å (mean distance between surface collisions in SiO_2 powders R = 35Å ρ =0.04 gcm^{-3}) into Equation AIII·3. yields ΔE^B =0.68 eV and n_c= 0.04.

According to this model, the probability that a Mu atom thermalizes directly in the voids of oxide powders is determined by processes occurring below the electron excitation threshold (E < 6 eV). It is most probable when the particle size is small and the work function for Mu at the oxide surface is large. The presence of a buffer gas such as He may enhance this probability provided that the mean free path between gas collisions is less than the mean free path between surface collisions.

APPENDIX IV ADSORPTION OF ATOMS ON A SURFACE

Consider gas atoms contained within a volume, V, in contact with an adsorptive surface of area A. Let ϵ_0 be the binding energy to the surface, and N_s be the number of atoms on the surface, N_g the number of atoms in the gas. Define $n_s = N_s/A$ and $n_g = N_g/V$. The adsorption isotherm n_s versus n_g at constant T will, in general, depend on the atom mobility on the surface. Two ideal situations, reviewed in more detail by (Dash 1975) are considered here.

1. Adsorption of a Van der Waals gas atom of area σ on a smooth surface.
2. Adsorption of tightly bound atoms on a surface with $1/\sigma$ adsorption sites per unit area.

A IV·1 Van Der Waals Two Dimensional Gas

The total energy of N_s atoms on the surface is

$$E = -N_s \epsilon_0 + \sum_{i=1}^{N_s} \frac{p_i^2}{2m} + U(r_1 r_2 \cdots r_{N_s}) \qquad \text{Equation AIV·1}$$

where ϵ_0 is the binding energy to the surface, p_i is the momentum of atom i, and $U(r_1 \ldots r_{N_s})$ is the total energy of interaction between atoms on the surface. In the case of hard discs,

$$U = \begin{cases} \infty & |r_i - r_j| < 2\left(\frac{\sigma}{\pi}\right)^{1/2}; \text{ for any } ij. \\ 0 & ; \text{otherwise} \end{cases} \qquad \text{Equation AIV·2}$$

The partition function, Z_s, for the adsorbed atoms

$$Z_s = \frac{1}{N!\,h^{2N}} \int e^{-E/kT}\, d\Gamma$$

$$= e^{N_s \epsilon_0 / kT} \frac{1}{N!\,\Lambda^{2N}}\, Q$$

Equation AIV·3

where $\Lambda = (h^2/2\pi mkT)^{1/2}$ is the thermal de Broglie wavelength, $d\Gamma$ is an element of phase space, and Q is given by:

$$Q = \int_A e^{-U/kT}\, d^2r_1 \cdots d^2r_N$$

Equation AIV·4

At low densities, where $N_s\sigma/A \ll 1$,

$$Q \sim A(A-4\sigma)(A-8\sigma)\cdots(A-4(N_s-1)\sigma)$$

$$\sim A^{N_s}\left[1-(2N_s-1)N_s\left(\frac{\sigma}{A}\right)\right]$$

Equation AIV·5

The free energy, F, for the adsorbed atoms is then

$$F = -kT \ln Z_s$$

$$= -N_s\epsilon_0 - N_s kT \ln[e n_s \Lambda^2] - kT \ln\left[1 - \frac{N_s(N_s-1)2\sigma}{A}\right]$$

$$\sim -N_s\epsilon_0 - N_s kT \ln[e n_s \Lambda^2] + \frac{N_s^2 kT 2\sigma}{A}$$

Equation AIV·6

The chemical potential

$$\mu_s = \left.\frac{\partial F}{\partial N}\right|_{T,A} = -\epsilon_0 + kT \ln[n_s \Lambda^2] + n_s kT 4\sigma$$

Equation AIV·7

The chemical potential for the atoms in the gas phase (assuming an ideal gas) is given by

$$\mu_g = kT \ln[n_g \Lambda^3]$$

Equation AIV·8

In equilibrium, $\mu_g = \mu_s$, and thus

$$n_s = n_g \Lambda e^{\epsilon_o/kT} e^{-n_s 4\delta}$$

Equation AIV·9

At very low densities, n_s is linear in n_g, since $n_s 4\sigma \ll 1$. Near monolayer completion as σn_s tends to 1 and Q (Equation AIII·1) tends to zero, so that n_s is bounded by $1/\sigma$ (we have ignored the geometric packing factor from the start).

A IV·2 Tight Binding Model

In this case, the free energy for the N_s atoms adsorbed on a surface with $N = A/\sigma$ tight binding sites is (Dash 1975)

$$F = -kT \ln\left[N! / \{(N-N_s)!\, N_s!\}\, e^{\epsilon_o N_s/kT} \right]$$

$$= -\epsilon_o N_s + kT N \{ n_s\sigma \ln[n_s\sigma] + (1-n_s\sigma) \times \ln[1-n_s\sigma] \}$$

Equation AIV·10

where $n_s\sigma$ is the fractional coverage. The chemical potentiial for the adsorbed atoms is

$$\mu_s = -\epsilon_o + kT \ln\left[\frac{n_s\sigma}{1-n_s\sigma} \right]$$

Equation AIV·11

In thermal equilibrium the chemical potential of gas phase atoms (given by Equation AIV·8) may be equated with that of the surface atoms, yielding:

$$n_s = \frac{1}{\sigma} \frac{n_g \Lambda^3}{n_g \Lambda^3 + e^{-\epsilon_o/kT}}$$

Equation AIV·12

At low coverage, $n_s\sigma \ll 1$, n_s is linear in n_g

$$n_s \sim \frac{1}{\sigma} n_g \Lambda^3 e^{\epsilon_0/kT}$$

Equation AIV·13

whereas for large n_g, $n_s = 1/\sigma$.

Note that at a low coverage, both Van Der Waals model and tight binding yield a linear relationship between n_s and n_g with the proportionality constant differing by a factor Λ^2/σ (~1 for He at 7°K).

A IV·3 Single Atom Adsorption

If a single atom (Ps or Mu) is thermalized in a system with surface area A and total free volume V_F, it is desirable to know the fraction of time spent on the surface, averaged over times much larger than the dwell time on the surface or the mean time between stickings. This fraction, α, may be obtained from the above low density approximations for n_s and n_g.

$$\alpha = \frac{n_s A}{n_s A + n_g V_F}$$

$$= \frac{1}{1 + \frac{n_g}{n_s}\frac{V_F}{A}}$$

Equation AIV·14

$$= \frac{1}{1 + e^{-\epsilon_0/kT}\frac{V_F}{A\Lambda}}$$

Equation AIV·15

for a 2-dimensional gas bound to the surface by ϵ_0.

$$\alpha = \frac{1}{1 + e^{-\epsilon_0/kT} \frac{\sigma V_F}{\Lambda^3 A}}$$

Equation AIV·16

for tightly bound atoms.

A IV·4 Mean Surface Dwell Time

It is also of interest to estimate the mean time spent on the surface per sticking to the surface before desorption occurs (Crampton 1980). The density of atoms on the surface can also be written

$$n_s = \frac{1}{4} n_g \upsilon \bar{t} P_t$$

Equation AIV·17

where υ is the mean thermal velocity and P_t is the probability that an atom which strikes the surface will adsorb. The sticking of an atom to a surface is an inelastic process in which the incident momentum of the atom and its binding energy are transferred to to the lattice via phonon interaction. In the case of a low density 2 dimensional gas, the above expression may be equated to Equation AIV·8 yielding

$$\bar{t} = \frac{4\Lambda e^{\epsilon_0/kT}}{\upsilon P_t}$$

Equation AIV·18

BIBLIOGRAPHY

Abragam, A., 1961, Nuclear Magnetism, Oxford Press, London, 126.

Anderson, C. D., 1933, Phys. Rev. 43, 491.

Anderson, C. D. and S. H. Neddermeyer, 1937, Phys. Rev. 51, 884.

Anderson, P. W., 1951, C. R. Acad. Sci. 82, 342.

Ashcroft, N. W. and N. D. Mermin, 1976, Solid State Physics, Holt Rinehart and Winston, 781.

Aston, J. G., S. V. R. Mastrangelo and R. J. Tykodi, 1955, J. Chem. Phys. 23, 1633.

Arthurs, A. M. and A. Dalgarno, 1960, Proc. R. Soc. London A256, 540.

Blackett, P. M. and G. P. Occhianlini, 1933, Proc. Roy. Soc. A139, 699.

Brandt, W, 1967, Positron annihilation, Academic Press, , 180, .

Brandt, W. and R. Paulin, 1968, Phys. Rev. 21, 193.

Brewer, J. H., 1981, Hyperfine Interactions 8, 375.

Brewer, J. H., K. M. Crowe, F. N. Gygax and A. Shenck, 1975, Muon Physics, Vol II, edited by V. W. Hughes and C. S. Wu, Academic Press, New York, 3.

Brunauer, S., P. H. Emmett and E. Teller, 1938, J. Am. Chem. Soc 60, 309.

Cabot Corporation, Technical Report, Cab-O-Sil Properties and Functions, available from Cabot Corporation, 125 High Street, Boston, MA 02110, U. S. A.

Canter, K. F., A. P. Mills and S. Berko, 1975, Phys. Rev. Lett. 34, 177.

Canter, K. F., A. P. Mills Jr. and S. Berko, 1974, Phys. Rev. Lett. 33, 7.

Canter, K. F., P. G. Coleman, T. C. Griffith and G. R. Heyland, 1972, J. Phys. B5, L167.

Casperson, D.E., T.W. Crane, V.W. Hughes, P.A. Souder, R.D. Stambaugh, P.A. Thompson, H. Orth, G. zu Putliz, H.F. Kaspar, H.W. Reist, A.B. Denison, 1975, Phys. Letts. 59B, 397.

Chuang, S.Y. and S.J. Tao, 1973, Can. J. Phys. 51, 823.

Chuang, S. Y. and S. J. Tao, 1974, Appl. Phys. 3, 199.

Crampton, S.B., 1980, Journal De Physique C7, 249.

Cronin, J. W., 1968, Proc. Int. Conf. High Energy Physics, 14th, 289.

Curry, S. M. and A. L. Shawlow, 1971, Phys. Lett. 37A, 5.

Dash, J. G., 1975, Films On Solid Surfaces, Academic Press, New York, .

Deutsch, M., 1951, Phys. Rev 83, 866.

Devonshire, A. F., 1938, Proc. Roy. Soc. A158, 269.

Dirac, P. A. M., 1930, Proc. Roy. Soc. A126, 360.

Fleming, D. G., D. M. Garner and R. J. Mikula, 1981a, Hyperfine Interactions 8, 337.

Fleming, D. G., R. J. Mikula and D. M. Garner, 1981b, Hyperfine Interactions 8, 307.

Foner, S. N., E. L. Cochran, V. A. Bowers and C. K. Jen, 1960, J. Chem. Phys. 32, 963.

Ford, G. W., L. M. Sander and T. A. Witten, 1976, Phys. Rev. Lett. 36, 1269.

Friedman, J. and V.Telegdi, 1957, Phys. Rev. 105, 1681.

Garner, D. M., 1978, Ph. D. Thesis, University of British Columbia, Chemistry Department.

Garwin, R.L., L.M.Lederman, and W.Weinrich, Phys. Rev., 105 1415 , .

Gidley, D. W., A. Rich, P. W. Zitewitz and D. A. L. Paul, 1978, Phys. Rev. Lett. 40, 737.

Golubev, V.B., 1965, Russian Journal of Physical Chemistry 39, 1395.

Goodman, F., 1971, Surf. Sci. 24, 667.

Goodman, F., 1972, Surf. Sci. 30, 1.

Gordon, E. B., B. I. Ivanov, A. P. Perminov, A. N. Ponomarev, V. L. Tal roze and S. G. Khidirov, 1973, JETP Letters 17, 395.

Hara, S.and P.A. Fraser, 1975, J.Phys.B Atom. Molec. Phys. 8, L472.

Hotz, H. P., J. M. Mathiesen and J. P. Hurley, 1968, Phys. Rev. 170, 351.

Huff, G.B. and J.G. Dash, 1976, J. Low Temp. Phys. 24, 155.

Hughes, V.W., D.W. McColm, K. Ziock, and R. Prepost, 1960, Phys. Rev. Lett. 5, 63.

Hughes, V.W. and T.Kinoshita, 1977, Muon Physics, Vol. I, edited by V.W. Hughes and C.S. Wu, Academic Press, New York, 11.

Ito, Y., B. W. Ng, Y. C. Jean and D. C. Walker, 1981, Hyperfine Interactions 8, 355.

Ito, Y. and Y. Tabata, 1979, Proc. 5th Intern. Conf. Positron Annihil., 325.

Iwasaki, M., K. Toriyama, H, Muto and K. Nunome, 1978, Phys. Lett. 56, 494.

Kiefl, R.F., 1978, M.Sc. Thesis, University of British Columbia, Department of Physics, .

Kiefl, R. F., J. B. Warren, G. M. Marshall, C. J. Oram, J. H. Brewer, D. J. Judd and L. D. Spires, 1979, Hyperfine Interactions 6, 185.

Kinugawa, K., T. Miyazaki and H. Hase, 1978, J. Phys. Chem. 82, 1697.

Klobuchar, R. L. and P. J. Karol, 1980, J. Phys. Chem 84, 483.

Knozinger, H., 1976, Adv. Catalysis 25, 184.

Knozinger, H. and P. Ratnasamy, 1978, Catal. Rev. - Sci. Eng. 17 , 31.

Leighton, R.B., 1959, Principles of Modern Physics, Mcgraw-Hill, New York, 149, .

Levine, I. N., 1957, Molecular Spectroscopy, John Wiley & Sons, New York, 160.

Marshall, G. M., J. B. Warren, D. M. Garner, G. S. Clark, J. H. Brewer and D. G. Fleming, 1978, Phys. Lett. 65A, 351.

Manaichev, E.V.,G.G. Myasishcheva,Yu V. Obukhov,V.S. Roganov,G.I. Savel ev and V.G. Firsov, 1970, JETP 31, 849.

Mobley, R.M., J. Amato, V.W. Hughes, J.E. Rothberg, and P.A. Thompson, 1966, J. Chem. Phys. 47, 3074.

Mogensen, O. E., 1974, J. Chem Phys. 60, 998.

Mohorovicii, S., 1934, Astron. Nachr., 94.

Oram, C.J., J.B. Warren, G.M. Marshall, and J. Doornbos, 1981, Nucl. Instrum. Meths. 179, 95.

Ore, A. and J. L. Powell, 1949a, Phys. Rev. 75, 1696.

Ore, A., 1949b, Univ. i Berger Arbok Naturvitenskap. Rekke 9, .

Pake, G. E., 1948, J. Chem. Phys. 16, 327.

Percival, P.W., 1981, Hyperfine Interactions 8, 315.

Pifer, A.E., T. Bowan, and K.R. Kendall, 1976, Nucl. Instr. Methods 135, 39.

Pirenne, J., 1946, Arch. Sci. Phys. et Nat. 28, 273.

Reif, F., 1965, Fundamentals of Statistical and Thermal Physics, McGraw-Hill, New York, 16, .

Spencer, D.P. and J.H. Brewer, 1981, Private Communication, .

Street, C. and E. Stevenson, 1937, Phys. Rev. 51, 1005.

Surin, S.A.,G.M. Zhidomirov,B.N. Shelimov and V.B. Kazanskii, 1970, Teoreticheskaya i Eksperimental naya Khimiya 6, 353.

Tawara, H. and A. Russek, 1973, Rev. Mod. Phys. 45, 178.

Temansky, M. W., 1968, Heat and Thermodynamics, 5th edition, McGraw-Hill, New York, 318.

Theriot, E. D. Jr., R. H. Beers, V. W. Hughes, 1967, Physics Reports 5, 215.

Tinkham, M., 1964, Group Theory and Quantum Mechanics, McGraw-Hill, New York, 253.

Townes, C.H. and A.L. Schawlow, 1955, Microwave Spectroscopy, McGraw Hill, New York, 183, .

Weil, J. A., 1981, Hyperfine Interactions 8, 371.

Walker, D.C., 1981, Hyperfine Interactions 8, 329.

Wallace, P.R., 1960, Solid St. Phys. 10, 1.

West, R. N., 1973, Advances in Physics 22, 263.

Wheeler, J. A., 1946, Ann. N. Y. Acad. Sci. 46, 221.

Williams, W. S. C., 1971, An Introduction to Elementary Particles, 2nd Edition, Academic Press, New York, 166 ; 349.

Wu, C. S., E. Ambler, R. W. Hayward, D. D. Hoppes and R. R. Hudson, 1957, Phys. Rev. 105, 1413.

Zemansky, M.W., 1968, Heat and Thermodynamics, McGraw Hill, New York, 318, .

PUBLICATIONS

R.F. Kiefl, J.B. Warren, G.M. Marshall, C.J. Oram, and C.W. Clawson, 1981, Muonium in the Condensed Phases of Ar, Kr, and Xe, J. Chem. Phys. 74, 308.

R.F. Kiefl, J.B. Warren, C.J. Oram, G.M. Marshall, J.H. Brewer, D. Harshman, and C.W. Clawson, 1981, Surface Interaction of Muonium in Oxide Powders at Low Temperature, Submitted for publication in Jan., 1982.

R.F. Kiefl, J.B. Warren, G.M. Marshall, C.J. Oram, J.H. Brewer, D.J. Judd, and L.D. Spires, 1979, Muonium and Positronium in Oxide Powders, Hyperfine Interactions 6, 185.

R.F. Kiefl, 1981, Thermalization of Muonium in Oxide Powders at Low Temperature, Hyperfine Interactions 8, 359.

G.M. Marshall, J.B. Warren, C.J. Oram, and R.F. Kiefl, 1981, A Search for Muonium to Antimuonium Conversion, To be published in Phys. Rev. D.

C.J. Oram, C.A. Fry, J.B. Warren, R.F. Kiefl, and J.H. Brewer, 1981, Observation of the 2S State of Muonium in Vacuum, To be published in J. Phys. B.

Y.J. Uemura, C.Y. Huang, C.W. Clawson, J.H. Brewer, R.F Kiefl, and A.M. de Graff, 1981, Zero-Field MSR in an Insulator Spin Glass, Hyperfine Interactions 8, 757.